RELATIONSHIPS BETWEEN MECHANICAL STRESS AND MARKERS OF INFLAMMATION IN DISEASED HUMAN CORONARY ARTERIES

A Thesis
Presented to
The Academic Faculty

By

Karen Melissa Hallow

In Partial Fulfillment
Of the Requirements for the Degree
Doctor of Philosophy in
Mechanical Engineering

Georgia Institute of Technology
August 2007

RELATIONSHIPS BETWEEN MECHANICAL STRESS AND MARKERS OF INFLAMMATION IN DISEASED HUMAN CORONARY ARTERIES

Approved by:

Dr. Raymond P. Vito, Advisor
School of Mechanical Engineering
Georgia Institute of Technology

Dr. Hamid Garmestani
School of Materials Science and Engineering
Georgia Institute of Technology

Dr. Rudolph Gleason
School of Mechanical Engineering
Georgia Institute of Technology

Dr. Robert Guldberg
School of Mechanical Engineering
Georgia Institute of Technology

Dr. Alexander Rachev
School of Mechanical Engineering
Georgia Institute of Technology

Dr. Robert Taylor
School of Medicine
Emory University

Date Approved: June 25, 2007

To my husband and my daughter

ACKNOWLEDGEMENTS

I would like to express my appreciation to the many people who have helped me along the way in accomplishing this research. First of all, I owe a debt of gratitude to my advisor, Dr. Ray Vito, for his direction, ideas, encouragement, and support throughout my Ph.D work. I've learned so much from him during my graduate school career. His guidance has helped cultivate my skills as a researcher, and I appreciate all the time and effort he has put into this work, and in helping develop my critical thinking, presentation, and writing skills. In addition, I would like to thank Dr. Alexander Rachev for his invaluable input, and for asking questions that really make me think (usually with a Bulgarian twist, i.e. which comes first, hen or egg?). He is a great teacher, and his door was always open when I needed help or advice. He has not only an incredibly sharp scientific mind, but also has a wonderful sense of humor. In addition to biomechanics, he taught me about the tenses of the English language (there are 16), and that "time flies like an arrow, but fruit flies like bananas." Also, I would like to thank Dr. Bob Taylor for his advice and insight, and for his patience in helping us engineers understand the complex biology of atherosclerosis. I would like to thank Dr. Hamid Garmestani, Dr. Rudy Gleason, and Dr. Bob Guldberg for their time and input in serving on my thesis committee.

As a mechanical engineering student, I entered graduate school knowing absolutely nothing about histology, but during my time here, I have had the opportunity to learn from several experts. First of all, I would like to acknowledge Tracy Couse for bestowing a portion of her incredibly vast knowledge of histology on me. Her thorough

technical knowledge was amazing, and on the rare occasion that she did not already know the answer to my question, she would always find it. This project could not have been completed without the training, skills, and expertise I received from Tracy. I would like to also thank Giji Joseph and Dr. Daiana Weiss, from Dr. Taylor's lab, for first teaching me immunohistochemical techniques, and for their patience with my silly mistakes and many non-working antibodies. In addition, I would also like to thank Daiana for her help in procuring arteries from explanted hearts. She has lost many hours of sleep receiving hearts from transplant patients in the middle of the night and dissecting out coronary arteries for us, and I am truly grateful for this. In addition, I would like to thank the transplant surgeon, Dr. J. David Vega of Emory, for making these explanted hearts available to us.

Working with my fellow graduate students has made my life in a graduate school much more enjoyable, and I would like to thank my fellow members of the Vito lab – Dr. Peter Carnell, Dr. Brian Wayman, Dr. Lori Lowder, Yu Shin Kim, and Zack Dominguez – for their friendship and camaraderie. Particularly, I would like to thank Lori Lowder for her collaboration, ideas, and suggestions, for sharing the work and many hours on the microtome in the histology lab, and of course, for her wonderful sense of humor. I also owe a special thanks to Dr. Peter Carnell, from whom I learned so much. His work provided a base for this research, and his collaboration, input, suggestions, and feedback were invaluable. I would also like to thank the fellow parents in the lab Dr. Brian Wayman, for his friendship and advice, and for being the "guinea pig" as the first parent in the lab. In addition to my fellow lab members, I also had the pleasure of working with a wonderful visiting REU student, Niki Florence, and I appreciate her hard work. Lastly,

I must thank our wanna-be Vito lab member, Dr. Srin Nagaraja, as well as my other friends from the histology lab – Samantha Andrews and Aqua Asberry – for good conversation and company during many long days in the histology lab.

I am fortunate to have a wonderful group of friends who I met primarily through GT Crew (I will not try to name you all, lest I leave someone out) and who have provided me with support and friendship, not to mention many many good times, throughout my time at Georgia Tech. I'm not sure I could have completed this work without the release and escape I find in spending time with you guys. I would particularly like to express my appreciation to Anne Marie Richards and Bart Debacker for their generous hospitality in opening their home to me during these last few months of graduate school. I also thank Suzanna Sayre and Anne Marie Richard, my fellow Warfield Women, for being the best friends a girl could ask for.

I am also blessed to have a wonderful family whose love and encouragement has guided me throughout my life. I have two wonderful parents, Jackie and Modena Deen, who have always supported me and given me the freedom to choose my own way. In addition, I would like to thank my grandmother, Doris Deen, for inspiring me to "have ambition" and for showing me that people can't limit you if you don't let them. Also, I would also like to thank my mother-in-law, Patricia Hallow, for her love, support, and hospitality.

And lastly, I would like to acknowledge my dear husband Daniel Hallow and my wonderful daughter, Ana Grace Hallow. Danny is my very best friend, my closest advisor, my biggest supporter, and my inspiration. Ana has brought a joy into my life that I never knew existed before the day she was born. I dedicate this work to Danny and Ana.

TABLE OF CONTENTS

LIST OF TABLES

LIST OF FIGURES

LIST OF SYMBOLS AND ABBREVIATIONS

2D ..... Two-dimensional

3D ..... Three dimensional

α ..... Significance level

ε ..... Strain

σ ..... Stress

A ..... Area fraction

AHA ..... American Heart Association

ANOVA ..... Analysis of Variance

CVD ..... Cardiovascular disease

d ..... Distance

E ..... Young's Modulus

EC ..... Endothelial cell

ECM ..... Extracellular matrix

GEE ..... Generalized Estimating Equations

IEL ..... Internal elastic lamina

IFN-γ ..... Interferon-gamma

IL-1 ..... Interleukin 1

iNOS ..... inducible isoform of Nitric Oxide Synthase

IVUS ..... Intravascular ultrasound

LDL ..... Low density lipoprotein

MAP ..... Mitogen-activated Protein Kinase

MCP1 ..... Monocyte-chemotactic protein-1

M-CSF ..... Macrophage Colony Stimulating Factor

MI ..... Myocardial infarction

MMA ..... Methyl methacrylate

MMP ..... Matrix Metalloproteinase

MRI ..... Magnetic resonance imaging

mRNA ..... Messenger Ribonucleic Acid

NF-kB ..... Nuclear Factor – kappa B

NO ..... Nitric Oxide

OCT ..... Optical coherence tomography

PDGF ..... Platelet derived growth factor

RCA ..... Right coronary artery

RGB ..... Red Green Blue

ROS ..... Reactive oxygen species

SMC ..... Smooth muscle cell

SRA ..... Scavenger receptor

T ..... Cauchy stress

TGF-β ..... Transforming Growth Factor-Beta

TIMP ..... Tissue Inhibitor of Matrix Metalloproteinase

TNF-alpha ..... Tumor Necrosis Factor – Alpha

W ..... Wilcoxon coefficient

SUMMARY

Rupture of atherosclerotic plaque and subsequent thrombus formation is the primary cause of death due to cardiovascular disease. The factors directing plaque progression to instability and rupture are poorly understood. It is known that arteries respond to changes in mechanical stress by remodeling, and that remodeling is mediated by the inflammatory response. Studies have shown that both mechanical stress and markers of inflammation tend to be localized in the fibrous cap and shoulder regions of atherosclerotic plaque, where rupture most often occurs. In this study we hypothesized that there are spatial relationships between the local mechanical environment and expression of markers of inflammation in atherosclerosis, and that these relationships are plaque progression dependent. To test these hypotheses, we analyzed cross-sections at regular intervals along the length of atherosclerotic human coronary arteries. For each cross-section, a 2D heterogeneous finite element model was developed to determine the spatial distribution of stress in the cross-section. In addition, novel techniques for quantifying inflammatory markers at high spatial resolution were used to determine the distributions of a set of inflammatory markers. The distributions of stress and five markers of inflammation – activated NF-kB, macrophages, MMP-1, nitrotyrosine, and microvessels - were then compared to determine whether spatial relationships exists between magnitude of mechanical stress and the presence of these inflammatory markers.

We demonstrated that the probability of activated NF-kB expression increases monotonically with increasing stress in all stages of plaque progression. This indicates that the relationship between mechanical stress and NF-kB activation is important

throughout the disease process. We found that the relationship between mechanical stress and macrophages is highly dependent on the state of plaque progression. In intermediate stages of progression macrophages increase with moderate stress but drop off again at very high stresses, while in the advanced stage macrophages continue to increase monotonically with stress. We found that MMP-1 increases with stress in stages of progression where active remodeling is occurring, but decreases with stress in mature stable plaque. We found no relationship between mechanical stress and nitrotyrosine expression or microvessels. Taken together, these results support the role of mechanical stress in instigating and maintaining the inflammatory response, and help explain how mechanical input is able to direct the complex biological changes involved in remodeling.

CHAPTER 1

INTRODUCTION AND BACKGROUND

Cardiovascular disease is the leading cause of death in the United States. CVD accounts for more deaths than the next four leading causes (cancer, chronic respiratory disease, accidents, and diabetes) combined, and costs over $400 billion annually (American Heart Association 2006). One of the primary causes of CVD is atherosclerosis, which is responsible for most instances of myocardial infarction and stroke. In the coronary arteries, atherosclerotic plaques sometimes progress to large highly stenotic plaques that cause blockage of blood flow, and are presented clinically in the patient as stable angina. More often, however, heart attacks are due to the rupture of lower grade stenotic plaques (Davies and Thomas 1981, Davies and Thomas 1985). It is the rupture and subsequent thrombosis, rather than stenosis, that blocks blood flow to the heart muscle and causes myocardial infarction. Plaques that are prone to rupture are often clinically silent until the time of rupture, when the patient experiences unstable angina.

The processes directing plaque progression to rupture are poorly understood. It is known that plaques that are vulnerable to rupture have several common characteristics. They tend to be large eccentric plaque with considerable positive remodeling, large lipid pools, thin fibrous caps, and significant inflammatory infiltration. Finite element studies have shown that mechanical stress is increased in the shoulder and fibrous cap region, where plaques most often rupture. Furthermore, inflammatory markers such as macrophages and MMPs have been found to localize in these regions.

Because cells are capable of sensing and responding to mechanical stress, it is reasonable to believe that associations between mechanical stress and inflammation may play a role in plaque progression and plaque rupture. However, there have been few attempts to compare the spatial distributions of inflammation and mechanical stress, and studies that do exist have very limited spatial resolution. In addition, previous histology-based finite elements models have used histologic methods that are highly susceptible to geometrical distortions, and have not captured the heterogeneous nature of plaque tissue.

A better understanding of the collocation of stress and inflammation in atherosclerosis will yield insight into the mechanisms of plaque progression and plaque rupture. The objectives of this research were to use a finite element model that limits geometrical distortions and accounts for the spatial heterogeneity of plaque, as well as quantitative methods for determining inflammatory cell distributions at high spatial resolution, to investigate spatial relationships between mechanical stress and important markers of inflammation.

ATHEROSCLEROSIS AND PLAQUE PROGRESSION TO RUPTURE

Atherosclerosis is a disease that is characterized by the progressive formation of plaque in large and medium-sized arteries. Although the mechanisms of plaque formation and progression to rupture are not yet fully understood, atherosclerosis begins with the deposition of lipid on the arterial walls. This occurs especially in regions with low wall shear stress (Giddens et al. 1993). These lipid molecules are ingested by macrophages, forming fatty streaks composed of macrophage-derived foam cells. Also, smooth muscle cells within the media wall proliferate and/or migrate into the intimal layer, where they secrete extracellular matrix (ECM). As the plaque burden increases, positive remodeling

may occur to accommodate the vessel's increased cross-sectional area without reducing lumen area (Glagov et al. 1997). Trapping of lipid molecules within the extracellular matrix, as well as foam cell necrosis, gradually leads to the formation of a soft lipid core. This lipid core is very thrombogenic, but is separated from the lumen by a fibrous cap comprised mainly of ECM and smooth muscle cells. Over time several factors, including inflammatory infiltration and apoptosis of SMCs, are thought to bring about a shift from ECM production to ECM degradation, causing thinning and eroding of the fibrous cap (Libby et al. 1996). Rupture of the fibrous cap exposes the lipid core to the blood stream, leading to thrombus formation and subsequent myocardial infarction or stroke.

As the fibrous cap thins and the lipid core increases in size, mechanical stresses within the plaque may be redistributed and concentrated in the fibrous cap, making the plaque more vulnerable to rupture. In addition, increased inflammation and neovascularization in the plaque shoulder and plaque base have been associated with plaque instability, Also, over time, calcification of plaque tissue occurs, especially in more advanced lesions. However, calcification has not conclusively been shown to indicate increased vulnerability to rupture, and may even act as a means of stabilizing plaque (Glagov et al. 1997, Kilpatrick 2001).

PLAQUE STRUCTURE AND COMPOSITION

Structure of Healthy Arteries

Arteries are comprised of three layers – the intima, media, and adventitia. In healthy vessels, the intima is very thin, consisting of the endothelial cell layer and the internal elastic lamina, which separates the intima from the media. The medial layer

consists mainly of smooth muscle cells and bundles of collagen fibers (primarily type III collagen), and is also interspersed with sheets and fibers of elastin. The adventitia is separated from the media by the basement membrane known as the external elastic lamina. The adventitia consists mainly of collagen fibers (primarily type III collagen) and ground substances such as fibronectin. It also contains fibroblasts, inflammatory cells, nerve bundles, and the vasa vasorum, which supplies the blood vessel with oxygen and nutrients (Fung 1993).

Structure and Composition of Plaque

The major structural components of plaque are the extracellular matrix (ECM), lipid, and calcification. Inflammatory cells, smooth muscle cells, and endothelial cells, though not inherently structural components, may also play significant regulatory roles in plaque structure.

Extracellular Matrix. The extracellular matrix (ECM) is the main structural component of plaque. Production, regulation, and degradation of ECM are important to plaque stability, because excess ECM leads to arterial stenosis, while degradation of ECM weakens the plaque and makes it more vulnerable to rupture. Besides providing structural integrity, ECM also helps regulate the adhesion, migration, proliferation, and apoptosis of cells embedded in the ECM. In addition, it can serve as a network onto which substances such as oxidized LDL or growth factors that aid in plaque progression can be deposited (Lindstedt and Kovanen 2004).

The ECM is comprised of different types of collagen, with contributions also from elastin, proteoglycans, and various glycoproteins. Collagen, the principle constituent of blood vessel ECM, serves to provide mechanical integrity to the vessel

wall. There are thirteen types of collagen present in the arterial wall, although type I and type III, fibrillar collagens, are the most common. Type I collagen accounts for 70% of the collagen in plaque, and is quite rigid, while type III collagen, the main collagen type in healthy vessels, is more elastic. Deposition of each collagen type changes with lesion progression, indicating changes in SMC collagen synthesis, since SMCs are the main synthesizers of ECM. The types of collagen present in plaque are important because different matrix metalloproteinases (MMPs) found in plaque are responsible for breaking down each of the different collagen types. (Katsuda and Kaji 2003, Rekhter 1999).

Elastin fibers in plaque, though much less abundant than collagen, are essential to plaque structure because they provide elasticity and resilience. However, elastin fibers often become disrupted as plaque progresses, and have been shown to decrease in number with increasing lipid deposition, meaning that the plaque loses elasticity as it progresses. Furthermore, elastin fibers may become sites of calcium deposition, further decreasing the flexibility and increasing the rigidity of plaque (Katsuda and Kaji 2003).

Although much less abundant than collagen and elastin, proteoglycans help organize the ECM and help it maintain its viscoelastic properties. They are also critical to permeability, hemostasis, and lipid metabolism, and influence cell adhesion, migration, and proliferation. (Katsuda and Kaji 2003)

The final component of the ECM is glycoproteins, such as fibronectin, vitronectin, osteopontin, thrombospondin, and laminin. Each of these plays a role in regulating the function of cells embedded in the ECM. For instance, fibronectin is an adhesive glycoprotein that can influence the proliferation, morphology, and migration of

SMCs. Osteopontin has a strong affinity for collagen, promotes SMC migration, and may accelerate fatty streak formation (Katsuda and Kaji 2003).

Vascular Smooth Muscle Cells. Vascular smooth muscle cells (VSMCs) are the main cellular component of plaque, and are also the primary source of ECM. They regulate ECM metabolism, remodeling, and degradation. SMCs in plaque may arise through proliferation of pre-existing SMCs in the intimal layer. However, disruption of the internal elastic lamina (IEL) and wasting of the medial layer as plaque progresses suggests that they migrate from the medial layer to the intima (Newby and Zaltsman 1999).

Early on in the development of plaque, migration and proliferation of SMCs and their subsequent synthesis of ECM leads to the build up of fibrous tissue. However, in more advanced plaque, loss of SMCs through apoptosis can lead to a loss of the plaque's ability to repair itself. This, along with the release of matrix degrading enzymes such as MMPs and cathepsins by inflammatory cells, can decrease the strength of the plaque. Furthermore, in the presence of cytokines IL-1 and TNF-alpha released by macrophages and T-lymphocytes, SMCs are also capable of releasing MMPs that may destabilize the plaque. Thus, SMCs are very influential in determining plaque stability (Newby and Zaltsman 1999, van der Wal and Becker 1999).

Lipid Deposits. Lipid accumulation begins in the very early stages of plaque formation, as low density lipoproteins (LDL) are transported into the artery wall and trapped in the ECM. The cells in the wall then release products that oxidize LDL. The oxidized LDL induces monocytes to migrate into the wall and differentiate into macrophages. These macrophages ingest oxidized LDL, forming large foam cells. Overtime, these foam cells,

as well as extracellular lipid trapped in the ECM and debris from necrotic foam cells, aggregate to form a lipid core. The lipid core is comprised of crystalline cholesterol, cholesteryl esters, phospholipids, cellular debris from apoptotic or necrotic foam cells, and collagen remnants (Schroeder and Falk 1995, Berliner et al. 1995).

The lipid content of plaque is a critical factor in plaque instability. Because the lipid pool is several orders of magnitude softer than the fibrous tissue surrounding it, it is relatively non-load bearing, and causes stresses within the plaque to be redistributed across the vessel wall and to become concentrated in the fibrous cap. The proximity of the lipid core to the lumen, as well as the proportional size of the lipid core relative to the rest of the plaque, have been found to be major factors in elevating and concentrating stresses in the plaque cap (Davies et al. 1994,Glagov et al. 1997). Furthermore, the material in the lipid pool is extremely thrombogenic, and when rupture occurs, this material is exposed to the blood stream. It is the subsequent thrombotic response, rather than the actual stenosis of the plaque, that blocks blood flow and leads to unstable angina and myocardial infarction.

Calcification. Another major constituent of atherosclerotic plaque is calcification. The calcification in plaque consists of hydroxyapatate and is biochemically and ultrastructurally similar to bone tissue. The formation of calcification in plaque was at first thought to occur through a passive precipitation process, but is now believed to happen through a more organized process similar to that of bone formation (Bostrom et al. 1993, Watson 2000). Plaque calcification may arise from a subpopulation of cells within the wall that differentiate into osteoblasts, or may come from osteoblasts that migrate into the cell wall (Bostrom et al. 1995).

Because calcification accumulates in plaque over time, it is a good indicator of the presence of atherosclerosis and general plaque burden. However, it does not necessarily correlate with plaque vulnerability. Many highly calcified plaques are relatively stable and biologically inert, with little cellular activity and fewer inflammatory cells than plaque with less calcification. In fact, a strong inverse correlation has been found between extent of calcification and extent of inflammatory infiltration (Shaalan et al. 2004), as well as between percent calcification and occurrence of unstable angina (Beckman et al. 2001). Plaque that rupture tend to have only mild to moderate calcification (Burke et al. 2001). Plaque calcification may actually be an adaptive attempt to stabilize plaque. Glagov et al found that while calcification causes increased stress concentrations in plaque, especially at material interfaces, these concentrations are shifted away from the lumen and more toward the interior of the plaque. Thus, calcification may be a biological attempt to alleviate stress concentrations near the surface of the plaque cap (Glagov et al. 1997).

Inflammatory Cells. Inflammatory cells, such as macrophages, T-lymphocytes, and mast cells, are another important component of plaque. While these cells do not contribute directly to the structural integrity of the plaque, they do play a critical role in the regulation of structural components. Inflammatory cells can ingest lipid to form foam cells, regulate ECM turnover through the release of MMPs, and induce SMC apoptosis. The presence of inflammatory cells and markers has been correlated positively with incidence of plaque rupture. In fact, inflammatory cells, especially macrophages, are often found in high concentrations at the immediate site of plaque rupture (van der Wal et

al. 1994). Therefore, inflammation is considered an important feature of vulnerable plaque.

Endothelial Cells. While the endothelium is not in itself a load bearing entity, it is essential to plaque stability. The endothelial layer acts as a buffer, separating the underlying plaque from the blood stream. When this layer is disrupted or denuded, thrombosis and myocardial infarction can occur, even without actual plaque rupture (Davies 2001). Also, the endothelial cells release mediators that interact with the SMCs and inflammatory cells, and are involved in the recruitment of monocytes into the arterial wall.

STAGES OF PLAQUE PROGRESSION

In order to describe the process of plaque progression, the American Heart Association has classified atherosclerotic lesions into 8 categories based on their composition and structure. Extensive discussion of this classification scheme can be found in three papers (Stary et al 1992, Stary et al 1994, Stary et al 1995), and updated in a fourth paper (Stary et al 2000). These classifications are useful in understanding the path of progression that lesions may take. The categories are briefly summarized here, and illustrated in Figure 1.1.

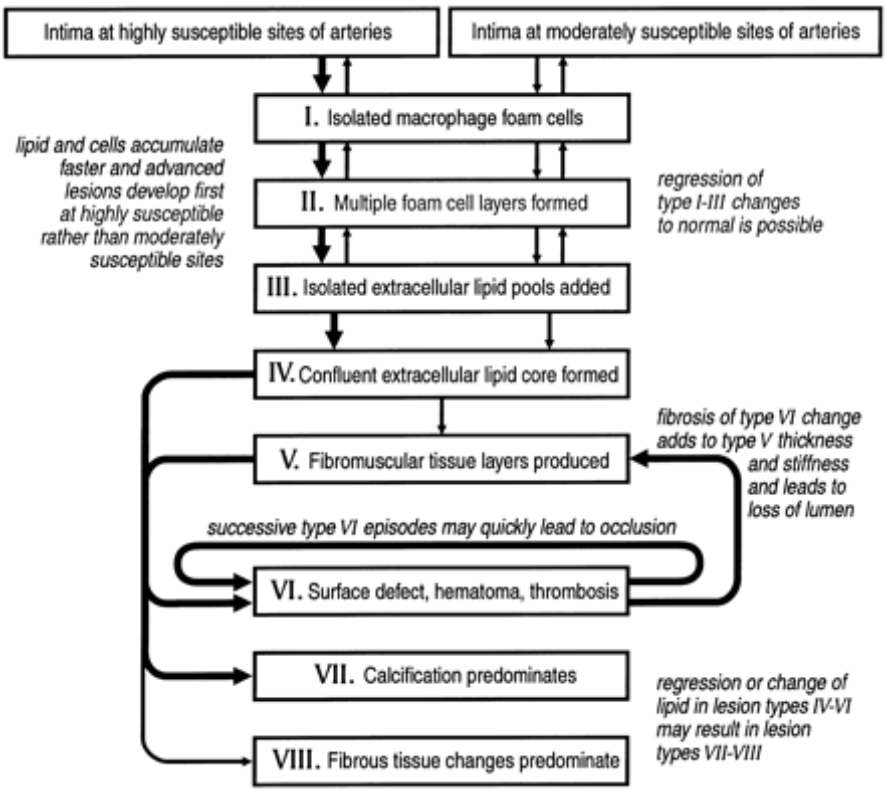

Figure 1.1 Stages of Plaque Progression (Stary et al. 2000)

Adaptive Intimal Thickening

Adaptive thickening of the intima occurs in arteries as early as the first week of life. It is a normal physiologic process that occurs in response to changes in the mechanical environment of the artery, including changes in shear and/or wall tension, and is not considered part of the atherosclerotic process. However, it is mentioned here because advanced atherosclerotic lesions do tend to form preferentially in regions that previously showed intimal thickening, particularly when the thickening was eccentric.

The thickened intima is comprised primarily of SMCs, extracellular matrix, and endothelial cells. Isolated macrophages may be present, but lipid deposits are absent. Intimal thickening does not block the lumen.

Type I Lesions

Type I lesions are identified by the first accumulations of lipid droplets, which are confined mainly to isolated groups of macrophages. These lesions are clinically silent, and may be found beginning in infancy.

Type II lesions

Type II lesions are also known as "fatty streaks," and begin developing in the coronary arteries around puberty. In these lesions, foam cells increase in number and form stratified layers. In addition, lipid droplets may be found in smooth muscle cells as well as macrophages. Still, most lipid is contained intracellularly, with very little extracellular lipid. Mechanical forces applied to the vessel wall and lumen surface are thought to be responsible for the increased influx and accumulation of lipid.

Type II lesions are subdivided into "progression-prone" lesions and "non-progression prone" lesions. Type II progression-prone lesions typically have more intimal SMCs, and foam cell layers are found deeper within the intimal layer than progression-resistant lesions. Why these types of lesions are more progression prone than others remains unknown, but it is thought that mechanical forces acting on the vessel may dictate whether the lesion is progression-prone or progression resistant (Stary et al 1994).

Type III lesions

Some type II lesions may stay in this stage for a long period of time, while others may progress more quickly to type III lesions. Type III lesions are considered the bridge between the clinically silent type II lesions, and the more advanced and dangerous type IV – type VI lesions.

The characteristic feature of type III lesions is the formation of small pools of extracellular lipid among the layers of smooth muscle cells. In addition, SMCs show increased expression of type I and type III interstitial collagen, but there are minimal changes in the ECM composition and intimal structure. There is no significant change in elastin content, and the internal elastic lamina remains intact. In addition, the media adjacent to the lumen is not diseased.

Type IV lesions

Type IV lesions are characterized by extensive, dense accumulations of extracellular lipid. These lesions have a true "lipid core" and "plaque cap." The lipid core is thought to form from the coalescence of the smaller isolated lipid pools of type III plaque. The plaque cap is composed primarily of proteoglycans and smooth muscle cells. The dense fibrotic tissue found in more advanced plaque has not yet formed. Smooth muscle cells of the intima are more dispersed. Also, calcium particles are sometimes found within the lipid core.

These lesions typically do not obstruct the lumen, so they are difficult to detect in vivo. However, because of the large lipid core and potentially thin fibrous cap, they are vulnerable to rupture and may therefore be quite dangerous.

Type V lesions

Like type IV lesions, these plaques are characterized by large lipid pools. In addition, they are also characterized by the deposition of fibrous tissue, particularly in the fibrous cap and in regions where the large lipid accumulations have disrupted the normal

arterial structure. They show a substantial increase in interstitial collagen. These arteries are typically more stenotic than type IV plaque, and are also vulnerable to rupture.

Some type V lesions may consist of multiple irregular layers of lipid cores, separated by thick fibrotic tissue. These layers may be the result of previous rupture and healing events. In addition, it is thought that the layers of lipid cores could be the result of changes in mechanical forces due to narrowing and asymmetry of the lumen caused by the morphological changes of the vessel wall. These morphological changes may alter the mechanical forces exerted on the wall such that the areas that are susceptible to lesion development change dynamically as the lesion progresses (Stary et al 1995).

Type VI lesions

Type VI lesions are ruptured plaque. These plaques show disruption of the lumen surface, hematoma or hemorrhage, and thrombosis. Typically, they are type IV or type V plaques that have undergone a rupture event. These are the plaques that are responsible for most cases of unstable angina and myocardial infarction.

Type VII lesions

The morphology of type VII lesions is dominated by calcification, with or without the presence of a lipid pool. Like type V plaque, they often have increased fibrous tissue. While lipid pools may still be present, it is thought that calcification is deposited to replace the lipid core.

Type VIII lesions

These lesions are characterized by the presence of extensive fibrous tissue with minimal or no lipid. These lesions could result from resorption of the lipid core,

remodeling of a previously formed thrombus, or may be extensions of adjacent atheromatous plaque. These lesions are not vulnerable to rupture, but may present clinically if the lumen is extensively obstructed.

VULNERABLE PLAQUE AND THEORIES OF PLAQUE RUPTURE

Those affected by atherosclerosis typically have a large number of plaques throughout their arterial tree. Some plaques remain in the early phases of plaque progression for decades. Others progress to form highly calcified and stenotic plaque, but these plaques typically do not rupture. Only a few plaque will actually progress to the point of rupture (Stary 1995).

It is currently unknown why some plaque progress to rupture, while many others do not. It is known that plaques that are prone to rupture share several common characteristics. First of all, they typically have large lipid pools, covered by thin fibrous caps depleted of smooth muscle cells. They are frequently large, eccentric plaque with significant positive remodeling, so that the lumen area is not significantly encroached. They also tend to have greatly increased levels of inflammatory cells and markers, especially in the plaque cap and shoulder region. Furthermore, the shoulder region of vulnerable plaque has been characterized by increased neovascularization (Schroeder and Falk 1995, Gronholdt et al. 1998, Shah 2003).

While several theories have been proposed to explain the occurrence of plaque rupture, including vessel injury due to turbulent flow (Loree et al. 1991), rupture of the vasa vasorum (Barger and Beeuwkes 1990), fatigue (McCord 1992, Bank et al. 2000, Versluis et al. 2006), and more recently, stress-induced debonding around small calcification deposits in the plaque cap (Vengrenyuk et al 2006), the currently held

theory is that rupture is due to a combination of two factors: 1) disregulation of the extracellular matrix (Lee and Libby 1997, Shah 2003), and 2) stress concentrations in and around the fibrous cap (Glagov et al. 1997, Golledge et al. 2000). As a plaque progresses, several factors, including inflammatory infiltration and apoptosis of SMCs, are thought to bring about a shift from ECM production to ECM degradation, causing thinning and eroding of the fibrous cap (Libby et al. 1996). As the fibrous cap thins and the lipid core increases in size, mechanical stresses within the plaque may be redistributed and concentrated in the fibrous cap, making the plaque more vulnerable to rupture. Because of this, understanding the interactions between the mechanical environment and biological activity of plaque is critical to understanding the pathology of plaque rupture.

MECHANICAL STRESSES IN PLAQUE RUPTURE

The current theory of plaque rupture is that rupture is a combination of mechanical stress concentrations within the cap and shoulder region of plaque, coupled with disregulation of the ECM. Blood vessels are not static entities, but are constantly changing and adapting in response to various stimuli such as mechanical stress and strain (Glagov et al. 1997). Remodeling due to changes in the mechanical environment occurs in healthy vessels, as well as in all stages of atherosclerosis (Glagov et al. 1997). Normal vessels adapt to changes in shear and tensile stress to maintain wall stability and adequate perfusion of nutrients and oxygen. Positive remodeling in diseased vessels is thought to be an attempt by the vessel to preserve luminal area by maintaining shear stress levels on the vessel wall at normal physiologic levels. Also, diseased vessels are thought to deposit and degrade ECM in an attempt to maintain wall tensile stress at normal physiologic

levels (Lehoux et al. 2006). In addition, cultured endothelial cells, SMCs and macrophages have all been found to respond to their mechanical environment in vitro by proliferating and/or releasing matrix metalloproteinases, which degrade ECM (Katsuda and Kaji 2003). This is especially significant since the disregulation of ECM, along with concentration of stresses in the plaque cap and shoulder regions, is thought to be responsible for plaque rupture. Therefore, understanding the mechanical environment is vital to understanding the atherosclerotic disease process.

Because atherosclerotic plaques are heterogeneous and have very complex geometries, most mechanical analyses of plaque have utilized the finite element method. This method is ideal for modeling diseased vessels because it breaks very complex geometries into a set of geometrically simple subdomains. Then, with the input of material properties and boundary conditions, an approximate stress solution can be solved for over the subdomains (Reddy 1993).

Mechanical Behavior of Plaque

While some work has been done to investigate the material behavior and properties of plaque constituents, this remains one of the most uncertain components in the mechanical analysis of diseased arteries. The mechanical behavior of atherosclerotic tissue is very complex. Even healthy vessels are heterogeneous, anisotropic, nonlinear, viscoelastic (exhibiting creep, relaxation, and hysteresis), insensitive to strain rate, and incompressible if fluid exchange is ignored. Residual stresses and strains are present within the wall when all loads are removed. Furthermore, normal vessels exhibit different behavior depending on the activation state of SMCs (Vito and Dixon 2003). Understanding the mechanical environment of diseased tissue is made even more difficult

because plaques are extremely anisotropic, and generally have heterogeneous and disorganized structure and composition.

An extensive review of efforts to determine plaque material properties may be found in Salunke and Topoleski 1997. The first studies to experimentally investigate the mechanical behavior of plaque utilized strips of fibrous cap tissue dissected from the underlying plaque and artery. These strips were mechanically tested under radial compression (Lee et al. 1991, Lee et al. 1992) and circumferential tension (Loree et al. 1994). These studies found that the stiffness is quite variable due to the underlying histologic variation of the tissue specimens. In addition, Lendon et al tested ruptured and non-ruptured plaque caps in circumferential tension, and found that ruptured plaque show increased extensibility, decreased maximum stress at fracture, and increased macrophage content relative to non-ruptured plaque (Lendon et al. 1991, 1993). While these studies give insight into the mechanical behavior of plaque tissue, they have several limitations. Testing on isolated strips of tissue ignores the effects of interactions with surrounding tissue, and acquiring homogeneous strips of tissue is very difficult considering the extreme heterogeneity of plaque. In addition, all of these experiments used uniaxial loading, but blood vessels are loaded trixially in vivo. Therefore, it is difficult to draw more than general observations about the relative behavior of plaque tissues from these types of experiments.

Other studies avoided some of these problems by using whole atherosclerotic lesions. Beattie et al, in our laboratory, was the first to use whole diseased human aortic segments to study material properties of plaque constituents. She used biaxial mechanical testing, coupled with histology in a finite element model, to determine the bilinear elastic

isotropic properties of the four main structural constituents of plaque – media, fibrous plaque, lipid, and calcification. The material properties of the four constituents were characterized using a bilinear model with three parameters – initial modulus, break point, and modulus above the breakpoint (Beattie and Vito 1996, Beattie et al. 1998). While Beattie et al did not account for the directional properties in the material parameters, their use of whole human aortic segments avoided the limitations and uncertainties posed by the use of isolated tissue segments in previous studies.

Besides direct mechanical testing of tissue, another method that has been used more recently to assess plaque material properties is elastography based on intravascular ultrasound (IVUS) coupled with finite element analysis (Vonesh et al. 1997,Chandran et al. 2003, De Korte et al. 2000). Due to current limitations in IVUS imaging resolution, these studies have thus far yielded only relative strengths of materials, rather than numerical material property data. However, as the resolution of image modalities is improved, this method may allow more accurate determination of mechanical properties.

Finite Element Models and Plaque Rupture

Over the past twenty years, finite element models of diseased arteries have contributed much to our understanding of the mechanical factors influencing plaque rupture. Because of the complex mechanical behavior of plaque constituents, simplifications and assumptions about material properties must be made when performing a finite element analysis. Finite element analyses in the literature have utilized a variety of assumed material property models, including linear elastic isotropic (Vito et al. 1990, Lee et al. 1996, Saijo et al. 2001, Huang et al. 2001,Chau et al. 2004), bilinear isotropic (Beattie et al. 1998, Kilpatrick et al. 2001, Kilpatrick et al. 2002),

nonlinear isotropic (Keeny and Richardson 1987, Hayashi and Imai 1997,Li et al. 2005), and linear transversely isotropic (Loree et al. 1992, Cheng et al. 1993, Lee et al. 1993, Ohayon et al. 2001, Finet et al. 2004, Imoto et al. 2005, Baldewsing et al. 2004).

There are three main sources of plaque geometry for these models – idealized models, histologic sections, and geometries obtained from imaging modalities such as intravascular ultrasound, magnetic resonance imaging, and optical coherence tomography. Table 1.1 gives a summary of the advantages and disadvantages of each geometry source, along with the studies that have utilized each source. Idealized models are advantageous because they allow independent variation of geometrical parameters such as cap thickness, lipid pool, size, shape, and location. Also, use of symmetry in idealized models can make these models much less computationally intense. However, the relevance of results from these models is limited, because they do not necessarily reflect realistic plaque configurations. This problem can be avoided by the use of real plaque geometries obtained from histology or imaging. Mechanical analyses based

Table 1.1 Geometry Sources for Finite Element Models of Plaque

Geometry Source	Papers	Advantages	Disadvantages
Idealized Models	Keeny et al. 1987 Vito et al. 1990 Loree et al. 1992 Hayashi et al. 1997 Finet et al. 2004	Easy to obtain Allow independent variation of geometrical parameters	Not directly physiologically relevant
Histology	Cheng et al. 1993 Lee et al. 1996 Beattie et al. 1998 Saijo et al. 2001 Kilpatrick et al. 2001 Huang et al. 2001	Physiologically relavant High resolution Structural and cellular detail	Geometrical distortions introduced by processiong (fixation, imbedding, and sectioning)
Imaging (IVUS, MRI, OCT)	Lee et al. 1993 Ohayon et al. 2001 Baldewsing et al. 2004 Finet et al. 2004 Imoto et al. 2005 Tang et al. 2004 Li et al. 2005	Can be aquired in vivo Non-destructive No processing artifact	Low resolution Segmentation uncertainty Inability to differentiate structural and biological elements

on these realistic geometries offer more physiologically relevant information about the stress distribution of real vulnerable plaque. Imaging modalities such as intravascular ultrasound (IVUS), magnetic resonance imaging (MRI), and optical coherence tomography (OCT) are appealing because they are nondestructive, and offer the possibility of in vivo acquisition of plaque geometry, so that analyses could be performed on living patients. They also avoid artifacts and distortions introduced by histologic processing. However, current imaging techniques still offer poor resolution relative to that available from histologic sections, and there is still a great deal of uncertainty in the segmentation of the acquired images. For these reasons, histology is currently considered the gold standard for determining plaque geometry and constituents (Chau et al. 2004). Still, one must consider the effect of distortions and artifact when using this method. These effects can be limited by pressure fixation of tissue and the use of stiffer embedding medium such as methyl methacrylate, rather than paraffin and frozen sections, which are more susceptible to distortions (Lowder et al. 2006).

Finite element analyses have contributed many important findings to our understanding of plaque rupture. A summary of results of these studies is given in Table 1.2. One of the first findings of finite element studies was that mechanical stress is often increased at the immediate location of rupture. Cheng et al developed finite element models based on histologic specimens from patients who died from plaque rupture. They found that peak stress was significantly higher in plaques that had ruptured, relative to the control group, and that most ruptures occurred near a region of high stress, although not necessarily at the location of maximum stress (Cheng et al. 1993). Lee et al found similar results using geometries obtained by ex vivo pre-angioplasty IVUS imaging. They

Table 1.2 Summary of Important Findings of Finite Element Models of Plaque Rupture

Papers	Model Source	Results
Cheng et al 1993	Histology	Mechanical stress is increased at site of rupture
Lee et al 1993 Ohayon et al 2001 Huang et al 2001	IVUS images pre- and post-angioplasty	Rupture occurs at locations of high stress, but not necessarily highest stress Discrepancy attributed to local variations in mechanical strength due to heterogeneity of plaque
Keeny and Richardson 1987 Vito et al 1990 Lee et all 1992	Idealized models	Plaque cap thickness is dominant factor affecting peak stress. Lipid pool size and degree stenosis are less important
Beattie et al 1998	Histology	Mechanical stress distribution is highly dependent on the underlying plaque structure and composition
Imoto et al 2005	Ex vivo IVUS images of ruptured plaques	Critical cap thickness for rupture varies from 10 to 200 microns, depending on the underlying vessel geometry
Finet et al 2004	IVUS + idealized model	Reducing plaque cap thickness exponentially increases peak stress Reducing lipid core stiffness exponentially increases peak stress
Loree et al 1992	Idealized models	Peak stress is particularly sensitive to elastic modulus, and less sensitive to shear modulus and poisson's ratio
Li et al 2005	In vivo MRI	Increasing fibrous plaque stiffness relative to lipid pool stiffness increases maximum circumferential stress, while increasing fibrous stiffness in direct proportion to lipid stiffness had little effect on stress

compared high stress regions predicted by finite element analysis with the actual sight of rupture in post-angioplasty images, and found that in 14 of 17 cases, rupture occurred at a high stress region, although not necessarily at the location of highest stress. This discrepancy was attributed to local variations in mechanical strength due to the heterogeneous nature of plaque (Lee et al. 1993). Ohayon et al repeated this experiment using in vivo images, and found that rupture occurred at high stress regions in all four cases considered (Ohayon et al. 2001). In addition, Huang et al considered 10 ruptured and 10 non-ruptured human coronary plaque, modeled as isotropic, incompressible nonlinear materials, and found that maximum principle stress was greater in ruptured than in non-ruptured plaque (Huang et al. 2001).

Finite element analysis has also been used to identify the features of plaque that increase mechanical stresses and contribute to plaque rupture. Idealized models have been especially used for this purpose, because they allow easy variation of geometrical

parameters. Keeny et al developed one of the first idealized finite element models of plaque, and used it to investigate the effect of lipid and calcification on stress distributions. They used a plaque geometry consisting of 12 concentric layers with lipid or calcification inclusions, and used a step-wise linear approach to approximate the nonlinear behavior of the vessel wall. They found that stresses were concentrated in the plaque tissue overlying a lipid pool, but were relieved in tissue overlying a calcium deposit, suggesting that the presence of lipid increased vulnerability, while presence of calcium may stabilize plaque (Keeny and Richardson 1987). Vito et al represented the diseased vessel wall using two non-concentric circles with an arc of plaque on the thicker side, between the media and lumen. They then looked at the effect of changes in lumen radius, plaque size, and relative stiffness of plaque and media wall (Vito et al. 1990). Loree et al combined these two models, using a geometry consisting of two non-concentric circles with an arc of lipid inserted in the wall. They varied the plaque cap thickness, size of the lipid pool, and degree of stenosis. They found that, of the parameters varied, the plaque cap thickness was the dominant factor affecting peak stress, and thus plaque stability, while size of the lipid pool and degree of stenosis were less important (Lee et al. 1992). Hayashi et al developed idealized models that mimicked early and intermediate stages of fibrous plaque. One model considered plaque uniformly distributed on the vessel wall, while a second model considered plaque localized to one side of the wall. They used a nonlinear isotropic strain energy density function, fit to experimental data from tension tests on atherosclerotic plaque in cholesterol fed rabbits, to represent material properties of plaque tissue and healthy vessel wall. In the localized plaque model, they found that high stresses occurred in the media wall near the border of

the plaque. In the uniformly distributed plaque model, they found that stresses were highest at the luminal surface, and decreased toward the outer layers of the vessel wall (Hayashi and Imai 1997).

Models based on actual plaque geometries, either from histology or imaging, have also been used to study factors affecting plaque stability. Beattie et al used histology-based finite element analysis to show that mechanical stress distribution in plaque is highly dependent on the underlying plaque structure and composition (Beattie et al. 1998). In addition, they showed that replacing the lipid core with calcification lowered peak stress in the plaque cap, while replacing calcification with lipid greatly increased plaque cap stress (Kilpatrick et al. 2001).

Imoto et al used ex vivo IVUS images of ruptured human coronaries to look at the critical cap thickness for plaque rupture. While most finite element analyses have been based on circumferential cross-sections, their models looked at two dimensional axial slices through the vessel. Because lipid deposits could not be distinguished from fibrous tissue in the IVUS images with confidence, plaque were assumed fibrous. Then, an arc of lipid was artificially inserted in the vessel wall. By varying the proximity of the lipid pool to the lumen surface, the "critical thickness" for rupture was determined for each vessel, based on a fracture stress of 300 kPa (Huang et al. 2001). They found that the critical cap thickness varied from 10 to 200 microns, and was very dependent on the underlying geometry of the vessel (Imoto et al. 2005). Finet et al also used IVUS imaging to develop parametric models of plaque. The plaque cap thickness was varied by adjusting the size of the lipid core. From this analysis, they found that reducing the plaque cap thickness caused an exponential increase in peak stress (Finet et al. 2004).

In addition, finite element studies have also looked at the effect of constituent material properties on stress distributions. In their idealized model, Loree et al found that peak stress was particularly sensitive to the elastic modulus of plaque tissue, but less sensitive to shear modulus and Poisson's ratio (Loree et al. 1992). Finet et al found that reducing the lipid core stiffness caused an exponential increase in peak stress (Finet et al. 2004). Using images of human carotid arteries obtained from in vivo MRI, Li et al found that increasing the stiffness of fibrous plaque relative to the lipid pool stiffness increased the maximum circumferential stress, while increasing the stiffness of fibrous plaque and the lipid pool in direct proportion had little effect on stress (Li et al. 2005). These results show the importance of the mechanical strength of plaque components in determining stability. It also indicates that care should be taken in representing material properties of plaque constituents in mechanical models.

ECM REGULATION AND INFLAMMATION IN PLAQUE RUPTURE

While the mechanical environment is critical to plaque rupture, the biological environment is equally important. Atherosclerotic vessels are not static structural entities, but are biologically very active and are constantly changing (Lee 2000).

Extracellular Matrix Regulation

While many connective tissues appear dormant with little active ECM turnover, the synthesis and degradation processes in plaque are greatly accelerated due to the impetus of inflammation (Arroyo et al 1999). A balance between synthesis and degradation of ECM is critical to plaque stability. Excess synthesis without degradation causes a shift toward accumulation of ECM, leading to vessel stenosis. On the other

hand, a shift toward degradation leads to loss of ECM. Since ECM, and particularly fibrillar collagen, provides the mechanical strength of plaque, stability is decreased when ECM is lost (Rekhter 1999).

ECM turnover is regulated by complex biological interactions. These interactions affect ECM turnover in three main ways: (1) direct changes in collagen synthesis by smooth muscle cells, (2) indirect changes in ECM production through proliferation or apoptosis of SMCs, and (3) changes in degradation rates of ECM. Smooth muscle cells are the primary producers and organizers of extracellular matrix. Cytokines such as Transforming Growth Factor-beta (TGF-β) stimulate SMCs to synthesize collagen, while other cytokines such as interferon-gamma (IFN-γ) inhibit SMC collagen synthesis (Arroyo and Lee 1999). Factors such as Platelet Derived Growth Factor (PDGF) stimulate smooth muscle cell proliferation and subsequently increase collagen synthesis in plaque, while SMC apoptosis may be induced by factors such as Reactive Oxygen Species (ROS) and leads to a decrease in collagen production (Lee 2000). ECM turnover is also regulated by proteolytic enzymes such as matrix metalloproteinases (MMPs) and cathepsins that break down ECM and also stimulate other cells in the plaque to release additional proteolytic enzymes (Arroyo and Lee 1999). All of these mechanisms are regulated by the inflammatory response.

Inflammation

Inflammation in atherosclerotic plaque causes rapid acceleration of extracellular matrix turnover. Inflammatory cells release products that either stimulate or inhibit collagen synthesis, but are thought to be most important for their role in degrading collagen through release of proteolytic enzymes such as MMPs and Cathepsins (Lee

2000). While there are a vast number of inflammatory markers that participate in atherosclerosis, a few of particular interest with respect to plaque progression and plaque rupture are discussed here.

Macrophages. Macrophages are the most prominent inflammatory cell in atherosclerotic lesions. While SMCs are the primary cell type in fibrous plaque, macrophages have been found to outnumber even SMCs in highly atheromatous lesions (van der Wal et al. 1994b). They tend to localize in the vulnerable shoulder region and in the plaque cap, and are the predominant cell type at the immediate site of rupture in culprit lesions (van der Wal et al. 1994a, Carr et al. 1996, Pasterkamp et al. 1999, MacNeill et al. 2004). Concentrations of macrophages are greater in plaque of patients experiencing MI and unstable angina than in patients with stable angina (Davies et al. 1994, Moreno et al. 1994) and are greater in disrupted than in intact plaque (Felton et al. 1997). Lendon et al found that plaque caps that had ruptured had significantly more macrophages, as well as increased extensibility and decreased stress at fracture, compared to intact plaque caps (Lendon et al. 1991).

As the primary cell responsible for the inflammatory response, macrophages release a large number of biological agents, including cytokines, chemokines, growth factors, MMPs, Tissue Factor, and reactive oxygen species. They also interact with and stimulate SMCs, endothelial cells, and other inflammatory cells like T lymphocytes and mast cells (Takahashi et al. 2002).

Macrophages are involved in all stages of atherosclerotic progression. In atherogenesis, migration of macrophages into the vessel and their subsequent ingestion of oxidized LDL through scavenger receptors results in formation of foam cells and fatty

streaks (Nicholson et al. 2001). As plaque progresses, macrophage foam cell apoptosis and necrosis lead to formation of the necrotic lipid core (Libby et al. 1996). Macrophage release of tissue factor greatly increases the thrombogenic nature of the lipid core (Moreno et al. 1996). Later in plaque development, macrophages localize in the shoulder and fibrous cap. Clusters of macrophages found in and around microvessels in the shoulder region and base of plaque suggest that macrophages may enter these regions through the microvasculature (de Boer et al. 1999). Once they have infiltrated the shoulder, macrophages facilitate degradation of the ECM. They inhibit SMC growth and proliferation in the shoulder and cap, and also decrease SMC expression of procollagen (Halloran et al. 1997). Furthermore, they can release cytotoxic substances such as ROS that result in SMC apoptosis (Schroeder and Falk 1995,Boyle et al. 2003). More importantly, macrophages are capable of releasing proteolytic enzymes such as MMPs that can actively degrade all components of the ECM (Galis et al. 1994, Sukhova et al. 1999, Takahashi et al. 2002, Katsuda and Kaji 2003, Liu et al. 2006). Macrophages in atherosclerosis have been shown to secrete the matrix metalloproteinases MMP-1, MMP-2, MMP-3, MMP-7, MMP-8, MMP-9, and MMP-13, as well as tissue inhibitors of MMPs TIMP-1 and TIMP-2 (Galis et al. 1994, Nikkari et al. 1995, Sukhova et al. 1999, Takahashi et al. 2002, Katsuda and Kaji 2003, Yamamoto et al. 2003, Molloy et al. 2004). They also produce the cysteine proteases Cathepsin S, Cathepsin K, and Cathepsin L (Sukhova et al. 1998,Liu et al. 2006). All of these enzymes have been implicated in degradation of components of the ECM in atherosclerosis.

Recent advances in medical imaging indicate that it may be possible to detect macrophage concentrations in plaque in vivo. Optical coherence tomography (MacNeill

et al. 2004), near infrared spectrometry (Moreno et al. 2002), magnetic resonance imaging (Kooi et al. 2003), and thermal imaging (Casscells et al. 1996,Stefanadis et al. 1999) have all shown potential for detecting local distributions of macrophages, at least near the luminal surface. As these technologies advance, determination of macrophage distributions in lesions in vivo may allow clinical identification of unstable plaque.

Nuclear Factor – Kappa B (NF-κB). Nuclear Factor – kappa B (NF-κB) is a transcription factor that regulates over 150 genes involved in initiating and sustaining the body's inflammatory and immune responses (Kumar et al. 2004). Activated NF-κB has been detected in SMCs, macrophages, and endothelial cells of atherosclerotic lesions. Initiation of inflammatory signaling pathways by NF-κB has been implicated in all stages of atherosclerosis (Brand et al. 1996)..

NF-κB is normally present intracellularly, bound to its inhibitor IkB. A variety of stimuli, including vascular injury, oxidized LDL, advanced glycation end products (AGEs), microbial agents, cytokines such as TNF-α and IL-1, and T lymphocyte signaling, are capable of activating NF-κB by causing the release of IkB. Once activated, NF-κB moves into the nucleus of the cell where it controls gene transcription.

One important role of NF-κB is in regulating cell survival and cell death. In most cases, NF-κB is thought to have a pro-survival, anti-apoptotic effect. Its activation can lead to the production of several proteins that prevent programmed cell death (Escarcega 2007). However, in some situations it has been shown to increase a cell's sensitivity to apoptotic stimuli. Because of its role in cell survival and death, NF-κB is important not only in atherosclerosis, but in other pathologies such as cancer, neurodegenerative diseases, and acute lung injury (Dutta 2006).

In addition to regulating cell survival and cell death, NF-κB regulates genes encoding for inflammatory markers such as Tumor Necrosis Factor-alpha (TNF-α), interleukin-1 (IL-1), Macrophage Colony Stimulating Factor (M-CSF), Tissue Factor, and MMPs (Brand et al. 1996, Monaco and Paleolog 2004).

NF-κB activation can have varying results, and the signaling cascades and genes that are affected depend on the specific stimuli and type of cell in which NF-κB is acting. In atherogenesis, NF-κB activity can lead to the activation of endothelial cells and to monocyte recruitment. As the plaque progresses toward a more vulnerable state, NF-κB-controlled pathways may be involved in the expression of MMPs and tissue factor, which may lead to destabilization and thrombosis (Vincenti and Brinckerhoff 2002, Monaco and Paleolog 2004).

Matrix Metalloproteinases (MMPs). Matrix metalloproteinases (MMPs) are a family of proteolytic enzymes capable of breaking down all components of the ECM (Katsuda and Kaji 2003). MMPs play a vital role in physiologic behaviors such as wound healing and vascular remodeling, as well as in pathologic processes such as rheumatoid arthritis, periodontal disease, tumor metastases, aneurysms, and atherosclerosis (Ennis and Matrisian 1994,Loftus et al. 2002).

Although there are at least 20 different MMPs, each controlled by a different gene, 50-70% of the structure of these different MMPs are the same. Their structure consists of five domains. Each has a signaling domain which is critical for cellular release of the MMP into the ECM. The propeptide domain helps maintain the enzyme in inactive zymogen form. The catalytic domain binds to the zinc catalyst. There is also a hinge

domain that allows enzyme folding, and one other domain whose function is unknown (Loftus et al. 2002).

MMPs are classified based on the extracellular matrix components that they degrade. Collagenases, which are MMP-1, -8, -13, and -18, are of particular interest in atherosclerosis because they degrade fibrillar collagen type I and III, the main structural component of the fibrous cap. The gelatinases, MMP-2 and MMP-9, digest collagen fragments, basement membrane collagen, and elastin, while stromelysins, MMP-3, -10, -11, -19, and -20, are responsible for breaking down proteoglycans and glycoproteins (Galis et al. 1994, Sukhova et al. 1999, Ferrans 2002, Molloy et al. 2004).

MMP activity is very tightly controlled, both intracellularly and extracellularly. At the transcriptional level, expression of MMP is regulated by cytokines, hormones, and growth factors. Interleukin-1, platelet-derived growth factor, and tumor necrosis factor-alpha all have a stimulatory effect on MMP expression, while heparin, TGF-β, and corticosteroids act to inhibit expression (Ferrans 2002, Loftus et al. 2002). Once they have been synthesized, MMPs also require activation. This activation can be by means of plasmin, thrombin, furin, reactive oxygen species (Rajagopalan et al. 1996), other activated MMPs (Kaartinen et al. 1998), and by chymase and tryptase released by mast cells (Leskinen et al. 2003, Kaartinen et al. 1998). An additional level of control is exerted by tissue inhibitors of MMPs (TIMPs) which form inactive complexes with MMPs. MMPs and their inhibitors react in a 1:1 molar ratio, and their reaction is irreversible (Galis et al. 1994, Ferrans 2002, Katsuda and Kaji 2003). Therefore, MMPs are only capable of degrading the ECM when they have been activated and are in stochiometric excess over their inhibitors (Galis et al. 1994).

Some MMPs are produced endogenously in non-diseased vessels. However, atherosclerotic plaque show greatly increased expression of MMPs, probably due to the influence of inflammatory infiltration (Galis et al. 1994, Ennis and Matrisian 1994, Loftus et al. 2002). Galis et al found that SMCs in both normal and diseased arteries express MMP-2. However, in diseased vessels, SMCs as well as macrophages also produced MMP-1, MMP-3, MMP-8, and MMP-9 (Galis et al. 1994). Galis et al also showed that lipid-laden macrophages isolated from rabbit aortic lesions contained MMP-1 and MMP-3, while macrophages isolated from the lungs of the same animal did not (Galis et al. 1995). In addition, using a novel method of in situ zymography, they found that atherosclerotic tissue contained activated MMPs, while non-diseased tissue did not (Galis et al. 1994).

All major cell types within atherosclerotic plaque, including SMCs, macrophages, and ECs, are capable of participating in matrix breakdown by producing MMPs (Ferrans 2002,Herman et al. 2001). Horton et al showed that CD40 ligation of SMCs leads to loss of ECM by increasing SMC release of MMPs, while having no effect on SMC synthesis of ECM (Horton et al. 2001). Shah et al showed that macrophages do indeed break down fibrous caps via activity of MMPs. They placed fibrous caps in cultures of macrophages, with and without MMP inhibitors. Using levels of hydroxyproline released in the medium as a measure of collagen degradation, they found that collagen was degraded in the presence of macrophages when inhibitors were excluded, but that no degradation occurred in the presence of both macrophages and MMP inhibitors (Shah et al. 1995).

MMP-1 is of particular interest in plaque rupture, because it breaks down type I collagen – the primary structural collagen of plaque (Dollery et al. 2003). MMP-1 is

expressed much more strongly in symptomatic than in asymptomatic plaque (Guo et al. 2000, Dollery et al. 2003). Its expression has also been inversely correlated with the presence of disease-free media (Kilpatrick et al. 2002). In addition, intense expression of MMP-1 has been found to occur in a subset of macrophages in the fibrous cap and shoulder regions at the border of the lipid core (Nikkari et al. 1995, Galis et al. 1994, Dollery et al. 2003, Herman et al. 2001,Molloy et al. 2004).

Reactive Oxygen Species. Reactive oxygen species such as nitric oxide (NO), superoxide, and hydrogen peroxide are produced by cells during normal metabolic events, as well as in response to growth factors and cytokines (Rajagopalan et al. 1996). Under physiologic conditions, cells have antioxidant mechanisms to protect against their toxic effects. Under these circumstances, oxidants may even be beneficial. For example, NO in vascular tissue is required for vasodilation, and also helps protect against leukocyte adhesion and platelet aggregation. However, in atherosclerotic tissue, cytokines trigger expression of the inducible isoform of Nitric Oxide Synthase (iNOS), which can lead to a 100 fold increase in constitutive production of NO. This excessive production can cause oxidative stress – damage to cellular membranes, lipids, proteins, and DNA – within plaque tissue (Madamanchi et al. 2004). Excessive NO may also react with superoxide to form peroxynitrite, a substance which has been shown to enhance platelet adhesion and aggregation and alter protein structures (Depre et al. 1999). ROS are also responsible for oxidation of lipoproteins – one of the first steps in plaque formation (Berliner et al. 1995).

Reactive oxygen species are of interest in plaque rupture for several reasons. First of all, ROS production has been found to be significantly higher in patients experiencing

unstable angina and MI, compared with patients with stable angina, suggesting the ROS may modulate plaque stability (Madamanchi et al. 2004). Specifically, iNOS (inducible Nitric Oxide Synthase) expression by macrophages was increased in unstable patients but not in stable patients (Baker et al. 1999, Depre et al. 1999). Furthermore, ROS have been implicated in activation of MMPs and NF-κB (Davies 1998, Robbesyn et al. 2004), and may also induce macrophage and SMC apoptosis (Madamanchi et al. 2004).

Neovascularization. Neovascularization has been implicated as a potential contributor to plaque rupture. The presence of microvessels in the intima and media is a well-documented feature of advanced atherosclerotic lesions (Fleiner et al. 2004). Moreno et al found that the number of microvessels is increased in ruptured, compared with non-ruptured plaque. They also found that the presence of microvessels at the base of plaque correlates independently with plaque rupture (Moreno et al. 2004). Microvessel density is much greater in lipid-rich plaque than in fibrous plaque. Furthermore, neovascularization is particularly prominent in the vulnerable shoulder region, often asymmetrically, so that one shoulder may have many more blood vessels than the other (Jeziorska and Woolley 1999,de Boer et al. 1999).

Microvessels also contribute to plaque progression. Microvessel hemorrhaging within the lesion may cause sudden periods of plaque growth, contributing to lipid core expansion and inflammatory activation. In addition, Moulton et al showed that plaque progression was decreased by 70-80% in apoE deficient mice when angiogenesis was inhibited by administration of endostatins (Moulton et al. 2003).

The role of microvessels in atherosclerosis may be to supply nutrients to the plaque tissue as the vessel grows. However, they also promote inflammation by providing

a conduit for inflammatory cell infiltration (Jeziorska and Woolley 1999, Moreno et al. 2004, Moulton et al. 2003). Inflammatory cells – macrophages, T lymphocytes, and mast cells – are often clustered in and around microvessels (Jeziorska and Woolley 1999, de Boer et al. 1999,Kaartinen et al. 1996). In addition, since activated macrophages are capable of inducing angiogenesis, there may be a positive feedback loop involving neovascularization and inflammation. Microvessels assist in inflammatory cell recruitment. Inflammatory cells then stimulate angiogenesis, and in turn more inflammatory cells are recruited (Moulton et al. 2003).

LINKS BETWEEN MECHANICS AND INFLAMMATION

Almost all cells are subjected to mechanical deformation through contacts with surrounding ECM (Yang et al. 2000). Vascular cells, in particular, are constantly subjected to mechanical forces due to blood pressure and axial stretch. In atherosclerosis, these forces may be even greater due to the effects of high blood pressure and stress concentrations (Lehoux et al. 2006). Cells can convert mechanical stimuli to biochemical signals through numerous complex transduction pathways that may involve stretch-activated ion channels, mitogen-activated protein (MAP) kinases, integrins, tyrosine kinases, and growth factors (Lehoux and Tedgui 1998, Lehoux et al. 2006). These biochemical signals may then lead to a variety of cellular responses, including proliferation, apoptosis, and gene regulation (Aplin et al. 1998).

Because inflammation and mechanical stresses have both been noted to localize in the shoulder region of the plaque cap, it has been suggested that interactions between mechanical stress and inflammation may be responsible for plaque destabilization (Arroyo and Lee 1999). Mechanical stress may stimulate an inflammatory response

(Jiang et al. 1999), and this inflammatory response may then lead to matrix degradation and weakening and erosion of plaque cap and shoulder. This may cause further increases in mechanical stresses, leading to additional stimulation of the inflammatory response (Galis et al. 1994), and thus forming a positive feedback cycle that progresses the plaque toward destabilization and rupture.

Macrophages and Mechanics. The results of several studies have revealed that macrophages are mechanically sensitive cells. Martin et al used patch clamp studies to show that macrophages possess potassium ion channels that can be activated by stretching of the cell membrane (Martin et al. 1995). Furthermore, studies of cultured monocytes/macrophages exposed to physiologically relevant levels of cyclic stretch have shown that macrophages respond to deformation by changes in protein, gene, and receptor expression (Yang et al. 2000, Ohki et al. 2002,Yamamoto et al. 2003). Cyclic stretch of cultured macrophages selectively upregulates macrophage expression of MMPs (Yang et al. 2000, Yamamoto et al. 2003). This suggests that mechanical deformation may stimulate macrophages to participate in extracellular matrix degradation. Furthermore, immediate-early genes, which are involved in cell migration, proliferation, and differentiation, are also upregulated by mechanical stretch (Yang et al. 2000, Ohki et al. 2002,Yamamoto et al. 2003).). Particularly, Ohki et al found that the gene IEX-1, an NF-κB-inducible gene involved in NF-κB-mediated cell survival, was upregulated by biaxial stretch (Ohki et al. 2002). Cyclic stretch also induces upregulation and release of the inflammatory cytokine IL-8, which has chemotactic activity for other inflammatory cells including neutrophils and T-lymphocytes (Ohki et al. 2002,Yamamoto et al. 2003). In addition, Sakamoto et al found that mRNA and protein for Class A scavenger receptor

(SRA) – a receptor involved in macrophage uptake of lipoproteins - was induced by biaxial stretch in an amplitude dependent manner (Sakamoto et al. 2001). These results show that macrophages are capable of responding to their mechanical environment.

Macrophages have also been associated with loss of mechanical strength in the plaque cap. Lendon et al looked at the relationship between macrophage density and the mechanical strength of the plaque cap, and found that ruptured plaque had increased macrophage densities, as well as increased extensibility and decreased maximum stress at fracture. This suggests that macrophages decrease the mechanical strength of the plaque cap (Lendon et al. 1991).

Mechanical deformation may also stimulate macrophage infiltration of high stress regions. Jiang et al showed that cyclic strain of smooth muscle cells in culture caused expression of mRNA for monocyte-chemotactic protein-1 (MCP-1) – a protein that facilitates monocyte migration into tissue (Jiang et al. 1999). This suggests that macrophages may infiltrate high stress regions such as the shoulder and fibrous cap as a result of SMC response to their mechanical environment.

Thus far, few attempts have been made to determine whether macrophages spatially correlate with increased mechanical stress. Lee et al did attempt this, and found no statistically significant correlation. However, the mechanical models used in this study were based on geometries from non-pressure fixed, paraffin embedded vessels. The presence of significant geometrical artifact could have affected the spatial distribution of stress. In addition, the spatial correlation was limited to comparison of 8 large sectors. The lack of spatial resolution could have masked a possible relationship (Lee et al. 1996).

MMPs and Mechanics. Plaque destabilization may also be promoted by interaction between mechanical stress and MMP expression. MMPs break down the ECM and thin the fibrous cap, potentially raising stresses in the cap and increasing vulnerability (Galis et al. 1994,Libby et al. 1996). In additional, studies have shown that mechanical deformation induces selective release of MMPs by macrophages (Yang et al. 2000, Yamamoto et al. 2003, Yang et al. 2000) and SMCs (James et al. 1993).

Furthermore, a study by Lee et al has suggested that MMP-1 expression colocalizes with regions of increased mechanical stress. In this study, they divided histologic cross-sections of plaque into 8 sectors. For each sector, they determined the MMP-1-positive stained area fraction, as well as the peak circumferential stress. They found significant correlation between MMP-1expression and peak stress (Lee et al. 1996).

NF-κB and Mechanics. While the direct effect of mechanical stress on NF-κB activation in human diseased vessels has not been determined, some studies have shown that NF-κB may be activated in vascular cells in response to mechanical deformation. Cell culture studies have shown that pulsatile stretch can activate NF-κB in vascular smooth muscle cells (Hishikawa et al. 1997, Lehoux et al. 2006). Also, induction of NF-κB pathways has been noted in cultured endothelial cells exposed to shear stress (Lehoux et al. 2006). Lamarie et al used an organ culture system to mimic in vivo mechanical conditions in whole carotid arteries of mice, and found that high intraluminal pressure induced NF-κB activation (Lemarie et al. 2003). The effect of this activation is controversial. While NF-κB activates pro-inflammatory genes, it also activates anti-apoptotic genes, and thus may help protect vascular cells against apoptosis in high stress conditions (Lemarie et al.

2003, Lehoux et al. 2006). All of these things make NF-κB an interesting target in investigating the interactions between mechanical stress and inflammation in atherosclerotic plaque.

Reactive Oxygen Species and Mechanics. ROS production in atherosclerotic plaque may be enhanced by mechanical deformation and vascular injury (Madamanchi et al. 2004). Several studies have shown that superoxide production by vascular smooth muscle cells is increased in response to pulsatile stretch, and that it is increased in a time and amplitude dependent manner (Hishikawa et al. 1997,Harrison et al. 2006, Grote et al. 2003). This cyclic stretch-induced production of ROS by vascular cells is thought to contribute to NF-κB activation, MMP activation, activation of MAP kinase signaling pathways, and angiogenesis (Harrison et al. 2006, Grote et al. 2003).

Neovascularization and Mechanics. Little is known about the direct role of mechanics in the formation of plaque microvessels. However, it is known that the mechanical environment is generally an important stimulus in angiogenesis (Ingber 2002). Endothelial cells (ECs), the cells responsible for microvessel formation, receive both chemical and mechanical cues from their local environment. In angiogenesis, they respond to these cues through proliferation, differentiation, migration, and apoptosis, to form capillaries. (Ingber 2002, Eliceiri and Cheresh 1999). Ingber suggests that local thinning of the ECM, and subsequent ECM extension due to mechanical loading, subjects ECs to tension through their ECM adhesion receptors (Ingber 2002). Indeed, integrins, the primary cell-matrix adhesion receptors, have been shown to be critical to angiogenesis (Eliceiri and Cheresh 1999). These cellular and cytoskeletal distortions direct capillary formation by causing ECs to switch between growth, differentiation,

apoptosis, and motility (Ingber 2002). The fact that local thinning and stretching of the ECM is involved in microvessel formation also suggests a possible mechanism for vessel localization in the shoulder region, where ECM remodeling occurs due to localized MMP release.

Furthermore, a study by Joung et al looked at angiogenesis in 3D collagen gel constructs seeded with endothelial cells. They mimicked blood-pressure-induced cyclic stretch, and looked at tubulogenesis by vascular ECs. Their results showed that cyclic strain causes endothelial-cord-like structures to form and align perpendicular to the principle axis of stretch (Joung et al. 2006).

LIMITATIONS OF EXISTING STUDIES

Limited Heterogeneity. Limited attempts have been made in existing finite element models of atherosclerotic plaque to account for the heterogeneous nature of atherosclerotic plaque. Plaque is heterogeneous in both composition and organization, and variations in the biochemical nature and spatial orientation of plaque tissue influence the mechanical strength of plaque (Burleigh et al. 1992). The variability of plaque material properties has been noted by several researchers (Loree et al. 1994,Holzapfel et al. 2004).

Most current mechanical models divide plaque into broad discrete regions of fibrous, healthy, lipid, and calcified tissue, and assume homogeneity within these regions (Beattie et al. 1998, Huang et al. 2001, Finet et al. 2004, Li et al. 2005). However, in real plaque transitions between constituents are more gradual rather than distinct, and there is considerable intermixing of constituents. Failure to account for this intermixing may

cause the strength of some regions to be falsely represented. Also, representing plaque constituents as distinct regions may introduce unrealistic stress discontinuities and concentrations due to interfaces between materials with greatly differing material properties. While current models provide useful information about features contributing to plaque instability, it has been suggested that more realistic representations of plaque heterogeneity accounting for intermixing and gradual transitions between constituents are needed if plaque mechanics is to be related to biological markers such as inflammation (Beattie et al. 1998).

Histologic Distortions. For accurate and meaningful stress results, it is essential that finite element models be based on geometries that approximate the in vivo state as closely as possible. Because of the lack of resolution currently provided by imaging modalities, histology is still the gold standard for obtaining geometries of diseased vessels for finite element analysis. Histologic processing requires that the artery be removed from the body, imbedded in a cutting medium, and cut into thin sections. When the artery is removed from its supporting tissue and pressurization in vivo, the tissue shrinks and the vessel may collapse. Therefore, it is essential that pressure fixation of the artery is carried out at near physiologic pressure, in order to eliminate these distortions and maintain the vessel in a state that is closer to in vivo (Stary 1992). In addition, histological processing introduces distortions to the plaque geometry that can affect the stress distribution predicted by the model. The use of stiffer embedding media such as methyl methacrylate can be used to minimize sectioning distortions (Lowder et al. 2006). However, most histology-based finite element models to date have not used pressure-

fixed tissue, and have utilized frozen or paraffin embedded sections, which are more susceptible to sectioning distortions due to their lack of rigidity.

Spatial Immunohistochemical Quantification. Immunohistochemistry is a useful method for detecting the presence of inflammatory markers in situ. Most previous studies have used semi-quantitative methods to assess staining. One common approach is to grade each cross-section as either negative, mildly positive, or heavy positive staining (Pasterkamp et al. 1999,Moreno et al. 2002). More quantitative approaches have included measuring the stained area fraction (Nikkari et al. 1995,Moreno et al. 1994) or counting positively stained cells (Meuwissen et al. 2003) over the entire cross-sections. Mauriello et al quantified positive immunostaining by cell-counting in non-contiguous sample fields in regions of interest (Mauriello 2005). However, none of these methods quantify the *spatial* distribution of staining. Lee et al included a degree of spatial quantification by dividing the cross-section into eight sectors, and determining the stained area fraction for each sector (Lee et al. 1996). However, the resolution of this method is very low, and improved quantification methods are needed in order to allow spatial correlation of immunostaining with distributions of other plaque characteristics such as mechanical stress.

Analysis of a Single Location within Plaque. Studies of 2D cross-sections to date have compared either random or pre-selected cross-sections taken from arteries of many individuals. However, a range of disease states from completely healthy to extremely diseased may sometimes be found within a single vessel. Therefore, by considering many sites along the length of a single vessel, it may be possible to find plaque in different stages of development all within a vessel from a single patient. Comparing vessel cross-

sections in variable disease states but from the same patient could provide information about the progression of plaque to instability, while eliminating external factors such as age, sex, and patient health history. Also, by considering sections at locations along the length of the plaque, rather than at a single location, one may be able to determine whether trends being investigated are systemic factors or factors specific to plaque at certain disease states.

CHAPTER 2

HYPOTHESIS AND SPECIFIC AIMS

Mechanical stress and inflammation have been shown to localize in the shoulder and fibrous cap of atherosclerotic plaque. It is well known that cells respond to their mechanical environment. Part of this response may include induction or upregulation of an inflammatory response. However, few studies have attempted to correlate spatial distributions of inflammatory markers and increased mechanical stress in plaque. Previous studies have been limited by the difficulty of accurately quantifying inflammatory marker distributions in histologic cross-sections, in part due to insufficient imaging capabilities. Furthermore, most finite element models to date have not adequately accounted for the heterogeneous nature of plaque constituents. In addition, most finite element studies have looked at a single location within a plaque – typically selecting the most diseased section. However, analysis along the length of plaque may shed light on the progression of plaque toward instability. The overall objective of this study was to determine whether spatial relationships exist between mechanical stress and markers of inflammation in human coronary atherosclerotic plaque, and to determine whether these relationships depend on the state of plaque progression. To this end, improved methods for quantifying the spatial distribution of inflammation and for mechanically modeling the heterogeneity of plaque were developed.

HYPOTHESIS

Spatial relationships exist between inflammatory markers and the local mechanical environment in human atherosclerotic plaque. These spatial relationships are plaque progression dependent.

SPECIFIC AIMS

1) **Develop a heterogeneous 2D finite element model of diseased human coronary plaque based on histology.**

   The objective of this aim was to generate mechanical models that more accurately predict the stress distribution in cross-sections of atherosclerotic plaque relative to previous homogeneous models. Mechanical models of coronary plaque were developed using fresh human right coronary arteries that were pressure fixed at physiologically relevant levels in order to maintain the geometry in a configuration close to in vivo, and imbedded in MMA to minimize histologic distortions. Intermixing of constituents was accounted for by using a semi-automatic segmentation approach to segment the image into four constituents (media, fibrous plaque, calcium, and lipid) pixel-by-pixel. For each element of the finite element mesh, a rule of mixtures for constant strain was used to determine the effective Young's modulus from the Young's modulus and area fraction of each constituent.

2) **Use histologic sections of diseased human coronary arteries to quantify the spatial distribution of inflammatory markers important in plaque rupture.**

The objective of this aim was to develop a technique for high-resolution quantification of the spatial distribution of inflammatory markers in cross-sections of atherosclerotic plaque. The developed technique was designed in a way that would facilitate comparisons with other spatially quantified entities such as mechanical stress. Briefly, inflammatory markers of interest were identified by immunohistochemistry, and high resolution images were obtained. The same mesh used for finite element analysis of the cross-section was then overlaid on the immunostained image, dividing the section into very small regions. Cell-counting or area fraction measurements were used to quantify the presence of inflammatory markers in each grid element.

3) **Correlate the spatial distribution of inflammatory markers and stress measures in 2D cross sections along the length of a plaque.**

The first objective of this aim was to determine whether a spatial relationship exists between the mechanical environment and inflammation in atherosclerotic plaque. The spatial distributions of markers of inflammation and of mechanical stress were determined using serial histologic sections taken at regular intervals along the length of human right coronary arteries. Selected markers included macrophages, MMP-1, NF-κB, nitrotyrosine, and neovascularization. Various statistical methods were applied to compare these spatial distributions to determine whether a relationship exists.

The second objective of this aim was to determine whether relationships between the mechanical environment and inflammatory markers are dependent upon the stage of plaque progression. Cross-sections were categorized into four categories based on their state of disease progression, and the spatial relationship between mechanical stress and strain and each inflammatory marker was determined for each disease category. These spatial relationships were then compared to determine whether there were differences between the disease categories.

CHAPTER 3

MATERIALS AND METHODS

VESSEL ACQUISITION AND FIXATION

Eight explanted human right coronary arteries (RCA) were obtained from cardiac transplant patients at Emory University. All arteries were obtained from male patients 49 ± 8 years (minimum age: 43, maximum age: 62) with no known diabetes. Additional medical histories and medications at time of transplant for each patient can be found in Appendix A.1. RCA segments approximately 3 cm in length (typically 2-6 mm in diameter) were excised from the heart and stored in PBS on ice for transport to our laboratory within 2-4 hours of removal from the patient. The arteries were pressure-fixed in 10% buffered formalin at 80mmHg for two hours. Pressure fixation is critical in order to maintain the artery in a geometric configuration that is close to in vivo. A pressure of 80 mmHg was selected based on the average diastolic pressure in humans. After pressure fixation, the arteries remained in formalin for a total of 36 hours. Initial experiments showed that this fixation time provided sufficient cross-linking to maintain vessel morphology during histologic processing, without blocking immunohistochemical access to antigens. After fixation, arteries were stored in 70% alcohol at 4°C.

Justification of pressure fixation time. A study performed in our lab using a pig carotid artery under pressure fixation showed that during the first hour of pressure fixation, the artery diameter changed by 3.1% with respect to the final diameter (Figure 3.1). In the

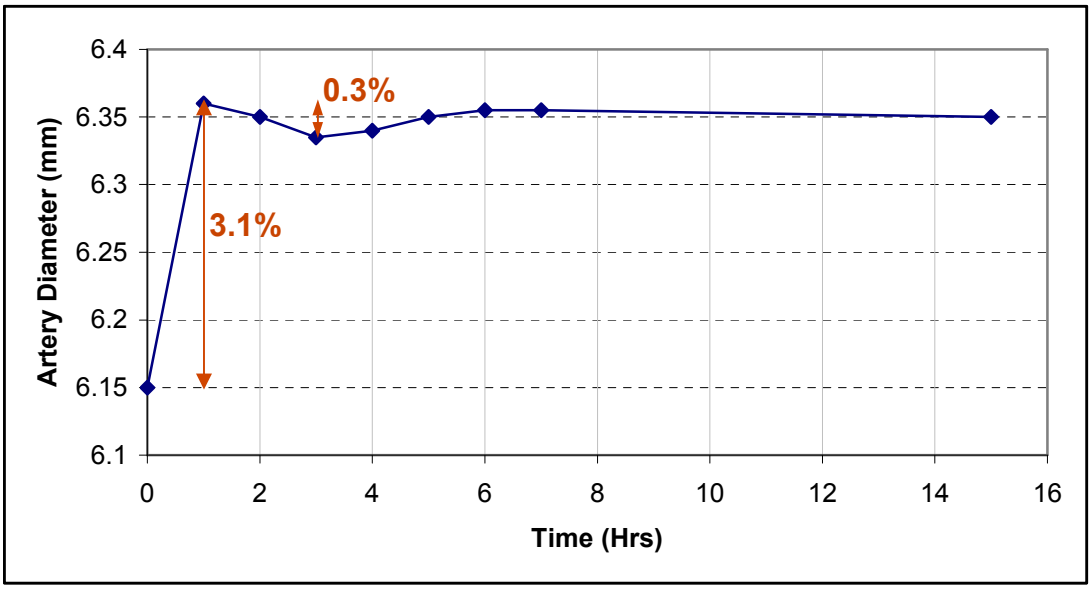

Figure 3.1 Pig carotid artery diameter change over time under 80mmHg formalin pressure fixation

following hours, the total change in artery diameter was 0.3% (Carnell 2006). Therefore, two hours of pressure fixation was deemed adequate to maintain the artery in a configuration close to in vivo.

HISTOLOGIC PROCESSING

MMA Embedding

Arteries were embedded in methyl methacrylate (MMA) resin. This embedding medium was selected over standard paraffin because it significantly reduces geometric distortions introduced during histologic processing (Lowder et al. 2006) and was chosen over alternative resinous embedding media because MMA can be removed before staining, thus allowing better access to tissue antigens during immunohistochemistry. In addition, MMA provides improved sectioning of calcified tissue, so that decalcification of arteries before imbedding was not necessary.

Before embedding, the arteries were dehydrated in graded alcohol and cleared with xylene using a Thermo Shandon Pathcenter (Thermo Electron Corporation, Pittsburgh, PA). They were then infiltrated with in a solution consisting of 75% (v/v) methyl methacrylate (Acros Organics, Morris Plains, NJ), 25% (v/v) dibutyl phthalate (Aldrich Chemical Company, Inc., Milwaukee, WI), and 5% (w/v) benzoyl peroxide (Sigma-Aldrich, Inc. St. Louis, MO). The arteries were embedded in acrylic blocks, consisting of 74.1% (v/v) methyl methacrylate, 24.7% dibutyl phthalate (v/v), 5% (w/v) benzoyl peroxide, and 1.2% (v/v) N,N-dimethyl-*p*-toluidine. The entire embedding protocol is given in Appendix B.

Due to damage to the ends of the arteries from cannulization during pressure fixation, approximately 0.5 cm of tissue was eliminated from each end of the artery before embedding. Therefore, approximately 2 cm of arterial segments were embedded in MMA. However, to achieve even thickness during sectioning, specimen blocks should ideally be no more than 1.5 cm in length. When specimen blocks are too long, the torque exerted on the specimen block can lead to deformation of the block. These changes are small, but because the sections being collected are already very thin, these changes can result in uneven sectioning. Particularly, a pattern of alternating thick and thin sections is seen when blocks exceed 1.5 cm in length. Therefore, to maintain uniform section thickness, embedded blocks were cut to approximately 1.5 cm in length.

Sectioning Along the Axial Length

Histologic sections with a thickness of 3 μm were cut using a retractable rotary microtome (Microm, Walldorf, GE). Sections were floated on a 50°C water bath to remove wrinkles introduced by cutting. They were then collected on slides coated with

poly-L-lysine to aid adherence. To further insure adherence of the sections to the slide, slides were clamped in a slide press and placed in an oven overnight at 50°C.

Sections were collected along the length of the artery as follows: At 1mm intervals along the length of the vessel, multiple serial sections were collected. A total of 12-24 sections were collected for each interval. The distance between the first and last section collected at each interval was no more than 100 microns (Figure 3.2) Over this region (~0.33% of total vessel length) axial variation in microstructure is assumed to be small, so that all sections collected within that interval can be assumed to represent the same artery cross-section. Two sections were collected per slide, for a total of 12 slides per interval. For each interval, the slide containing the two middle sections was stained for morphology, while the remaining slides were used to identify inflammatory markers.

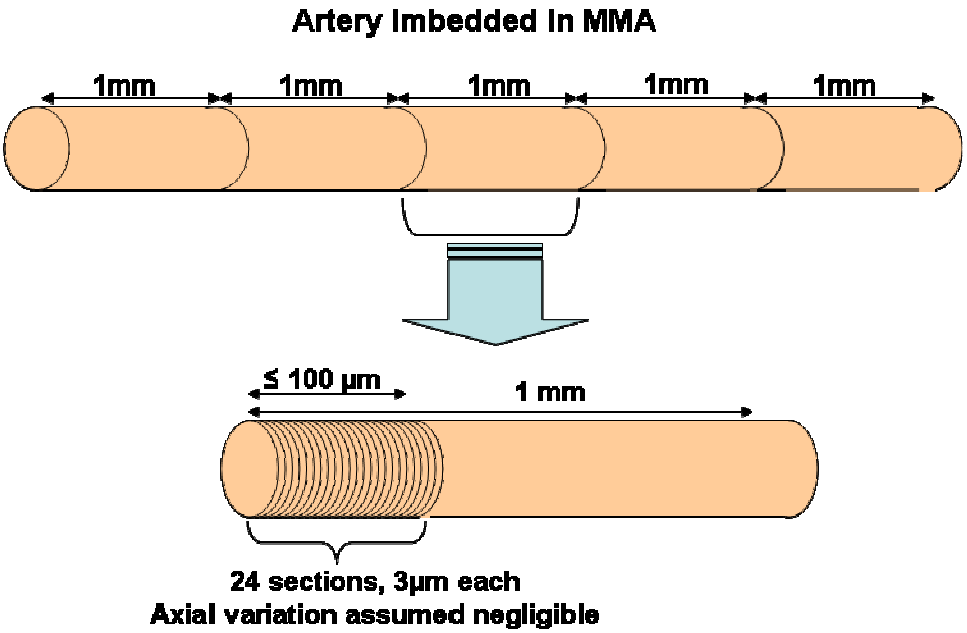

Figure 3.2 Schematic of protocol for collecting sections along the length of the artery

Staining

Morphological Staining. For each interval along the length of the artery, the middle histologic section was routinely stained with Masson's Trichrome and von Kossa's calcium stain to identify plaque constituents. The histologic protocols followed for these stains may be found in Appendix B. A representative morphologically stained cross-section is shown in Figure 3.3. Smooth muscle cells are stained red, collagen is stained blue, calcification is stained brown or black, and lipid is left unstained.

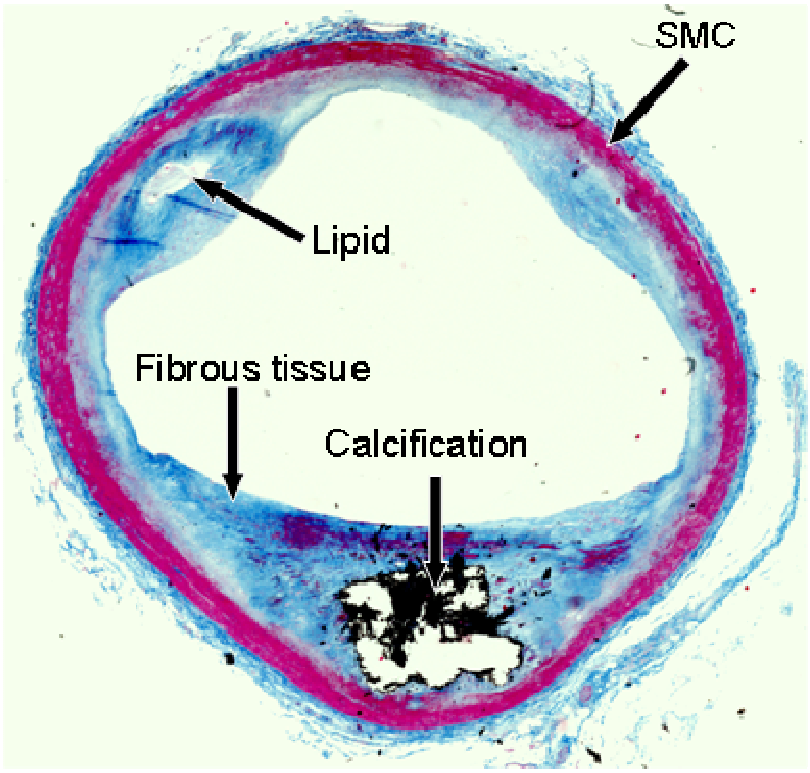

Figure 3.3 Representative image of cross-sections stained with Masson's Trichrome and von Kossa's calcium stain.

Immunohistochemistry. For each interval along the length of the artery, the remaining sections were used to identify inflammatory markers of interest by immunohistochemical

staining. Standard immunohistochemistry protocol was used, and is given in Appendix B. The markers that were studied are macrophages, MMP-1, activated NF-κB, reactive oxygen species (ROS) activity (detected by nitrotyrosine), and neovascularization. These markers were selected because, as discussed earlier, they each play an important role in atherosclerosis and plaque rupture, and each may interact with their mechanical environment. These markers may potentially respond to the mechanical stimuli, or they may act to affect changes in their mechanical environment.

The antibodies used to detect each marker, along with their working dilution, are given in Table 3.1. For some antibodies, antigen retrieval methods were needed to improve the quality of the signal, as suggested by the antibody provider. Any pretreatments used are also listed in Table 3.1. Standard pretreatment protocols were used, and can be found in Appendix B.

Figure 3.4 shows a region of serial cross-sections stained for macrophages, NF-κB, MMP-1, and nitrotyrosine. Figure 3.5 shows a different region of the same cross-section stained for microvessels. Macrophages, MMP-1, and activated NF-κB were detected using anti-HAM56 (DakoCytomation, Fort Collins, CO), anti-MMP-1 (EMD Biosciences, Darmstadt, Germany) and anti- NF-κB p65 subunit (Temecula, CA) antibodies, respectively. Reactive oxygen species activity was detected using an antibody against nitrotyrosine (Upstate Cell Signaling Solutions, Charlottesville, VA). Nitrotyrosine is formed in the presence of nitric oxide, and is a stable end-product of peroxynitrite oxidation. The presence of nitrotyrosine in the vessel wall indicates reactive oxygen species activity (Onorato et al. 1998). Neovascularization was detected by staining for endothelial cells using the lectin ULEX Europaeus Agglutinin 1 (Vector

Table 3.1 Immunohistochemical Antibodies and Pretreatments

Marker	Primary Antibody (Dilution)	Primary Source	Secondary Antibody	Pretreatment
Macrophages	Mouse anti-HAM56 (1:50)	DakoCytomation	horse anti-mouse IgM	proteinase K
MMP-1	Mouse anti-MMP-1 (1:200)	CalBioChem	horse anti-mouse IgG	citrate in pressure cooker
NF-kB	Mouse anti-NFkB p65 subunit (1:75)	Chemicon International	horse anti-mouse IgG	citrate in pressure cooker
Nitrotyrosine (ROS)	Rabbit anti-nitrotyrosine (1:2000)	Upstate Cell Signalling Solutions	goat anti-rabbit IgG	None
Endothelial Cells (Microvessels)	Biotinylated UAE1 (1:100)	Vector Labs	None	None

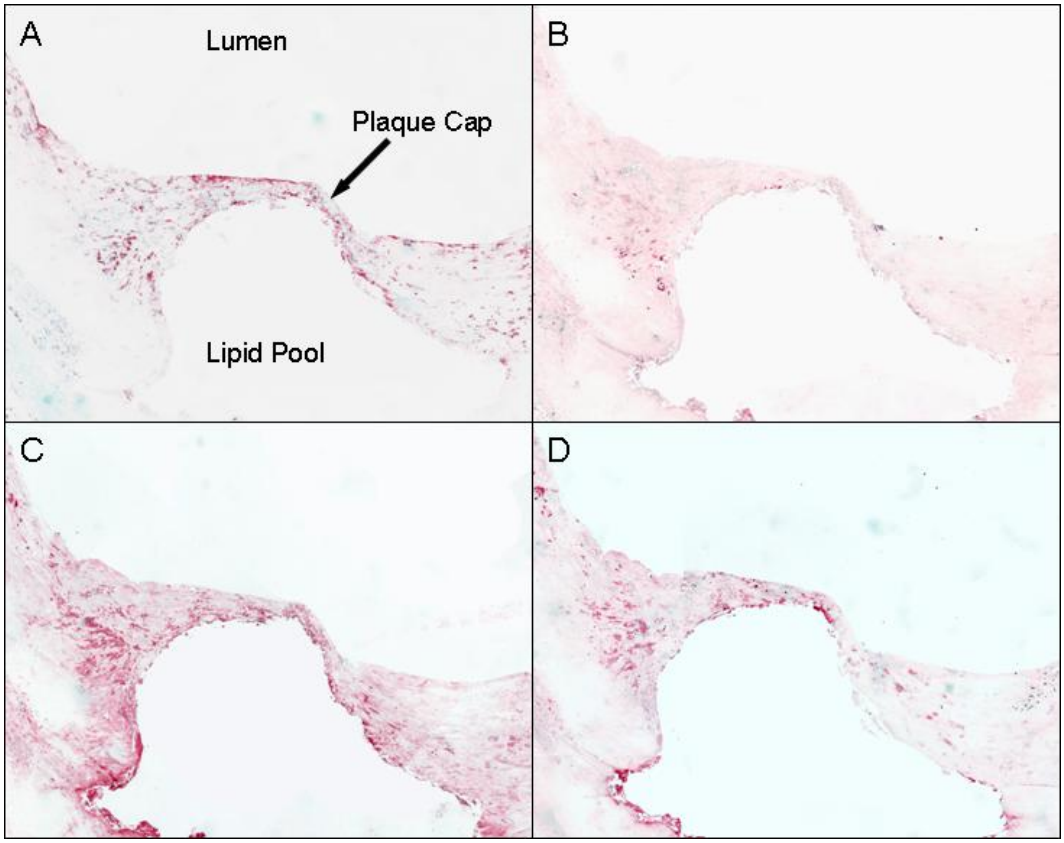

Figure 3.4 The shoulder and fibrous cap region of a cross-section stained for macrophages (A), NF-κB (B), MMP-1 (C), and nitrotyrosine (D).

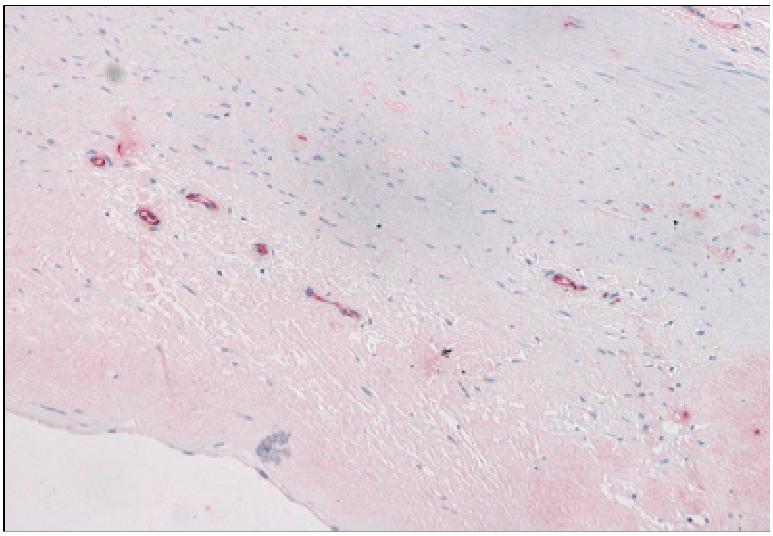

Figure 3.5 Positive staining for microvessels within the arterial wall.

Laboratories, Burlingame, CA). Circular patterns of endothelial cells within the vessel wall indicate microvessels.

For each marker, arterial tissue previously found to stain positively for that marker was used as a positive control. Many serial sections were collected from the positive control specimen. A positive control section was then included in each staining session. Because the positive controls were serial sections from the same tissue, they stained similarly from session to session. Thus, visual comparison of the positive control to a reference positive control during staining was used to reduce variability in staining intensity from session to session. Also, these positive controls were used to standardize the staining segmentation process, as discussed later.

IMAGE ACQUISITION

After Masson's and von Kossa's staining, images of the morphologically stained cross-section were captured using a Super CoolScan 9000ED slide scanner (Nikon Instruments, Tokyo, Japan) at a resolution of ~ 6 μm/pixel. This resolution is sufficient

for carrying out constituent segmentation, while still allowing the cross-section to be captured in a single frame. A representative cross-section captured in this way is shown in Figure 3.3 above.

After immunohistochemical staining, images of the immunostained cross-sections were captured at 4X magnification using a Nikon Eclipse E800 microscope with a motorized stage (Ludl, Ltd. Hawthorne, NY). Images of a representative cross-section captured in this way are shown in Figure 3.4 above. This magnification, which has a resolution of ~1.8 μm/pixel, was chosen because it provides sufficient resolution for quantification of markers, while keeping file sizes small. When needed, higher magnification images of specific regions were captured for reference during marker quantification.

IMAGE ALIGNMENT

For each interval along the length of the artery, there were six images representing the same cross-section: one stained for morphology, and one stained for each of the five inflammatory markers. In order to compare spatial data from these cross-sections, images must have the same orientation. Because the central section was stained for morphology, and all immunohistochemically stained sections were collected within ± 50 μm of this section, the morphologically stained image was used as a reference, and all immunohistochemically stained images were aligned with respect to this image. The alignment was performed in Amira 3.1 (TGS Inc., San Diego, CA) by manually aligning two images so that Amira's image similarity measurement was maximized.

Alignment Errors. Accurate alignment is important when comparing spatial data from two images. To determine the accuracy of this alignment method, the alignment error was

estimated as follows: Using pairs of aligned images, the inner and outer vessel wall boundaries were traced. This segmentation process introduces an additional segmentation error; however, this error can be determined independently. Next, masks containing the pixels inside the vessel wall were generated for each image. The number of non-overlapping pixels was determined by subtracting these masks. The alignment + segmentation error was calculated by dividing the number of non-overlapping pixels by the total number of pixels in the wall of the reference image. This error was found to be 5.8 ± 2.8% (n=7). The error due to segmentation alone was then determined by measuring the total number of pixels within the vessel wall for each mask. For each pair, the segmentation error is the difference in the total number of pixels between the two masks. As a percentage of total pixels in the wall, this segmentation error was found to be 2.2 ± 2.0% (n=7). Therefore, the total alignment error is estimated as 3.6 %.

In addition, the error in alignment was also estimated by determining the distance between corresponding points in pairs of aligned images. For perfect alignment, the distance should be zero. The locations of five corresponding points were determined in each of five cross-sections, for a total of 25 points. The mean distance between corresponding points was 12.3 ± 6.7 pixels, or 74 ± 40 μm.

SPECIFIC AIM 1: MECHANICAL MODELING

Because it is not possible to measures stresses in the vessel wall or to solve for them analytically, a finite element mechanical model was developed to replace the real problem with a mathematical representation that is solvable. Although it is desirable to mimic the real problem as closely as possible when developing a model, it is also necessary to balance the level of complexity included in the model with the ability to

obtain a solution to the mathematical equations. Assumptions and simplifications must be made in order to account for available information and to reduce the problem to one that is mathematically solvable.

There are four steps in development of a mechanical model: 1) modeling of the geometry, 2) modeling of mechanical properties, 3) modeling of boundary and loading conditions, and 4) modeling of the deformation process. Once the model has been developed, the equations of equilibrium and equations of motion can be solved to determine the parameters of interest.

Modeling of Vessel Geometry

Two-dimensional geometries were obtained from morphologically stained images of each vessel cross-section. As discussed previously, because the arteries were pressure fixed and embedded in MMA, distortions were limited and the geometries obtained closely represent the in vivo vessel geometries.

By modeling the arteries as 2D, we make the assumption that geometrical variations in the axial direction are small. For most cases, this is a good assumption. However, we are aware that there may be instances in which this assumption is not true.

Cross-Section Boundary Determination and Meshing. For each interval along the length of the artery, inner and outer boundaries of the plaque cross-section were determined from the morphologically stained image using a segmentation tool in Amira. This tool uses image gradients to fill in the boundary between manually selected points. The inner and outer boundaries were then imported into the commercially available finite element

software Ansys 7.0 (Ansys, Inc., Canonsburg, PA) and the entire area was meshed. Shape warnings were set within Ansys so that no elements had an aspect ratio greater than 1:4 or angles smaller than 65°. The ANSYS code used to generating the mesh is included in Appendix C.

In order to aid in the comparison of stress and inflammation distributions, the finite element mesh was used not only for determining stresses, but also for quantifying inflammatory marker spatial distributions in the cross-section. For each element in the mesh, von Mises stress, as well as inflammatory content, was determined, as discussed later. In order to compare these values, the elements must be large enough to account for alignment errors between the morphologically and immunohistochemically stained sections. However, the elements must be small enough to provide adequate information about the spatial distribution in the cross-section. Therefore, mesh parameters were set so that the characteristic element dimension was approximately 200 microns – significantly larger than the typical misalignment distance of 75 microns, but small enough to retain spatial resolution. This mesh will be referred to as the "coarse" mesh.

Because more accurate finite element stress solutions can be obtained by increasing mesh density, a finer mesh was generated from this coarse mesh before the finite element solution was obtained. The refinement was done in such a way that each element in the coarse mesh corresponds to a subset of elements in the fine mesh. Computing power is now such that a very fine mesh can be used over the whole cross-section. Therefore, it was not necessary to refine the mesh in specific areas of the cross-section.

Segmentation of Plaque Microstructure. For each interval along the length of the artery, the microstructure of the plaque cross-section was obtained from the morphologically stained image. Each artery was treated as a constrained mixture of four homogeneous materials – media, fibrous plaque, lipid, and calcium. To account for the heterogeneous intermixing of plaque constituents, rather than dividing the cross-section into distinct constituent regions, a semi-automatic segmentation approach was used to assign each pixel to one of the four materials based on image RGB values. Representative sections were used to "train" the algorithm as follows: for each constituent, regions clearly consisting of only that constituent were selected. Then, the average RGB values over the selected regions were determined for each constituent.

$(R,B,G)_{media}$

$(\overline{R},\overline{G},\overline{B})_{fibrous}$

$(\overline{R},\overline{G},\overline{B})_{calcium}$

$(\overline{R},\overline{G},\overline{B})_{lipid}$

} Average RGB values from representative regions

Once the average constituent RGB values were known, a minimum distance approach was used to assign each pixel to a constituent (Deng et al 1999). For the i^{th} pixel, the geometric distance between its RGB value and the average RBG value of each constituent will be calculated:

$$d^{i}_{media} = \sqrt{(R_{media} - R_i)^2 + (G_{media} - G_i)^2 + (B_{media} - B_i)^2} \qquad \text{Eq 3.1}$$

$$d^{i}_{fibrous} = \sqrt{\left(R_{fibrous} - R_i\right)^2 + \left(G_{fibrous} - G_i\right)^2 + \left(B_{fibrous} - B_i\right)^2} \quad \text{Eq 3.2}$$

$$d^{i}_{lipid} = \sqrt{\left(R_{lipid} - R_i\right)^2 + \left(G_{lipid} - G_i\right)^2 + \left(B_{lipid} - B_i\right)^2} \quad \text{Eq 3.3}$$

$$d^{i}_{calcium} = \sqrt{\left(R_{calcium} - R_i\right)^2 + \left(G_{calcium} - G_i\right)^2 + \left(B_{calcium} - B_i\right)^2} \quad \text{Eq 3.4}$$

The segmentation of plaque microstructure is illustrated in Figure 3.6 for a representative cross-section. Figure 3.6A shows the cross-section stained for morphology. Figure 3.6B shows the cross-section after semi-automatic segmentation into four constituents – healthy, fibrous, calcification, and lipid – on a pixel-by-pixel basis.

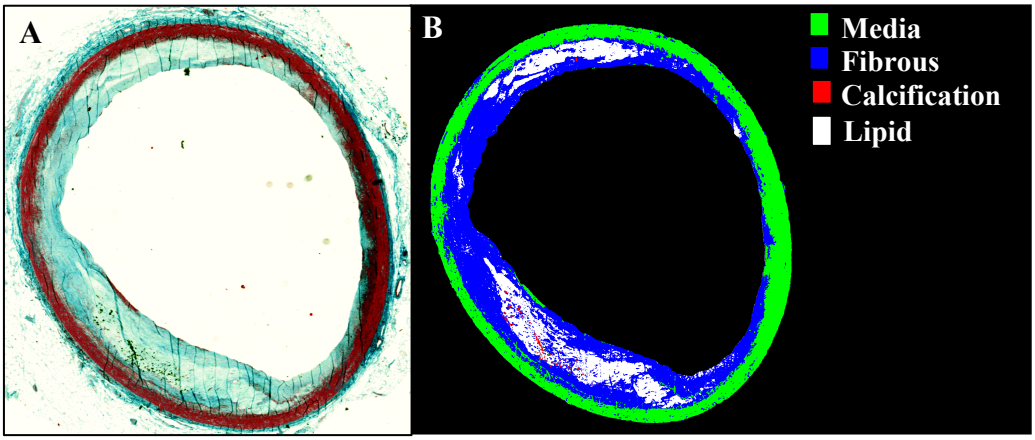

Figure 3.6 Representative cross-section stained for morphology (A), and segmented into four plaque constituents (B)

Modeling of Mechanical Properties

Modeling of mechanical properties involves selection of the appropriate constitutive equations to mathematically represent the mechanical behavior of the arterial tissue. In selecting these constitutive equations, it was necessary to make several assumptions. First of all, because the extreme heterogeneity of plaque precluded the use

of transversely isotropic or orthotropic properties, and anisotropic material properties for plaque constituents were unavailable, all tissue was assumed to behave isotropically.

In addition, because biological tissue is comprised of about 70% water, which is incompressible at physiologic pressure, blood vessels can be modeled as incompressible (Fung 1993). However, the finite element algorithms used in this work cannot tolerate incompressible materials when plane strain is assumed. Thus, in order to allow solution of the finite element equations, the materials were modeled as *nearly* incompressible, with Poisson's ratio of 0.49.

Furthermore, while blood vessels possess non-linear material properties, most non-linear deformation occurs at low pressures (Beattie et al 1996). Therefore, the constituents were modeled as linear elastic solids over the physiologic pressure range (greater than 80 mmHg), and the magnitudes of elastic moduli were taken from the physiologic pressure range of the bilinear properties measured by Beattie et al. As discussed previously, accurate material properties of plaque constituents are difficult to obtain, and there is a great deal of uncertainty in the measured values in the literature. For this work, the material properties measured by Beattie et al (1996) were selected over other measurements of constituent material properties because they were measured using intact human aortic plaque under biaxial loading. While there is uncertainty in the selection of material properties, previous finite element work has shown that stress distributions in plaque are relatively insensitive to small changes in the absolute values of constituent material properties (Williamson 2003). Stress distributions have also been shown to be insensitive to orders of magnitude changes in constituent properties when each constituent's properties are changed in direct proportion. However, they are

sensitive to changes in relative orders of magnitude of constituent material properties (Lee 1992, Kilpatrick 2001, Li 2005)

Using a bilinear elastic mechanical model, Beattie et al found that most nonlinear deformation occurs below 40 mmHg, and that the mechanical behavior of each constituent could be described well using a linear elastic model for pressures above 40 mmHg. Because the arteries in this study were fixed at 80 mmHg, the Young's moduli measured by Beattie et al were considered appropriate. These values are given in Table 3.2.

Table 3.2 Young's Moduli of Plaque Constituents

Constituent	E (kPa)
Media	6.15×10^2
Fibrous Plaque	4.83×10^3
Lipid	3.80×10^1
Calcification	4.00×10^4

Arteries were treated as constrained mixtures of four homogeneous materials – media, fibrous plaque, lipid, and calcification. In mixture theory, a differential volume is characterized by the co-existence of the homogenized constituents (Humphrey and Rajagopal 2002). For this differential volume dV, the mass density of the i^{th} constituent in that volume is:

$$\rho^i = \frac{dm^i}{dV} \qquad \text{Eq 3.5}$$

so that the average mass density of the mixture volume is

$$\rho = \sum \rho^i \qquad \text{Eq 3.6}$$

The mass fraction for the i^{th} constituent, ϕ^i, is defined as

$$\phi^i = \frac{\rho^i}{\rho} \qquad \text{Eq 3.7}$$

Thus,

$$\sum \phi^i = 1.$$

In a *constrained* mixture, each constituent has the same displacement and velocity as that of the mixture, and there is no exchange of momentum between constituents. In this case, the Cauchy stress, T_{xx}, is given by

$$T_{xy} = \sum \phi^i T^i_{xy} \qquad \text{Eq 3.8}$$

where T^i_{xx} is the Cauchy stress for the i^{th} constituent. It was assumed that under no-load conditions, all constituents within an element have compatible zero-stress states, so that there were no residual stresses present. Therefore, within an element, all constituents experience the same strain. So for the uniaxial case for linear isotropic materials:

$$T_{xx} = E_{eff}\varepsilon_{xx} = \sum \Phi^i E^i \varepsilon_{xx} \qquad \text{Eq 3.9}$$

If the densities of materials are comparable, then the mass fraction ϕ^i is equivalent to the volume fraction V^i. For the two dimensional case where materials are isotropic and

incompressible, the volume fraction V^i is equal to the area fraction A^i. Thus, the effective Young's modulus is:

$$E_{eff} = \sum \phi^i E^i \approx \sum A^i E^i \qquad \text{Eq 3.10}$$

Using this rule-of-mixtures, material properties were assigned to each element of the finite element mesh. The refined finite element mesh was overlaid on the segmented image. For each mesh element, the area fraction of each constituent was calculated. For the i^{th} element, the effective Young's modulus was determined from the Young's moduli and the area fractions of each constituent:

$$E^i_{eff} = E_{fibr} A^i_{fibr} + E_{media} A^i_{media} + E_{lipid} A^i_{lipid} + E_{calc} A^i_{calc} \qquad \text{Eq 3.11}$$

where $\boldsymbol{E}$ is Young's modulus and $\boldsymbol{A}$ is area fraction.

This process of material property assignment is illustrated in Figure 3.7 for the same segmented cross-section shown in Figure 3.6 above. Figure 3.7A shows the finite element mesh overlaid on the segmented image. Figure 3.7B shows material properties of each element, as determined using the rule-of-mixtures.

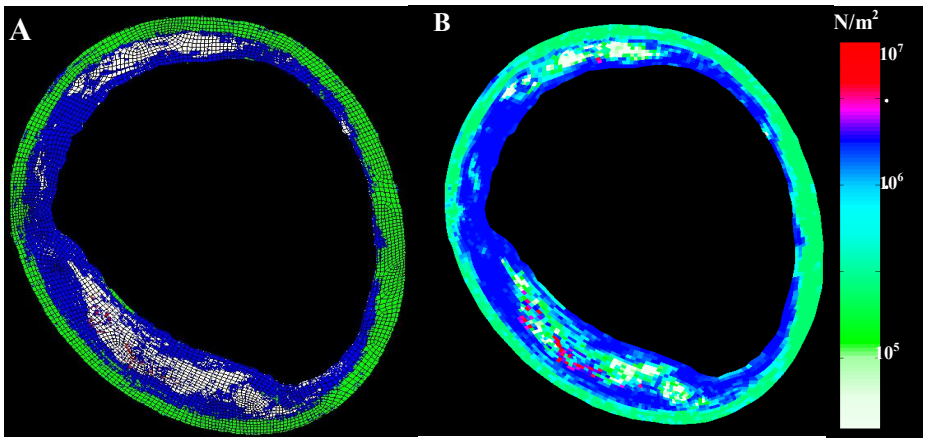

Figure 3.7 Refined FE mesh overlaid on segmented image (A). Map of element material properties

Modeling of Boundary Conditions, Loading Conditions, and the Deformation Process

Model geometries were obtained from cross-sections of arteries pressure fixed at the typical diastolic pressure of 80 mmHg. In order to simulate typical systolic blood pressure, an incremental pressure of 40 mmHg was applied as a static pressure on the lumen surface. Because the model geometries were obtained from pressure-fixed arteries, the deformation process was considered as a superposition of a relatively small deformation from the deformed state due to the additional pressure increase of 40 mmHg on a large deformation from the no-load state due to the transmural fixation pressure of 80 mmHg, as illustrated in Figure 3.8. Since Beattie et al found that arterial constituents are bilinear with a breakpoint around 40 mmHg, the fixation pressure of 80mmHg is well above the breakpoint. Therefore, deformation above this point can be considered linear.

Due to the deformation from the undeformed to the deformed state, a pre-stress (σ^*) exists in the deformed state. According to Rachev et al (2000), the final stress due to

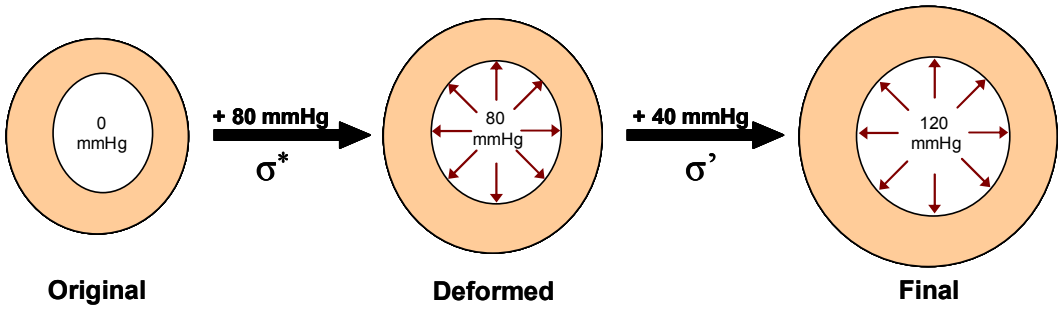

Figure 3.8. The deformation process was considered as a superposition of a small deformation on a finite deformation.

the superposition of a small deformation on a finite deformation is given by:

$$\sigma = (E + 2\sigma^*)\varepsilon \qquad \text{Eq 3.12}$$

Because the Young's modulus of each constituent is much greater than the stresses generated in the wall at 80mmHg ($E >> \sigma^*$), the pre-stress was neglected, so that the pressure-fixed configuration was considered stress free.

The stress field determined by this method does not represent the true absolute values of stress that exist at 120 mmHg. However, because the strains are small (<1%) and the mechanical response is linear, the stress field generated by the model provides reliable information on the *relative* spatial distribution of stress.

The deformation process was considered quasi-static, as is accepted in the field of vascular biomechanics (Humphrey 2002), and thus inertial effects due to the pulsatile nature of blood pressure are small and were ignored. Flow-induced shear stress acting on the luminal surface was also neglected, since its effect is small relative to the stresses generated within the wall. The effects of axial stretch may be substantial, but because no

information on axial stretch of these vessels was available to us, the effects of axial stretch were not included in our analysis. Because we are focused on the *relative* spatial distributions of stress, we believe that ignoring axial stretch will not affect the conclusions of this study. Also, external forces due to heart movement or tethering to the surrounding tissue were assumed small relative to blood pressure and were ignored. In addition, displacement constraints were applied within the finite element model to prohibit rigid body motion.

It should be noted that arteries in this study showed only moderate stenosis. If severe stenosis had been present, then the loading conditions would be much more complex due to pressure drop across the stenosis and possible negative pressure downstream of the stenosis.

Finite Element Stress Solution

Four-node plane strain elements were used to solve for the distribution of stress and strain. Plane strain is valid if geometrical variations in the axial direction are small. A large deformation, geometrically non-linear solution was used to account for possibility of large strain values.

The stress solution obtained provided von Mises stress and strain values for each element in the fine mesh. von Mises stress was selected because it gives an appreciation of the overall magnitude of the stress tensor. In order to compare stress and strain distributions with inflammatory marker distributions, stress and strain measures were calculated for the coarse mesh. Because each element in the coarse mesh corresponds to a subset of elements in the fine mesh, stresses and strains for the coarse mesh were determined using an area-weighted average of the elemental solution for the fine-mesh.

Figure 3.9 shows the von Mises stress distributions using the fine mesh (A) and coarse mesh (B) for a representative cross-section.

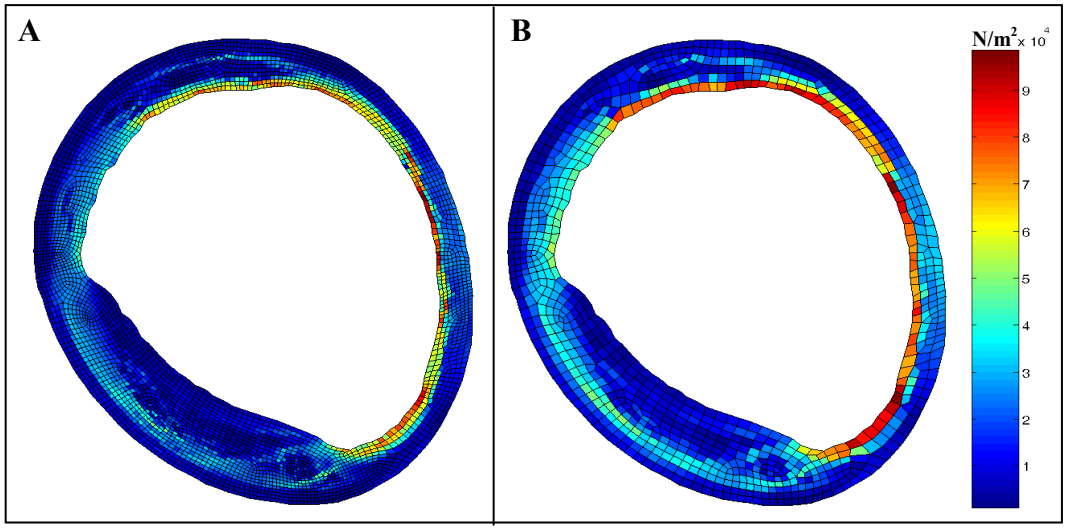

Figure 3.9 von Mises stress solution for representative cross-section – fine mesh (A), coarse mesh (B)

Element Selection for Statistical Analysis

For this work, we were interested primarily in the response of cells embedded in the extracellular matrix of the media and fibrous plaque to forces exerted on them due to their contacts with the ECM. Calcified regions of the artery are accellular, and few cells are present in lipid pools. For this reason, elements consisting of only lipid, only calcification, or a mixture of only lipid and calcification were excluded from statistical analyses.

SPECIFIC AIM 2: QUANTIFICATION OF INFLAMMATORY MARKER DISTRIBUTIONS

Marker Selection

While there are a vast number of inflammatory markers that play a role in atherosclerosis, for practical reasons it was necessary to narrow the list considered in this study to only a few markers. As mentioned above, the selected markers were macrophages, activated NF-κB, MMP-1, nitrotyrosine, and microvessels. Four criteria were used in selecting these markers from the long list of possible inflammatory markers:

1. *There are indications that that the marker plays a role in atherosclerosis and plaque rupture.*

   All five of the markers studied here have previously been detected in atherosclerotic plaque, as discussed in Chapter 1.

   Macrophages are found in large numbers in atherosclerotic plaque, and have been noted to be particularly prevalent in the plaque shoulder and fibrous cap, where rupture most often occurs. Macrophages also release a plethora of other inflammatory markers, including MMPs.

   MMP-1 is expressed in both macrophages and smooth muscle cells in the vessel wall, and has also been found to be highly expressed in the shoulder and fibrous cap. MMP-1 is the primary enzyme responsible for breaking down fibrillar collagen, the main structural component of the extracellular matrix.

   While NF-κB is present in all cells, the activated form of NF-κB has been found to be increased in atherosclerotic plaque. Activated NF-κB is involved early in the inflammatory signaling process - it initiates and maintains the inflammatory response through regulation of a large number of genes. NF-κB

may help protect cells from apoptosis, or in some cases, may sensitize cells to apoptotic stimuli.

Nitrotyrosine is a marker of oxidative stress caused by reactive oxygen species (ROS). ROS production is increased in patients experiencing unstable angina and MI. It is expressed by both macrophages and SMCs. In addition, ROS may activate NF-κB and MMP-1.

Microvessels have been found in higher concentrations in ruptured than in non-ruptured plaque. It has been suggested that they provide a conduit for macrophage infiltration of plaque.

2. *There are indications that the marker may be sensitive to the mechanical environment.*

Based on previous studies (see Chapter 1), it was reasonable to expect that each of these markers may be mechanically sensitive.

Macrophages in culture respond to mechanical stretch by upregulating their production of other inflammatory mediators. In addition, SMCs increase their production of Monocyte Chemotactic Protein 1 (MCP-1), a powerful attractant of macrophages, in response to stretch.

NF-κB activation, MMP-1 production, and ROS production have all been found to be upregulated by mechanical stretch in macrophage and/or SMC cell culture studies. Also, it is known that the mechanical environment is generally an important stimulus in angiogenesis, making microvessels an interesting target as well.

3. *The overall set of markers selected represents the spectrum of inflammatory processes.*

We attempted to select markers that cover a range of inflammatory processes. Macrophages were an obvious choice, since they are the primary cell involved in inflammation. NF-κB is involved early in the inflammatory signaling process. On the other hand, increased MMP-1 expression probably occurs as the *result* of the inflammatory process – due to direct upregulation of MMP-1 gene expression in macrophages and smooth muscle cells, as well an indirect increase in expression due to an increase in the number of macrophages and/or SMCs.

Reactive oxygen species, whose activity is detected by nitrotyrosine, may be involved at both ends of the process. Reactive oxygen species may be upregulated due to the inflammatory process, but may also stimulate inflammation.

Microvessels may help facilitate the inflammatory process by providing a means for inflammatory cell infiltration.

4. *It is possible to detect the marker in fixed tissue embedded in MMA using standard immunohistochemical methods.*

While there were other markers that fit the first three criteria, it was not possible detect all markers that might be of interest using immunohistochemistry on formalin-fixed tissue embedded in MMA. Some methods, such as in situ zymography, as well as some antibodies, require that frozen rather than fixed tissue be used. In addition, we found that some

antibodies do not work as well on MMA-embedded tissue as on paraffin for frozen sections.

The five markers used in this study were able to be detected in our formalin-fixed MMA embedded tissue using routine immunohistochemical techniques. Studies in our lab showed that the variability in staining in MMA sections was not significantly different from the variability of staining in paraffin (data not shown).

It should be noted that, while nitrotyrosine is the currently accepted method for detecting reactive oxygen species immunohistochemically, it is well-known in the field that this antibody has rather poor specificity, often resulting in substantial background staining, even at very low concentrations. Because it is the only method available, it was used here, and every effort was made to eliminate the inclusion of background staining during quantification. However, the limitations of this antibody should be considered when interpreting the results of this study.

Determination of Positive Immunostaining

Locations of positive staining were determined by one of two methods, depending on the marker being considered. Positive staining for very prevalent, extracellular markers (MMP-1 and Reactive Oxygen Species) was determined by color threshold segmentation, while locations of positive staining for sparsely distributed cellular or intracellular markers (macrophages, NF-κB, and microvessels) was determined by manual tagging of the individual cells or microvessels.

Color Threshold Segmentation. In this method, each pixel within the cross-section was classified as either stained or unstained based on its image RGB values. Threshold RGB values for positive staining were determined from the positive control section included in each staining session. Although there may be session to session variability in staining intensity, the positively stained area of the positive control in each session should be very similar, since all control sections are taken from approximately the same location within the control vessel. Threshold RGB values were determined for each staining session so that the area classified as positive staining in the control closely matches the original stained control. Then, this threshold value was applied to all other images from that staining session. Figure 3.10 shows a representative cross-section stained for MMP-1 (A) to which this method has been applied to generate a mask of positive staining (B).

Because this method can be automated, it provides an objective measure of positive staining that is not affected by user bias. However, this method is potentially susceptible to errors due to histologic artifacts such as tissue wrinkles and the presence of calcification shards. These artifacts may cause some pixels to be incorrectly classified. When the marker being considered is very prevalent, these errors have little effect on the segmented marker distribution. However, for less prevalent signals, these errors may be large, and may skew the distribution. In addition, this method is not sensitive enough to locate single, positively stained cells. Therefore, this method is appropriate only for very prevalent, extracellular markers.

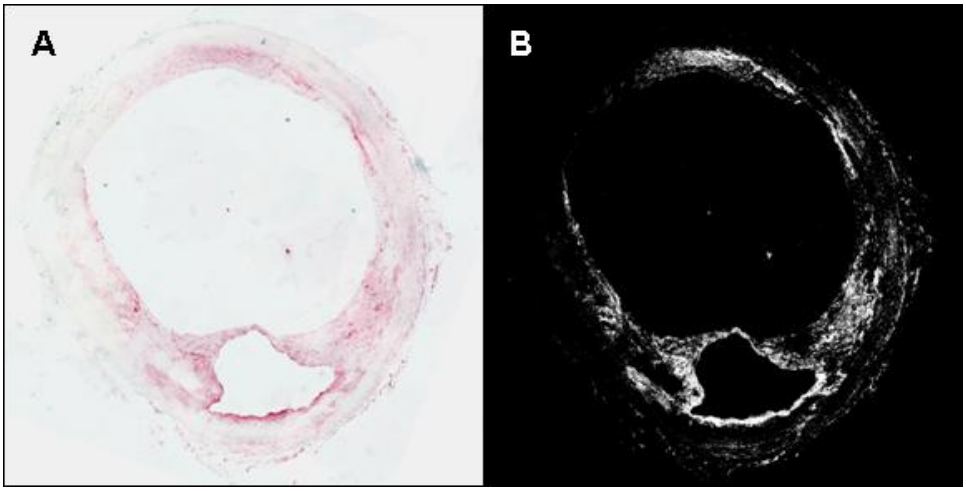

Figure 3.10 Determination of positive MMP-1 staining. Threshold RGB values were applied to cross-sections stained for MMP-1 (A) and a mask of positive staining was generated (B).

Manual Tagging of Cell/Microvessel Locations. For sparsely distributed cellular and intracellular markers where color thresholding is inappropriate, the locations of individual positively stained cells or microvessels in the cross-section were determined manually. Using the "manual tag" feature of Image Pro Plus 4.5, an X,Y point location for each positively stained cell or microvessel was determined by manually clicking on the center of each cell or microvessel. Because human cells are typically 10-50 microns in diameter and the image resolution is 1.5 microns, the error in identified cell locations was on the order of a few microns. The criterion used to dictate positive staining was the presence of a clear nuclei associated with some red staining. A representative image showing point locations of manually tagged cells in the cross-section are shown in red in Figure 3.11A.

While this method is less susceptible to errors due to histologic artifact, it is potentially more susceptible to user bias. One possible source of user bias is in the user's

definition of positive staining. To investigate this, a single section stained for macrophages was manually tagged twice – once using conservative criteria for positive staining, and once using liberal criteria. The conservative criteria required that only clearly distinguishable nuclei completely surrounded by red staining could be considered positive staining. The liberal criteria allowed any object present in the section that resembled a nucleus and that was associated with some red staining to be tagged as positive. Although there was a large difference in the total number of macrophages tagged between the two methods, Spearman rank analysis showed very high correlation ($R_s=0.41$, $N=530$, $p<0.00003$) between the two spatial distributions. Another potential source of user bias could be changes in user criteria over time. However, using two cell taggings performed on the same section 5 months apart, Spearman rank analysis showed very high correlation ($R_s=0.75$, $N=216$, $p<0.00003$) between the two spatial distributions. Therefore, this method appears to be insensitive to these types of user bias.

Quantification of Spatial Distribution

Once the locations of positive staining were identified, the spatial distribution of inflammatory markers was quantified. In order to represent the spatial variation of inflammatory content, the cross-section was broken into regions, and a value for inflammatory marker concentration was calculated for each region. These regions needed to be as small as possible, in order to retain information on the spatial distribution. But they also needed to be much larger than the size of a single cell. Because the goal was to compare inflammatory distributions with stress, the coarse mesh generated for the finite element analysis was also used here to divide the cross-section into elements over which inflammatory content was be quantified. The finite element mesh was overlaid on the

segmented, cell-tagged, or microvessel-tagged image, and the positive area fraction (stained pixels/total pixels), cell density (cells/mm^2), or microvessel density (microvessels/ mm^2), respectively, was calculated for each element. This process is illustrated in the case of macrophages in Figure 3.11.

The elements of the coarse meshes ranged in area from 5000-45000 μm^2, and the characteristic dimension of each element ranged from 80 – 220 μm. The median element area was 18000 μm^2, and the median characteristic length was 140 μm. Because the typical distance of misalignment between immunostained and morphologically stained images has been determined to be approximately 75 μm, these element sizes were considered sufficient to account for alignment errors, while still providing adequate spatial detail.

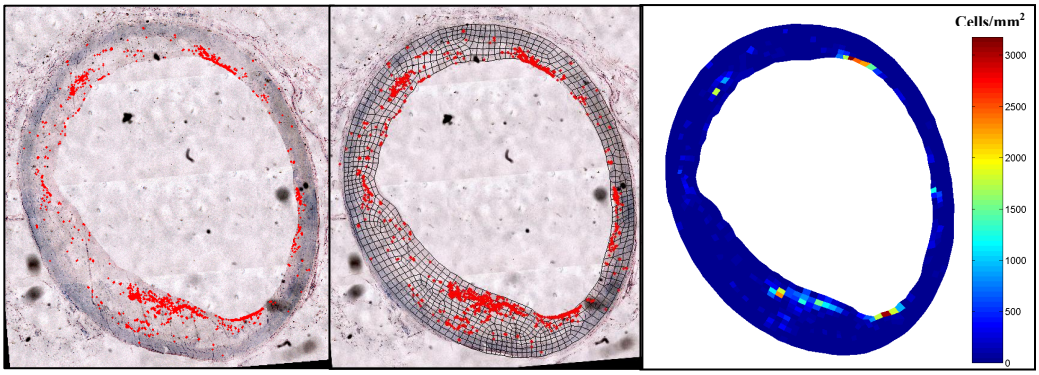

Figure 3.11 Locations of individual macrophages in the cross-section (A). A coarse finite element mesh (B) was used to quantify the distribution of macrophage cell densities (C)

Interpreting Quantified Immunohistochemistry Data

Immunohistochemistry is a very valuable tool, because it is currently the only method for visualizing antigens in their normal tissue environment. However, as discussed above, quantification of immunohistochemistry is subject to a degree of uncertainty due to variation in staining. Because care was taken to limit and account for this variation by comparison with a standard positive control, we believe that the methods presented here for quantifying immunostaining are a good measure of how much of the marker is present. Still, because it is impossible to completely eliminate variation in immunohistochemical staining intensity, we must be careful when interpreting numerical values for marker content determined from immunostaining. For some purposes in this study, the actual value (cell density or area fraction) were used. However, these values must be interpreted with care. Therefore, for most purposes, numerical values for marker concentrations were converted to binary values indicating the presence or absence of the inflammatory marker.

SPECIFIC AIM 3: COMPARISON OF SPATIAL DISTRIBUTIONS

We hypothesized that there is a spatial relationship between the expression of biological markers of inflammation – NF-κB, macrophages, MMP-1, nitrotyrosine, and microvessels – and the local mechanical environment. In order to test this hypothesis, the spatial distributions of von Mises stress, von Mises strain, and each of the five inflammatory markers of interest were determined at intervals along the axial length of 8 human right coronary arteries. Thus, for each interval, the cross-section is represented as a set of elements. Each element has corresponding stress and strain values, as well as inflammatory content values (area fraction, cell density, or microvessel density) for each of the five markers.

Several methods were used to compare the mechanical data sets with the inflammatory marker data sets to determine whether each marker collocates with mechanical stress and/or strain. These methods include visual comparisons, comparisons within individual cross-sections, and comparisons over the whole data set. While discussion of these methods will focus on von Mises stress as the mechanical measure, the methods were applied in the same way to the corresponding strain data.

Visual Comparisons

The simplest way to compare spatial distributions is by visual comparisons. By placing plots of the stress distribution and of each of the five markers side by side, general trends can be identified. These general trends were useful in developing hypotheses for testing by statistical analysis. However, while visual comparisons are helpful, their usefulness is limited, since they cannot provide a definitive answer about

whether collocation is occurring and the extent of this collocation. A side-by-side comparison for a representative cross-section is shown in Figure 3.12.

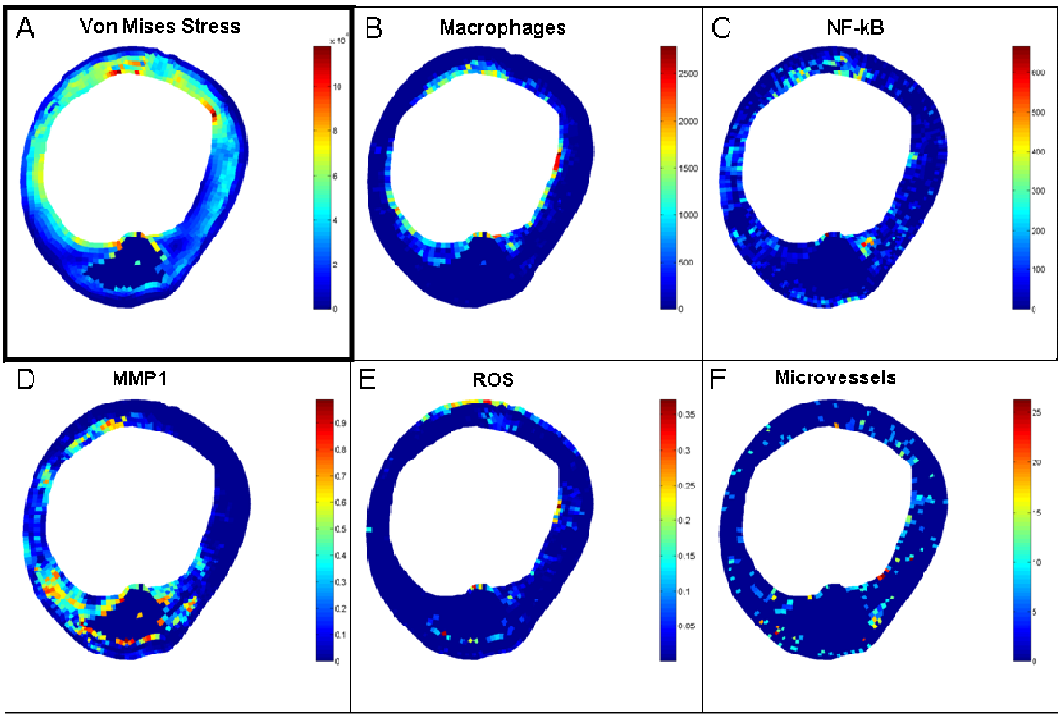

Figure 3.12 Visual comparison of the spatial distribution of von Mises Stress (A) with the spatial distribution of Macrophages (B), NF-κB (C), MMP-1 (D), Nitrotyrosine (E), and Microvessels (F).

Collocation within individual cross-sections

Because of the limitations of visual comparisons, statistical methods are needed to compare the distributions of stress and inflammatory markers within the cross-section. Because the data being considered was not normally distributed within the cross-section, a non-parametric statistical measure was required. In addition, because stress is one of possibly many stimuli that affect inflammatory marker expression, it was not necessarily expected that increasing inflammation would correlate with increasing stress in a monotonic fashion. Based on visual comparisons, it was only expected that inflammatory

markers would be preferentially located in regions where mechanical stresses were high. Therefore, the Wilcoxon Rank-Sum – a non-parametric method that does not require a monotonic relationship – was selected.

Wilcoxon Rank-Sum Test. The Wilcoxon rank-sum test is a non-parametric alternative to the two-sample t-test. Given samples of size n_A and n_B from populations A and B, it tests the hypothesis that the mean values μ_A and μ_B of the two populations are the same:

$$H_0: \mu_A = \mu_B$$

$$H_1: \mu_A \neq \mu_B$$

Briefly, observations from the two populations are combined into a single list and assigned a rank value based on their magnitude, from highest to lowest. Then, ranks of the observations of each population are summed. To account for different sample sizes, if the Wilcoxon coefficient W_A is the sum of the ranks of sample A, then W_B is given by:

$$W_B = \frac{(n_A + n_B)(n_A + n_B + 1)}{2} - W_A \qquad \text{Eq 3.13}$$

If the mean of the two groups are equal, the sum of their ranks should be close to the same value. For sample sizes larger than 20, the distribution of W_A is well approximated by the normal distribution. In this case, normal parameters can be calculated using Equations 3.14 – 3.16, and standard t-tables can be used to determine significance (Devore 1998).

$$\mu_{W_A} = \frac{n_A(n_A + n_B + 1)}{2} \qquad \text{Eq 3.14}$$

$$\sigma_{W_A}^2 = \frac{n_A n_B \left(n_A + n_B + 1\right)}{12} \qquad \text{Eq 3.15}$$

$$Z_0 = \frac{W_A - \mu_{W_A}}{\sigma_{W_A}} \qquad \text{Eq 3.16}$$

For each cross-section, elements with a cell density or area fraction greater than zero were assigned to an "Inflammation" group, while elements with a cell density or area fraction equal to zero were assigned to a "No Inflammation" group. After assignment to a group, all elements were then ranked based on their von Mises stress value. These ranks were then summed for each group. The null hypothesis was that the mean von Mises stress of the high inflammation group was equal to the mean von Mises stress of the low inflammation group:

$$H_0: \mu_{\text{inflammation}} = \mu_{\text{no inflammation}}$$

$$H_1: \mu_{\text{inflammation}} \neq \mu_{\text{no inflammation}}$$

The null hypothesis was rejected for p-values less than 0.05. If the null hypothesis was rejected and the Wilcoxon coefficient $W_{\text{inflammation}}$ was greater than $W_{\text{no inflammation}}$, then there was collocation of stress and inflammation.

Collocation across entire data set

Determining significance within individual cross-sections is helpful. However, from this data it was not possible to fully determine whether and to what extent inflammatory markers and stress collocate. No markers showed collocation in 100% of

cross-sections, and there was no means for determining how many cross-sections must show collocation in order to conclude that collocation indeed does occur. In addition, questions remained. For each inflammatory marker, does probability of that marker's expression strongly or weakly depend on stress? Are the relationships monotonic, or do they sometimes follow other trends? To answer these questions, collocation was considered across the entire data set.

Stress Excursion – Normalization by Median. To facilitate comparison of data among cross-sections across the entire data set, stress and strain data must be normalized for each cross-section. One option is to normalize by the maximum stress in each cross-section. However, some cross-sections may have stresses that vary over a large range, with focal concentrations of very high stresses, while stresses in other cross-sections may vary over a much smaller range, with no real regions of stress concentrations. If stresses were normalized by the maximum cross-sectional stress, then all of these points of max stress would be given a value of 1. This could cause masking of the effects of true stress concentrations.

To avoid this effect, cross-sectional data was normalized by the median cross-sectional value. Specifically, a term that will be referred to as "Stress Excursion" was calculated:

$$Stress\ \ Excursion = \frac{\sigma - \sigma_{median}}{\sigma_{median}} \qquad \text{Eq 3.17}$$

A stress excursion value of 0 indicates a stress that equals the median cross-sectional stress; a negative value indicates stresses below the median; a positive value indicates stresses above the median, with higher values being further from the median.

Accounting for Clustered Samples. In this research, 96 cross-sections were obtained at 1mm intervals from 8 right coronary arteries. Since the number of arteries available was limited, acquiring multiple cross-sections at intervals along each artery allowed us to increase the amount of data that could be obtained from a single vessel. In addition, it allowed us to investigate possible effects of changes along the length of the artery. Because 1 mm is much greater than the typical cell size of 10 μm, the assumption was made that there is no impact from direct cell-to-cell communication between cross-sections from consecutive intervals. Still, cross-sections taken from the same artery cannot be assumed to be completely independent. Their geometries may be more similar than cross-sections from other arteries. In addition, unknown systemic biological effects may be present. Because of this data clustering, one may expect some correlation, or non-independence, of cross-sections from the same artery. This non-independence may be important when comparing data over all cross-sections. Therefore, the Generalized Estimating Equations (GEE) approach was used to account for sample clustering.

If there was no clustering present, all samples could be treated equally. For clustered data, however, this approach would overstate the amount of information available. One approach to dealing with clustered data is to throw out all but one observation from each cluster. However, this wastes data which could provide additional information. Another approach could be to average the observations for each cluster, and

then average these averages. However, it can be shown that the Generalized Estimating Equations approach is a less variable estimator than each of these alternatives (Hanley 2003).

The GEE approach uses an iterative method to assign weights to the samples in each cluster, where the weights are determined based on the degree of correlation within a cluster, as well as the number of samples in each cluster. Clusters with a higher degree of correlation and/or more samples are weighted less than samples with less correlation and/or fewer samples. A simple but thorough explanation of the mechanics and application of GEE can be found in Hanley et al 2003.

Plots of Probability of Inflammatory Marker Expression vs Stress/Strain Excursion.

After normalization, element data for all cross-sections was combined into a single data set using the GEE approach to account for clustering. In order to investigate the variation of inflammatory markers with stress, elements were divided into bins of equal number of elements based on their stress value. Figure 3.13 illustrates the way in which elements were divided into bins. In this figure, elements have been sorted in ascending order based on their stress excursion values. The element number is given on the x-axis, and the stress excursion of each element is plotted on the y-axis. Although the curve appears to be a solid line, it actually consists of nearly 120000 separate data points. Because a very large number of elements have stress excursion values near zero (or in other words, stresses near the median), all elements with a stress excursion less than 0.25 were used to determine a baseline inflammation value. Then, the remaining elements were divided into 10 bins with equal number of elements and ascending stress excursion values.

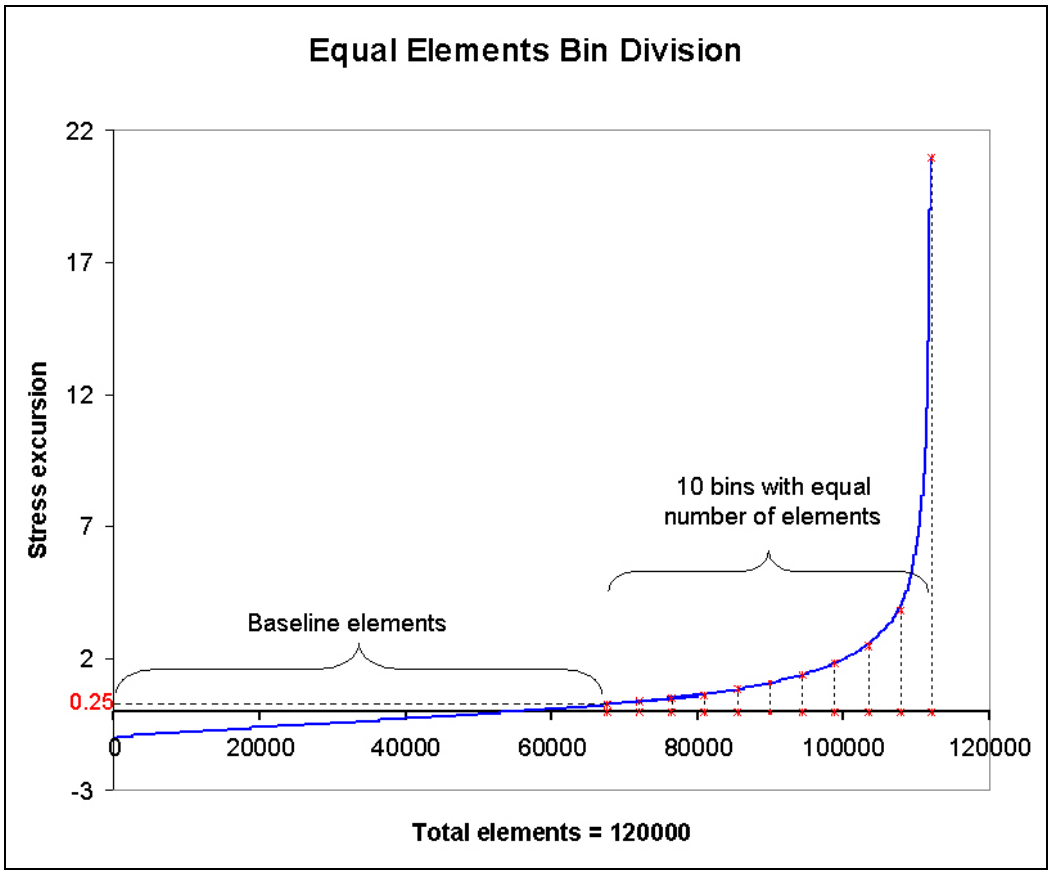

Figure 3.13 Division of elements into bins of equal number of elements and increasing stress.

For the baseline group of elements, as well as for each stress bin, the percentage of elements positive for the inflammatory marker of interest was calculated. These percentages can be viewed statistically as a probability of the presence of inflammation. For illustrative purposes, an example plot of the results of this type of analysis is shown in Figure 3.14. The baseline probability of inflammation is shown by the cross-hatched bar, while the probability of inflammation in each stress bin is shown by the solid bars. These results will be presented and discussed in detail in Chapters 4 and 5.

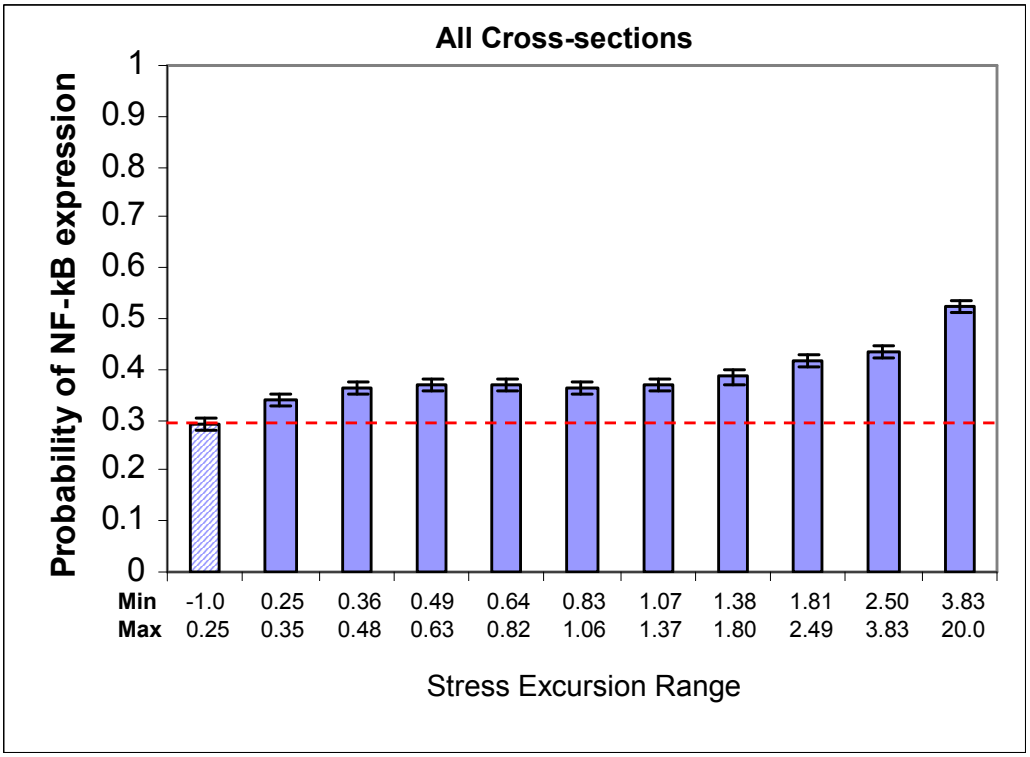

Figure 3.14 Representative plot showing variation of inflammatory marker with stress. Red dotted line represents the baseline value.

In addition to grouping elements from all cross-sections together, this analysis was repeated for cross-sections from each of four disease categories. These disease categories are discussed in detail later in this chapter. Also, this analysis was repeated using strain excursion rather than stress excursion.

Statistical Analysis. Statistical analyses were carried out using the software package Minitab 12.23. One-way ANOVA was used to determine whether there were significant differences between the any of the bins and also between each bin and the baseline. While ANOVA assumes that the data is normally distributed, it has been shown to be robust to violations of this assumption, particularly when the sample size is large

(Maxwell and Delaney 2003). Since the sample sizes in this study are quite large, the use of standard ANOVA was deemed reasonable.

If ANOVA indicated that there were significant differences, two-sample proportion tests were performed post hoc between each bin and the baseline to determine which bins showed significant differences. A two-sample proportion test is analogous to a two-sample t-test, but is applied to proportions rather than to means.

When performing multiple significance tests, the likelihood of finding false positives, or Type I errors, is increased. This was accounted for using Bonferroni's correction, which reduces alpha by a factor of N, where N is the number of tests being performed. Therefore, in these tests:

$$\alpha = \frac{\alpha_0}{N} \qquad \text{Eq 3.18}$$

where:

α = final significance level

α_o = original significance level

N = number of tests being performed

Comparing Collocation Trends at Different Stages of Plaque Progression

The second hypothesis of this study was that the spatial relationship between markers of inflammation and mechanical stress/strain is plaque progression dependent. Because the arteries are taken explanted from human subjects at transplant, each cross-section shows a snapshot of what is occurring within the plaque at one time point. Thus, it is not possible to study the relationship between inflammation and mechanics over time by looking at the same cross-section at multiple time points as the plaque progresses. An

alternative approach is to compare these relationships in multiple cross-sections of different disease states.

In order to compare results from cross-sections in different stages of progression, a simplified scheme for classifying the disease state of each cross-section was developed by adapting the classification scheme developed by the AHA and presented in the background section (see Figure 1.1). Each cross-section was assigned to one of four categories of plaque progression: Early, intermediate, advanced, and mature. This classification scheme is summarized in Table 3.3, and representative cross-sections for each category are shown in Figure 3.15. Early cross-sections were defined as cross-sections without detectable extracellular lipid accumulation, and included cross-sections with adaptive intimal thickening and type I plaque. Intermediate plaques were defined as cross-sections with layers of foam cells or small lipid accumulations present, and included types II and III lesions. Advanced plaques were defined as plaque with large lipid accumulations, without large calcification deposits, and included types IV, V and VI. Mature plaques were defined as plaque dominated by calcification or fibrous tissue, and included types VII and VIII.

After classifying cross-sections into categories, the same techniques discussed in the previous section to study collocation in the overall group were applied to each category.

Table 3.3 Plaque Classification Scheme

Progression Category	AHA Classification
Early	Intimal thickening - Type I
Intermediate	Type II - Type III
Advanced	Type IV - Type IV
Mature	Type VII - Type VIII

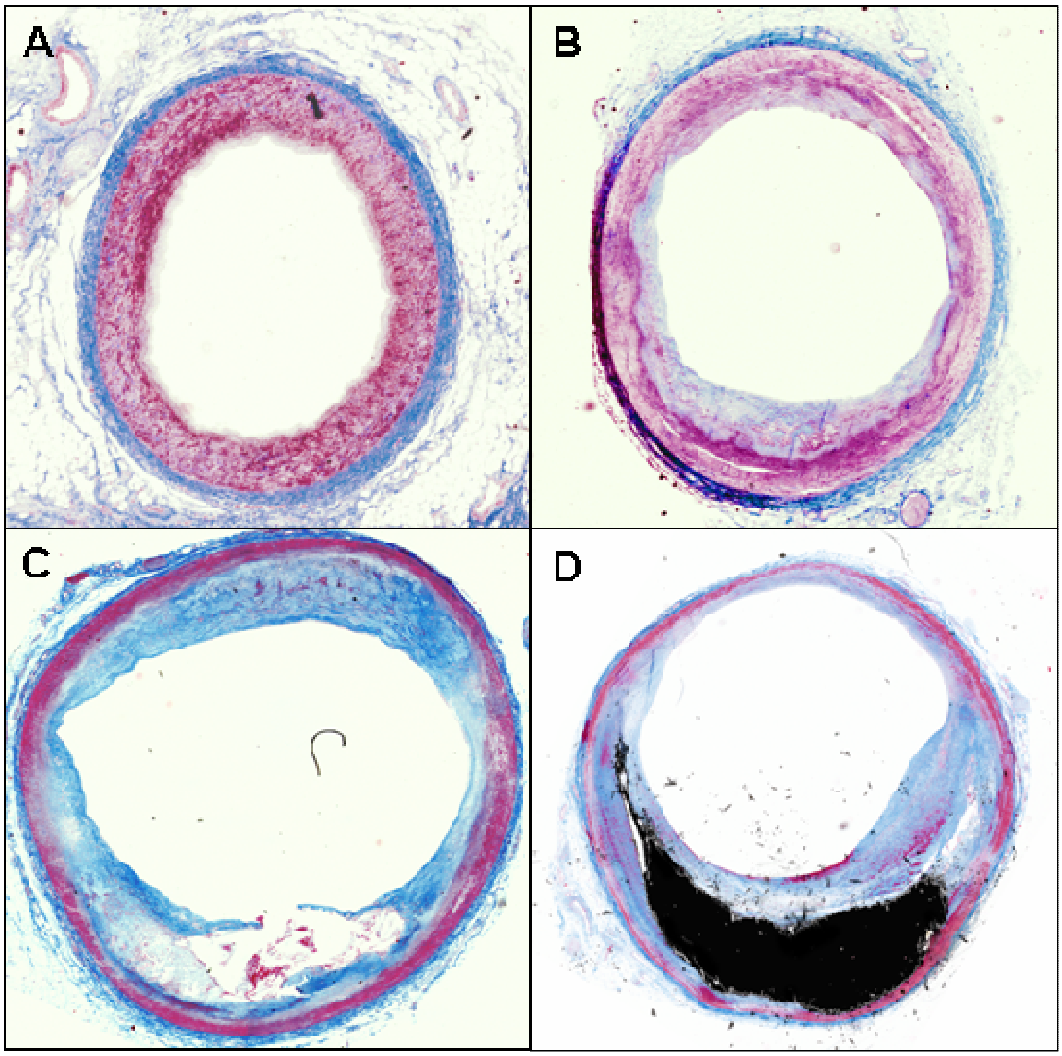

Figure 3.15 Representative cross-sections for each disease category – Early (A), Intermediate (B), Advanced (C), and Mature (D)

CO-EXPRESSION OF INFLAMMATORY MARKERS

One of the advantages of the methods developed in this study for quantifying inflammatory marker spatial distributions is that these methods facilitate not only comparison of each marker with mechanical measures, but also comparison of each marker distribution with other marker distributions. Because each cross-section is divided

into elements with an associated value for each inflammatory marker, as well as stress and strain values, marker spatial distributions can be easily compared to each other. Also, rather than looking at the probability of a single marker as a function of stress/strain excursion, it is possible to look at the probability of co-expression of two or more markers as a function of stress/strain excursion.

Determining Co-expression of Two Markers

Consider two markers: Marker A and Marker B. For all cross-sections, each element has a content value for both Marker A and B. For the purpose of determining whether markers are co-expressed, all content values were converted to binary: a value of 1 if the marker content was greater than zero, and a value of 0 if the marker content equaled zero. Using these binary marker values for Marker A, elements were divided into two groups – "*A-Positive*" (Marker A value = 1) and "*A-Negative*" (Marker A value = 0). Then, for both groups, the proportion of elements that were positive for Marker B (Marker B value > 0) was determined. A two-proportion test was performed in Mini-tab 12.23 to determine whether the proportion of elements positive for the Marker B was significantly greater in the "*A-Positive*" group than in the "*A-Negative*." Marker B was considered to be co-expressed with Marker A for $p < 0.05$. This analysis could also be repeated, dividing elements into groups based on Marker B and determining proportions based on marker A.

For markers showing co-expression, we were also interested in understanding how this co-expression varies with stress. To determine this, plots of marker expression as a function of stress excursion similar to the one shown in Figure 3.14 were generated. However, instead of determining the probability of expression from the proportion of

elements in each stress bin positive for a *single* marker, the probability of expression was determined from the proportion of elements in each stress bin positive for *both* markers being considered.

It should be noted that while these methods allow us to determine which markers are co-expressed within the same element, it is not possible to definitively determine which markers are being co-expressed within the same cell. The term "co-expression" as used here simply means that both markers are expressed in the same element area (characteristic element length: 200 microns). Since the element sizes are relatively small, it is a fairly reasonable assumption that the same cells are expressing both markers. However, because there may be many cells within an element, it is possible that different cells are expressing different markers.

CHAPTER 4

RESULTS

The goals of this study were to determine whether there is a spatial relationship between expression of inflammatory markers and mechanical stress and strain, and to determine whether these relationships are plaque progression dependent. To address these goals, a total of 99 cross-sections were analyzed, taken at 1mm intervals from 8 human right coronary arteries, with 12±5 cross-sections per artery. As discussed in Chapter 3, for each interval, 2D heterogeneous finite element mechanical models were developed to the spatial distribution of von Mises stress and strain. Also, novel methods for quantifying immunohistochemistry were used to determine the spatial distributions of each of five inflammatory markers – NF-kB, macrophages, MMP-1, nitrotyrosine, and microvessels. The distributions of mechanical stress/strain and markers of inflammation were then compared to determine whether there is a spatial relationship between inflammatory marker expression and the mechanical environment.

In order to determine whether this spatial relationship depends on stage of plaque progression, each cross-section was categorized by disease state as early, intermediate, advanced, or mature based on its gross morphology. Table 4.1 summarizes the number of cross-sections analyzed for each marker, as well as the classification of these cross-sections. Due to the loss or damage of cross-sections that occasionally occurs during histologic staining, there was some variation in the number of cross-sections analyzed for each marker.

Table 4.1 Summary of classification of cross-section disease states for each marker

	# of Cross-sections				
Category	**NF-kB**	**Macrophages**	**MMP-1**	**Nitrotyrosine**	**Microvessels**
Early	25	34	22	17	18
Intermediate	19	24	20	20	15
Advanced	22	21	23	21	22
Mature	17	19	15	16	11
Total	**83**	**99**	**81**	**75**	**67**

SPECIFIC AIM 1: MECHANICAL MODELING OF ATHEROSCLEROTIC PLAQUE

The goal of Aim 1 was to develop two-dimensional, histology-based heterogeneous finite element models of human coronary atherosclerotic plaque in order to determine the spatial distribution of mechanical stress and strain within the vessel wall. Figure 4.1 shows representative segmented cross-sections for each of the four disease categories. Figures 4.2 and 4.3 show spatial distributions of stress and strain excursion (Eq 3.17), respectively, resulting from the developed models for each of the cross-sections shown in Figure 4.1. These cross-sections were selected because they show the morphological features, as well as the associated trends in stress and strain typically seen in each disease category.

The spatial distributions of stress varied depending on the disease category. In early and intermediate plaques (Figure 4.2A and 4.2B), stress was fairly evenly distributed around the circumference. However, for advanced plaque (Figure 4.2C), stresses were increased in the shoulder and fibrous cap. In contrast, stresses in the shoulder and fibrous cap of mature plaque (Figure 4.2D) were not particularly high. Instead, high stresses were shifted to relatively plaque-free wall opposite the plaque bulk.

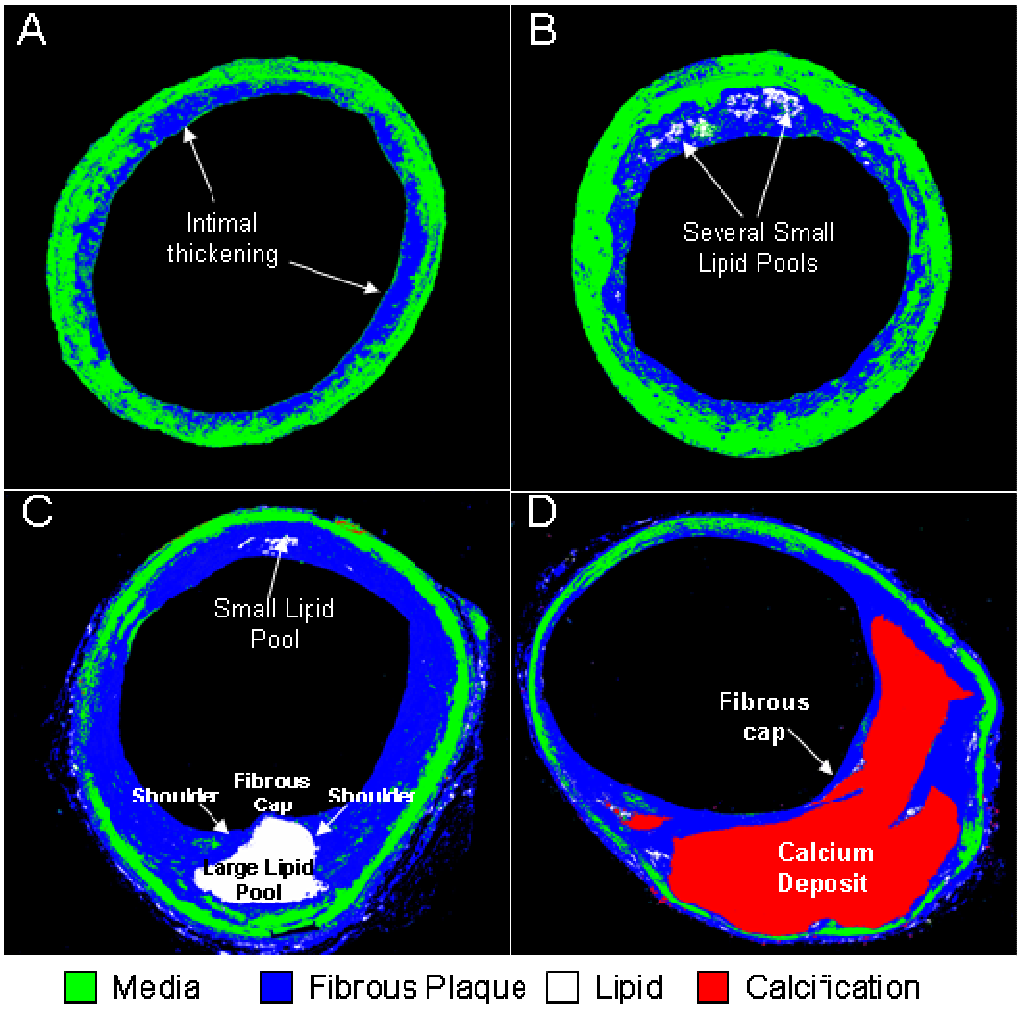

Figure 4.1 Representative segmented cross-sections of each of the four disease categories showing the typical morphological features of each category: Early (A), Intermediate (B), Advanced (C), and Mature (D)

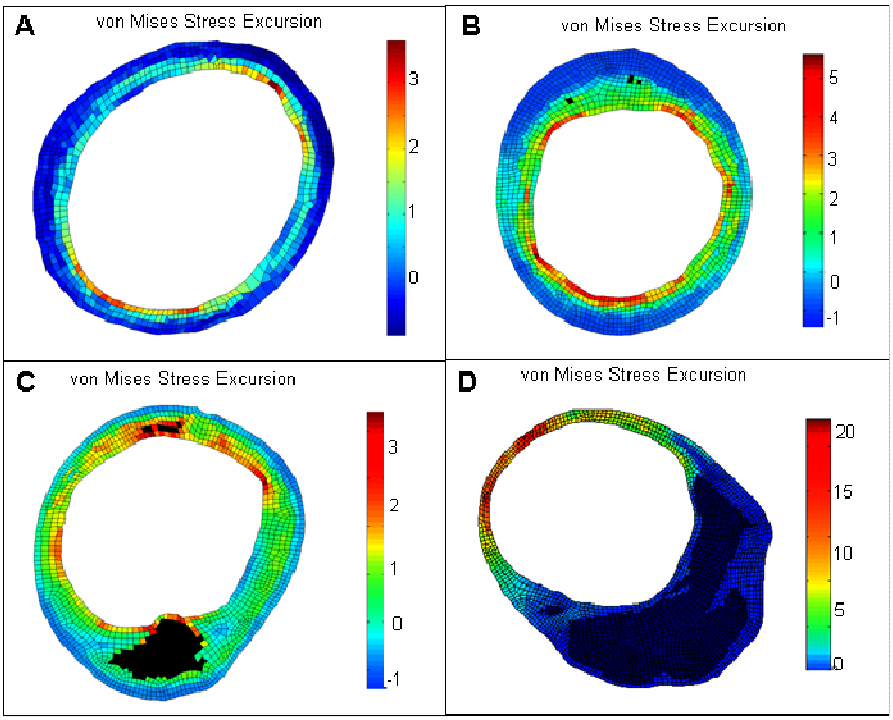

Figure 4.2 Representative spatial distributions of stress excursion for each disease category: Early (A), Intermediate (B), Advanced (C), and Mature (D). Lipid and calcification elements are shown in black.

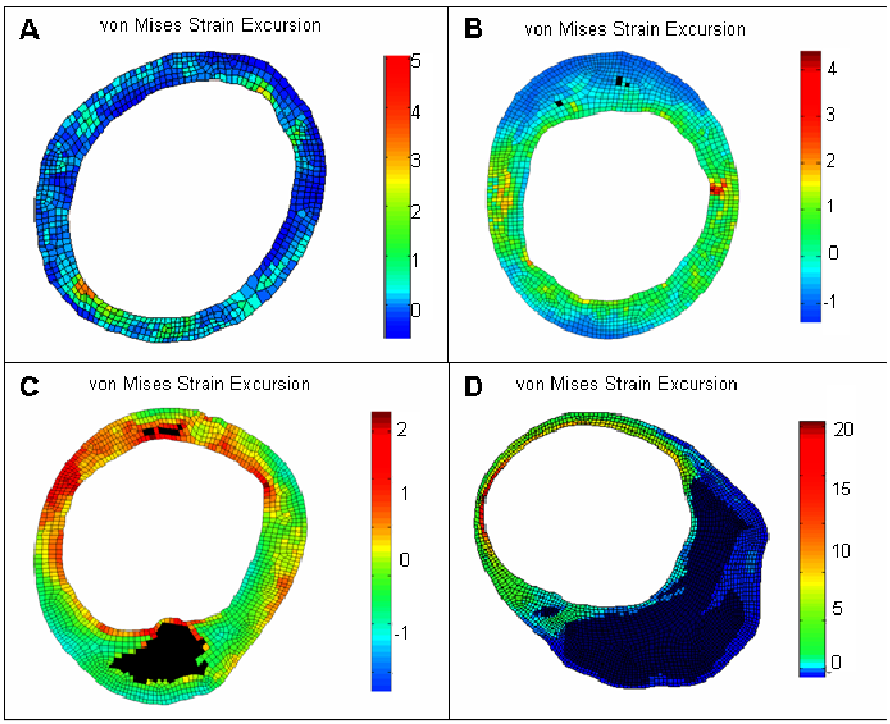

Figure 4.3 Representative spatial distributions of strain excursion for each disease category: Early (A), Intermediate (B), Advanced (C), and Mature (D). Lipid and calcification elements are shown in black.

SPECIFIC AIM 2: QUANTIFICATION OF INFLAMMATORY MARKER SPATIAL DISTRIBUTIONS

The goal of Aim 2 was to develop a technique for high-resolution quantification of the spatial distributions of inflammatory markers in the cross-section of atherosclerotic plaque. By utilizing the same finite element mesh used in the mechanical analysis (Aim 1) to quantify the marker spatial distribution for each cross-section, the developed technique obtained high-resolution spatial distributions while also facilitating comparison with mechanical data.

Figures 4.4-4.8 show representative spatial distributions in cross-sections in each disease category for each of the five markers – NF-kB, macrophages, MMP-1, nitrotyrosine, and microvessels. The cross-sections in these figures correspond to the cross-sections shown above in Figures 4.1-4.3.

As shown in Figures 4.4C, 4.5C, and 4.6C, NF-kB, macrophages, and MMP-1 respectively were strongly expressed in the fibrous cap and/or shoulder region of the advanced plaque cross-section, where stresses were also high (Figure 4.2C). In the mature cross-section, NF-kB and nitrotyrosine (Figures 4.4D and 4.7D) were both strongly expressed in the relatively plaque-free portion of the vessel wall opposite the plaque bulk, where stresses were also particularly increased (Figure 4.2D).

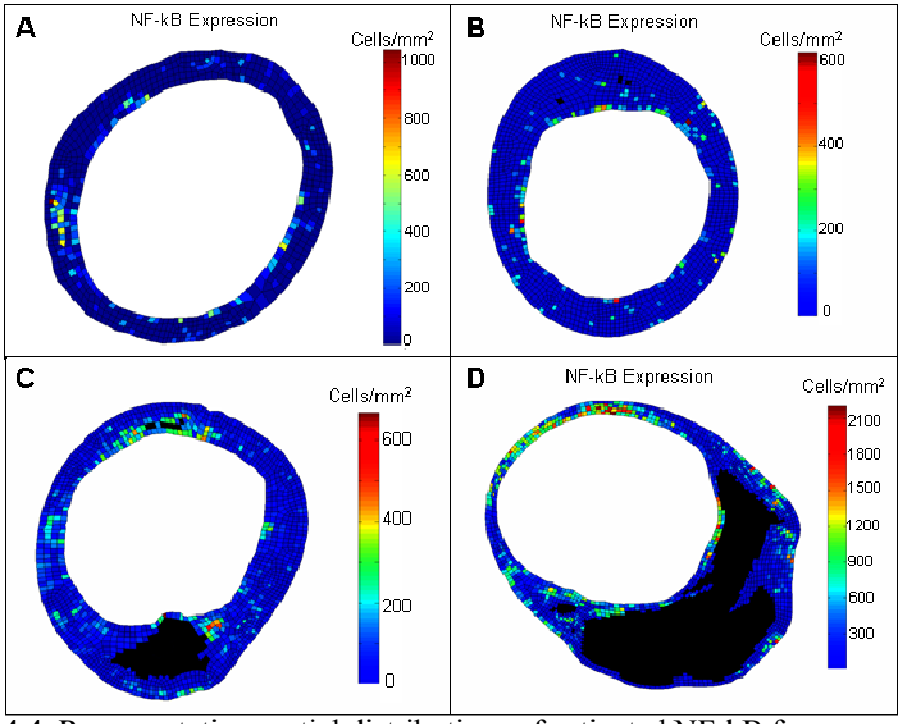

Figure 4.4 Representative spatial distributions of activated NF-kB for representative cross-sections from each disease category: Early(A), Intermediate(B), Advanced(C), Mature(D)

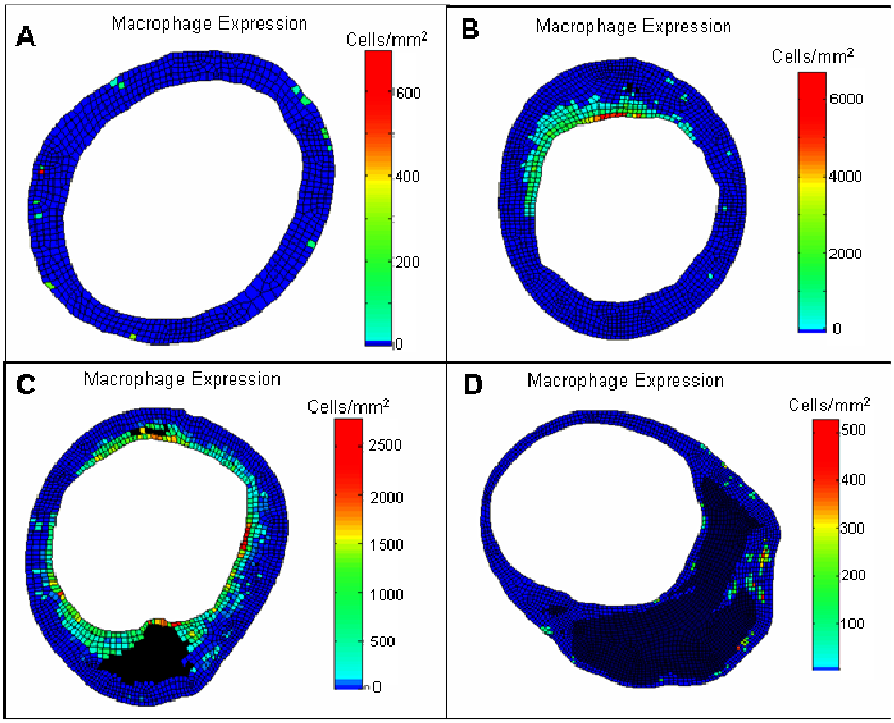

Figure 4.5 Representative spatial distributions of Macrophages for representative cross-sections from each disease category: Early(A), Intermediate(B), Advanced(C), Mature(D)

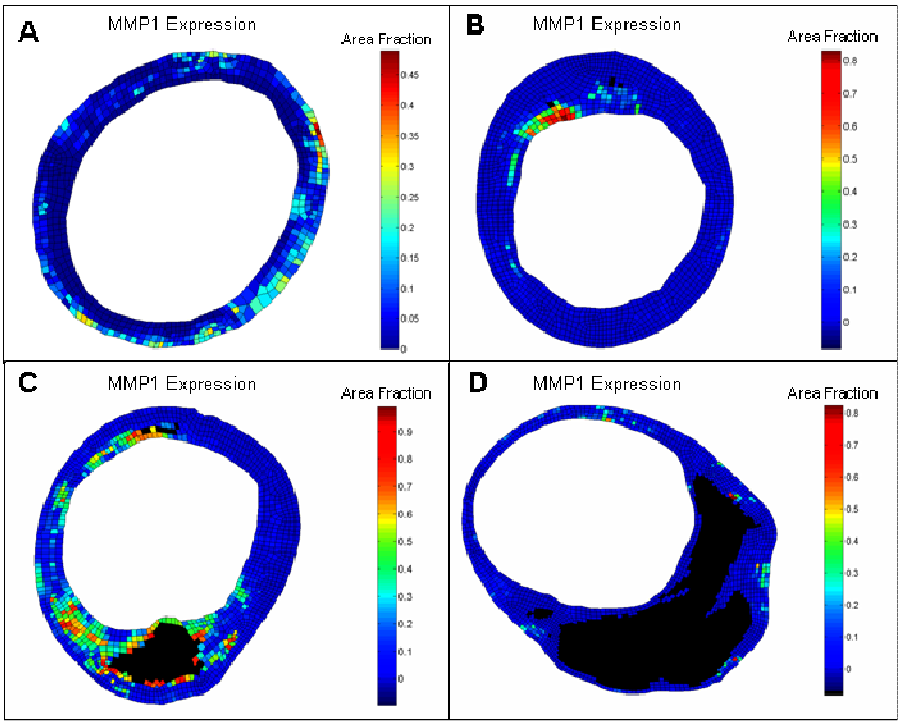

Figure 4.6 Representative spatial distributions of MMP-1 for representative cross-sections from each disease category: Early(A), Intermediate(B), Advanced(C), Mature(D)

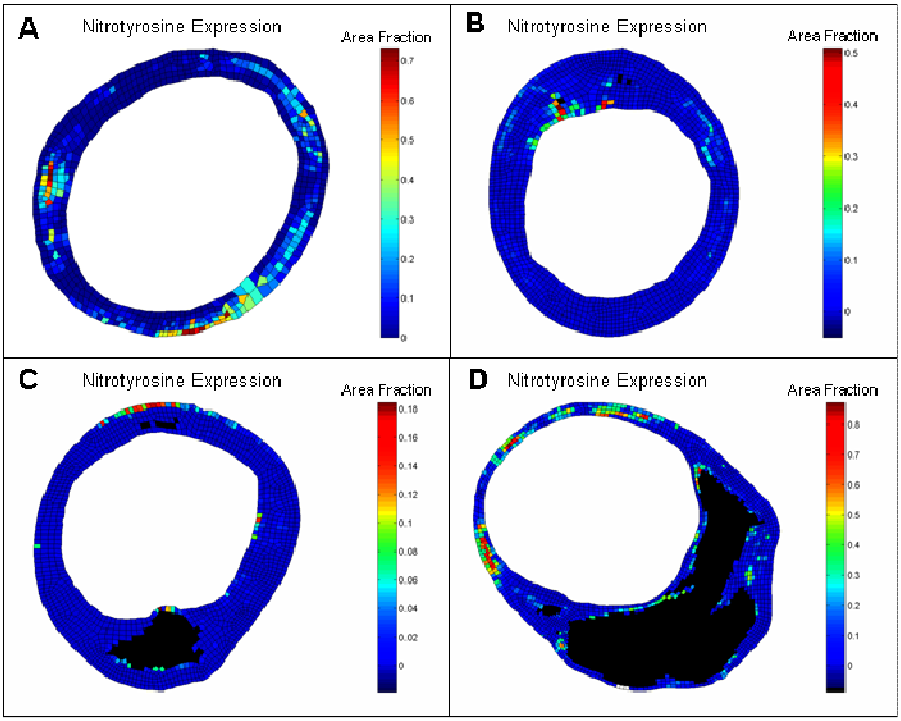

Figure 4.7 Representative spatial distributions of nitrotyrosine for representative cross-sections from each disease category: Early(A), Intermediate(B), Advanced(C), Mature(D)

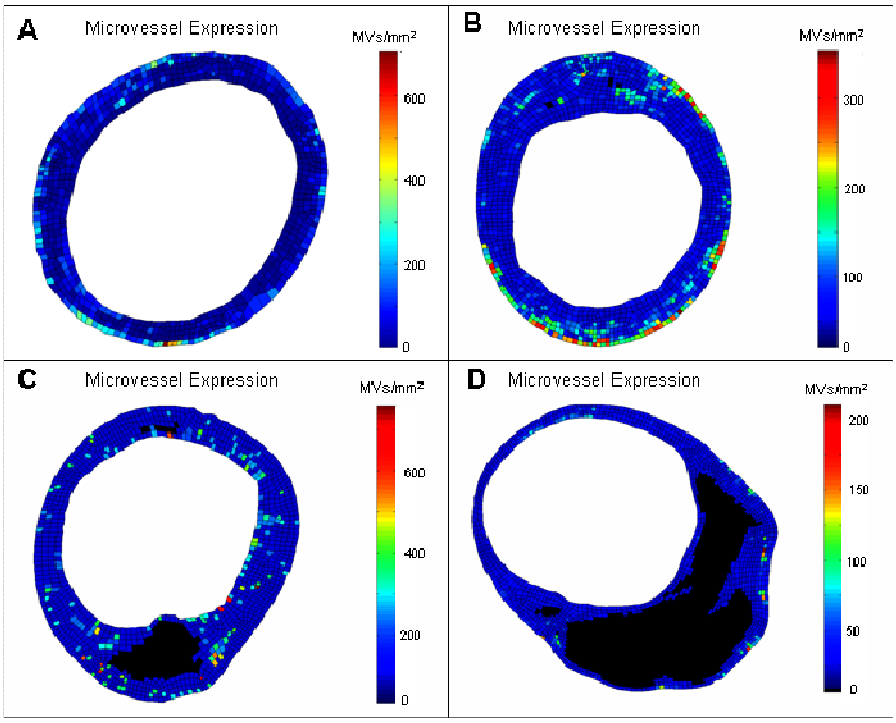

Figure 4.8 Representative spatial distributions of microvessels for representative cross-sections from each disease category: Early(A), Intermediate(B), Advanced(C), Mature(D)

SPECIFIC AIM 3: COMPARISON OF SPATIAL DISTRIBUTIONS

The goals of Aim 3 were to determine whether there are spatial relationships between inflammation markers and the local mechanical environment, and whether these spatial relationships are dependent upon the stage of plaque progression. Results are presented here for each of the five markers – NF-kB, macrophages, MMP-1, nitrotyrosine, and microvessels. For each marker, first the average overall concentration of the marker in each of the four disease categories – early, intermediate, advanced, and mature – is presented. This data shows the phases of plaque progression where the marker is most prevalent, and gives an indication of whether the marker might play a greater role in certain stages of plaque development. Next, the probability of marker expression as a function of stress excursion (Eq 3.17) over the entire data set is

considered. The trends from this data indicate whether there is an overall relationship between the marker and mechanical stress, and give an indication of the type of trend. Following this, the variation of marker expression with increasing stress is given for each disease category. The same overall and categorical data is then presented with strain excursion as the mechanical measure instead of stress. This is repeated for each of the five markers of interest. After results are presented for each marker separately, results of analysis of the co-expression of markers are presented.

NUCLEAR FACTOR – KAPPA B (NF-κB)

Overall Expression Levels of NF-kB

NF-kB was expressed more strongly in some disease categories than in others. Figure 4.9 shows the average overall expression level of NF-kB for each disease category (ANOVA, $p < 0.001$). The overall NF-kB expression was determined for each cross-section by dividing the total number of NF-kB positive cells in the cross-section by the

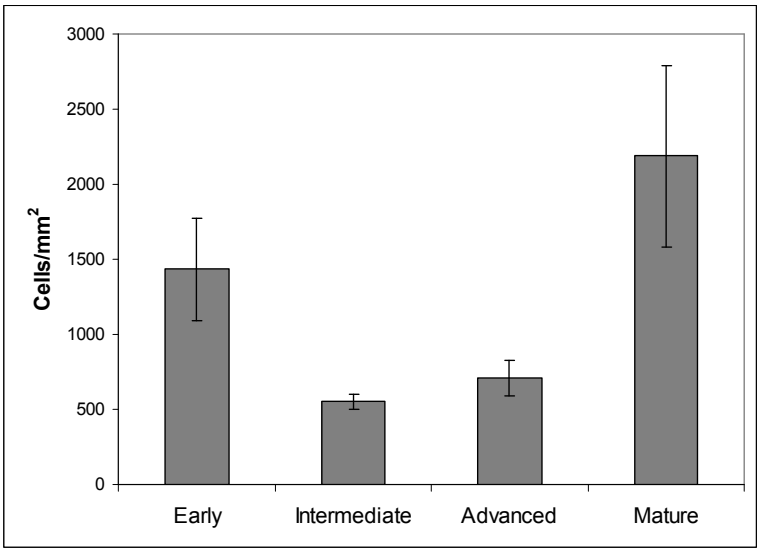

Figure 4.9 Overall expression of NF-kB by disease category

total cross-sectional area. The expression values for all cross-sections in each category were then averaged. NF-kB expression in the intermediate category was significantly less than in the early ($p=0.008$) and mature ($p=0.007$) categories (Bonferonni correction: $\alpha = 0.008$). NF-kB expression in advanced plaque was less, but not significantly less, than in early ($p=0.025$) or mature ($p=0.012$) plaque. There was no significant difference in NF-kB expression between the early and mature groups ($p=0.27$) or between the intermediate and advanced groups ($p=0.22$). Because of potential variation in staining, care must be taken when interpreting the meaning of numerical values of marker concentrations. Still, this information gives an indication of the relative NF-kB expression in each group.

Collocation of NF-kB expression and von Mises Stress

NF-kB expression showed a strong dependence on von Mises stress. Figure 4.10 shows the probability of NF-kB expression as a function of stress excursion (see Eq 3.17). As discussed in Chapter 3, all elements with a stress excursion less than 0.25 were used to determine the baseline probability, represented in the figure by the cross-hatched bar. The remaining elements were divided into bins of equal number of elements and increasing stress excursion, as represented by the solid bars. The probability of NF-kB expression increased monotonically with increasing stress excursion (ANOVA, $p<0.001$). In addition, for all stress excursions above the baseline threshold of 0.25, the probability of NF-kB expression was significantly greater than the baseline expression, as indicated by asterisks ($p<0.001$, Bonferroni's correction: $\alpha=0.0045$). In particular, there was a significant jump (indicated by †) in NF-kB expression for the last bin, which contains the elements with highest stress excursion.

NF-kB expression increased with increasing stress for all four disease categories, as shown in Figure 4.11, (ANOVA, $p<0.001$ for all). This trend was stronger in mature and advanced plaque than in early and intermediate. The probability of NF-kB expression in all bins for all four categories was higher than the baseline, although not all bins were significantly higher (Bonferroni's correction: $\alpha=0.0045$). The trend of monotonically increasing NF-kB expression with increasing stress was clearly seen in the intermediate, advanced, and mature categories, but was not as clear in the early category. This trend was strongest in the mature group. Although a dip was seen in the trend in intermediate plaque indicating possible non-monotonicity (for stress excursion between 1.92 and 2.54), this dip was not significant ($p=0.34$). In both the advanced and mature groups, there was a significant jump (indicated by † in figure) in the probability of NF-kB expression for the last bin, which contains the highest stress elements.

Collocation of NF-kB expression and von Mises Strain

NF-kB expression also increased monotonically with increasing strain. Figure 4.12 shows the probability of NF-kB expression as strain excursion increases for all cross-sections (ANOVA, $p<0.001$). While in the case of stress excursion, the probability of NF-kB expression was significantly greater than the baseline for all bins, the probability of NF-kB expression was only significantly greater than the baseline for strain excursions greater than 1.06 ($p<0.004$). Also, there was a significant jump in the probability of NF-kB expression for the two bins containing the highest stress elements.

NF-kB expression increased with increasing strain for all four disease categories, but this trend was strongest in mature plaque. Figure 4.13 shows the probability of NF-kB expression as a function of strain excursion for each disease category (ANOVA, $p<0.001$

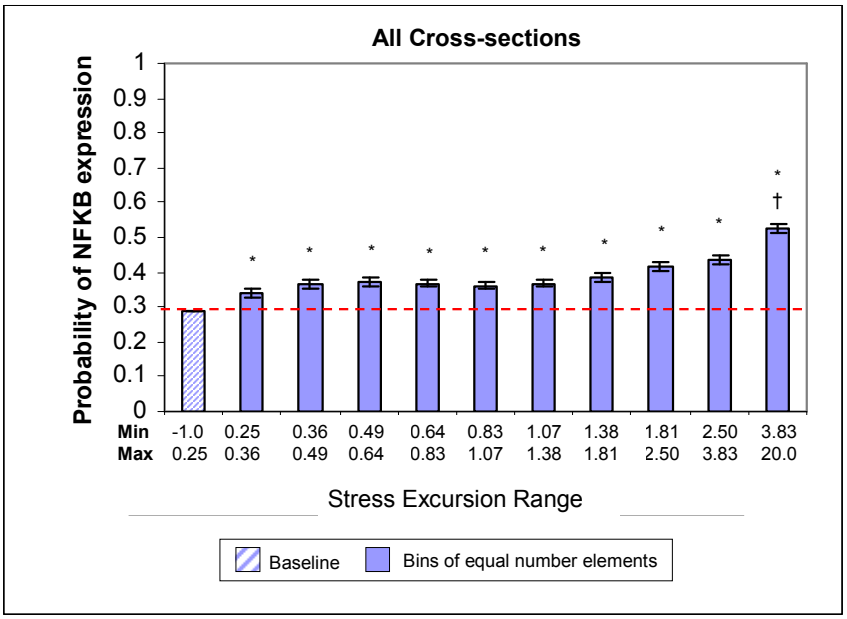

Figure 4.10 Probability of NF-kB expression as function of stress excursion over all cross-sections. * Significantly greater than baseline, † Significantly greater than preceding bin (Bonferonni correction: α=0.008)

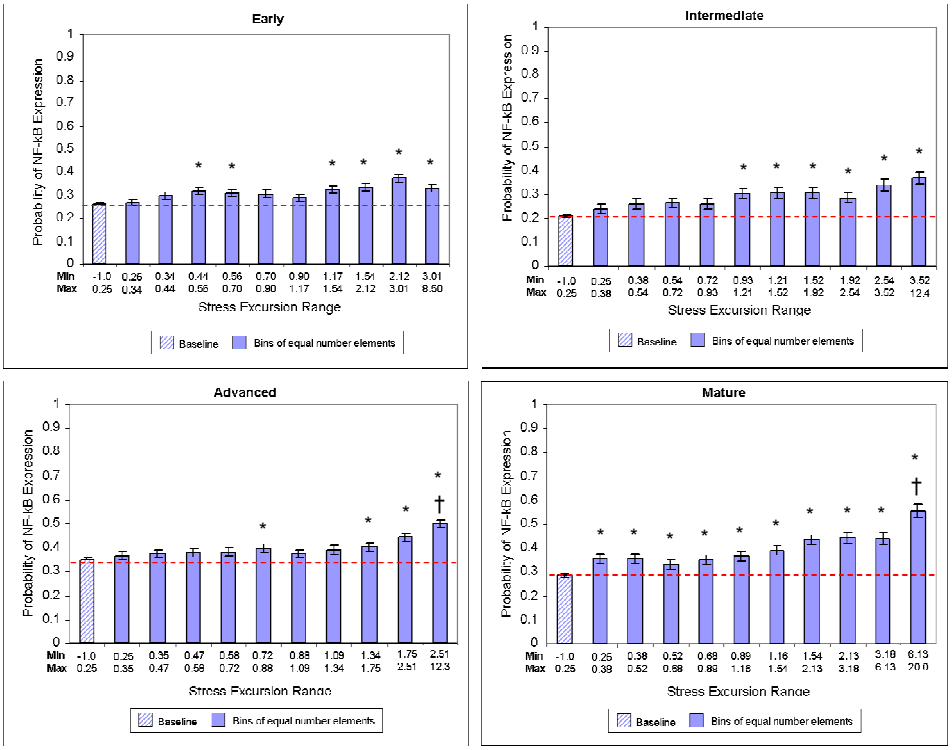

Figure 4.11 Probability of NF-kB expression as a function of stress excursion for each disease category: Early (Top Left), Intermediate (Top Right), Advanced (Bottom Left), and Mature (Bottom Right). * Significantly greater than baseline, † Significantly greater than preceding bin

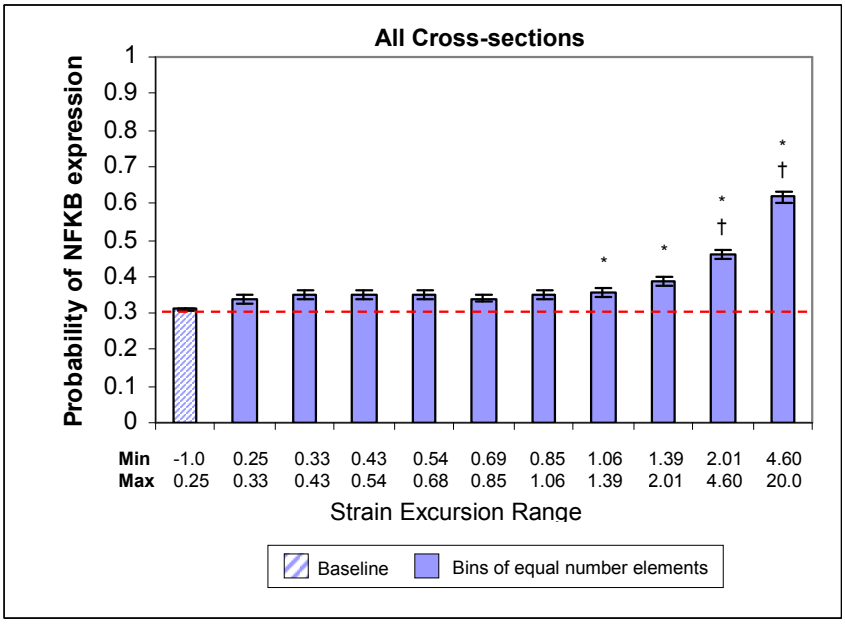

Figure 4.12 Probability of NF-kB expression as a function of strain excursion for all cross-sections. * Significantly greater than baseline, † Significantly greater than preceding bin

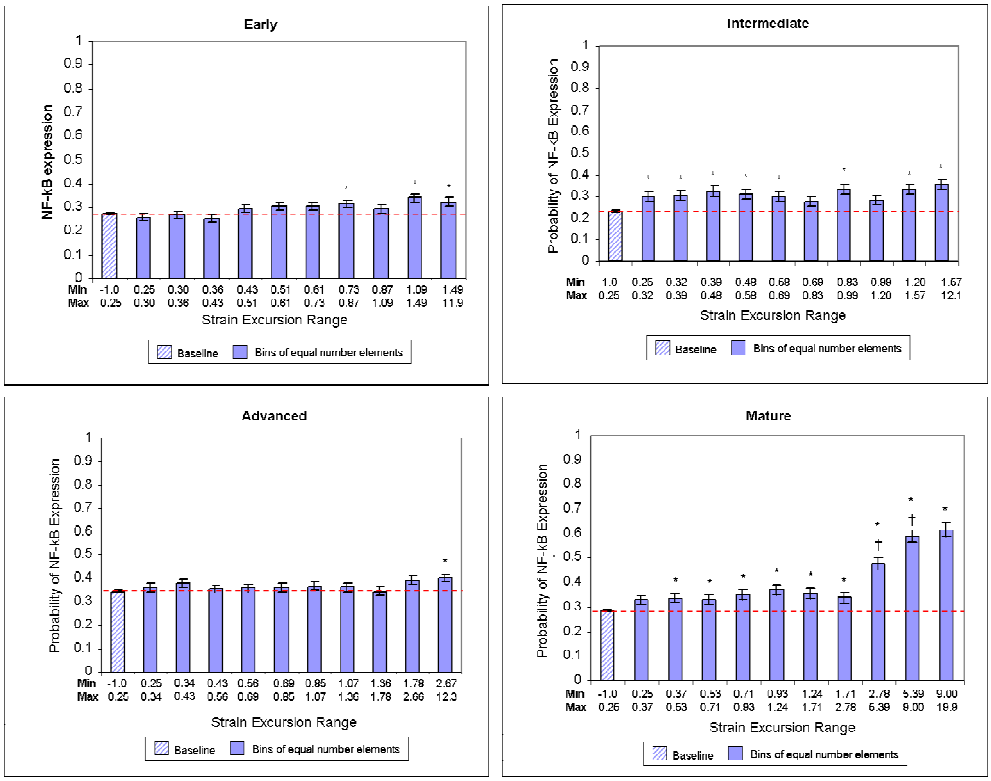

Figure 4.13 Probability of NF-kB expression as a function of strain excursion for each disease category: Early (Top Left), Intermediate (Top Right), Advanced (Bottom Left), and Mature (Bottom Right). * Significantly greater than baseline, † Significantly greater than preceding bin

for all). For early plaque, three of the final four bins had expression probabilities significantly greater than the baseline ($p<0.002$). In the intermediate category, all but one bin was significantly greater than the baseline, indicating that NF-kB expression is greater when strain is greater than the median. However, the trend of monotonically increasing expression was not seen in this group. In the advanced category, the last bin had an NF-kB expression probability that was significantly greater than the baseline ($p<0.003$). The trend of monotonically increasing expression was much stronger in mature plaque than in early, intermediate, and advanced plaque. In the mature category, there was a particularly strong increase in expression probability in the three highest-strain bins, with strain excursions greater than 2.78.

MACROPHAGES

Overall Macrophage Cell Density

Macrophage concentrations were highly variable, depending on the disease state. Figure 4.14 shows the average overall macrophage cell density for each disease category (ANOVA, $p<0.001$). Macrophage cell density in early lesions was very low - significantly less than in intermediate ($p<0.0001$), advanced ($p=0.0034$), and mature ($p=0.072$) lesions. Macrophages were also significantly less prevalent in mature than in intermediate lesions ($p<0.0001$), and less, but not significantly less prevalent in mature than in advanced lesions ($p=0.041$). Macrophages were very prevalent in both intermediate and advanced plaque, and was no significant difference in macrophage cell density between these two groups ($p=0.12$).

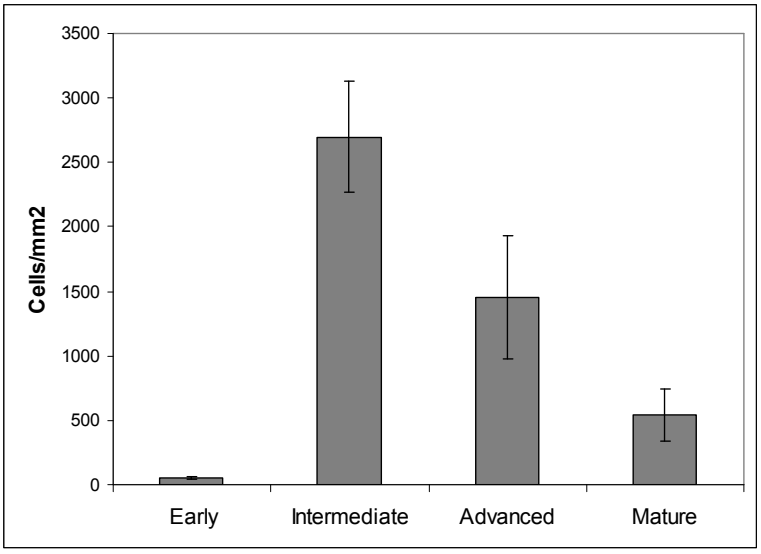

Figure 4.14 Overall Macrophage cell density by disease category

Collocation of Macrophages and Von Mises Stress

The probability of macrophage presence increased monotonically with increasing stress excursion for moderate ranges of stresses, but dropped off sharply at very high stresses, as shown in Figure 4.15 (ANOVA, $p<0.001$). Although the probability of macrophage presence dropped significantly in the highest-stress bin ($p<0.001$), the probability remained significantly greater than the baseline. In fact, for all stress excursions above the baseline threshold of 0.25, the probability of macrophage presence was significantly greater than the baseline ($p<0.001$).

The relationship between the probability of macrophage presence and stress is quite dependent on the stage of plaque progression. Figure 4.16 shows the probability of macrophage presence as a function of stress excursion for each disease category (ANOVA, early: $p = 0.016$; intermediate, advanced, and mature: $p < 0.001$). In intermediate plaque, the probability of macrophage presence in all bins was

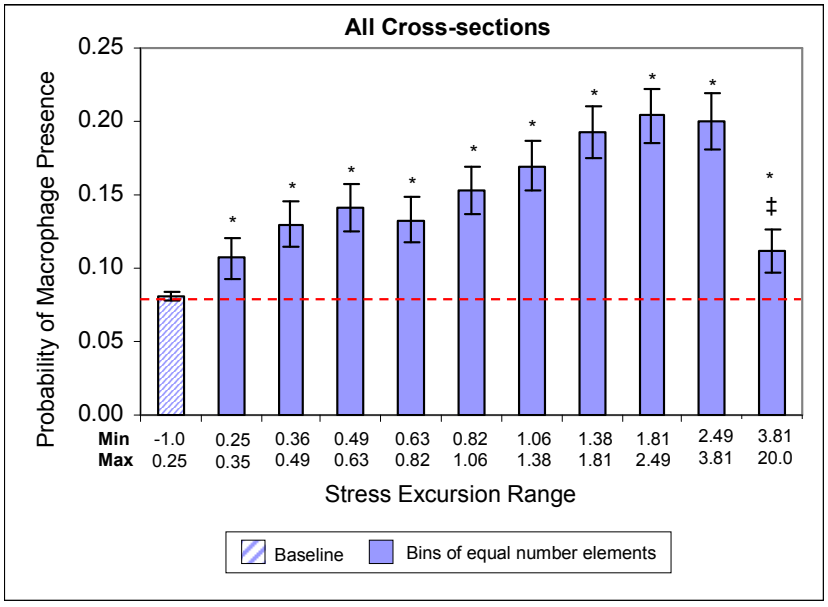

Figure 4.15 Probability of Macrophage presence as function of stress excursion over all cross-sections. * Significantly greater than baseline, ‡ Significantly less than preceding bin

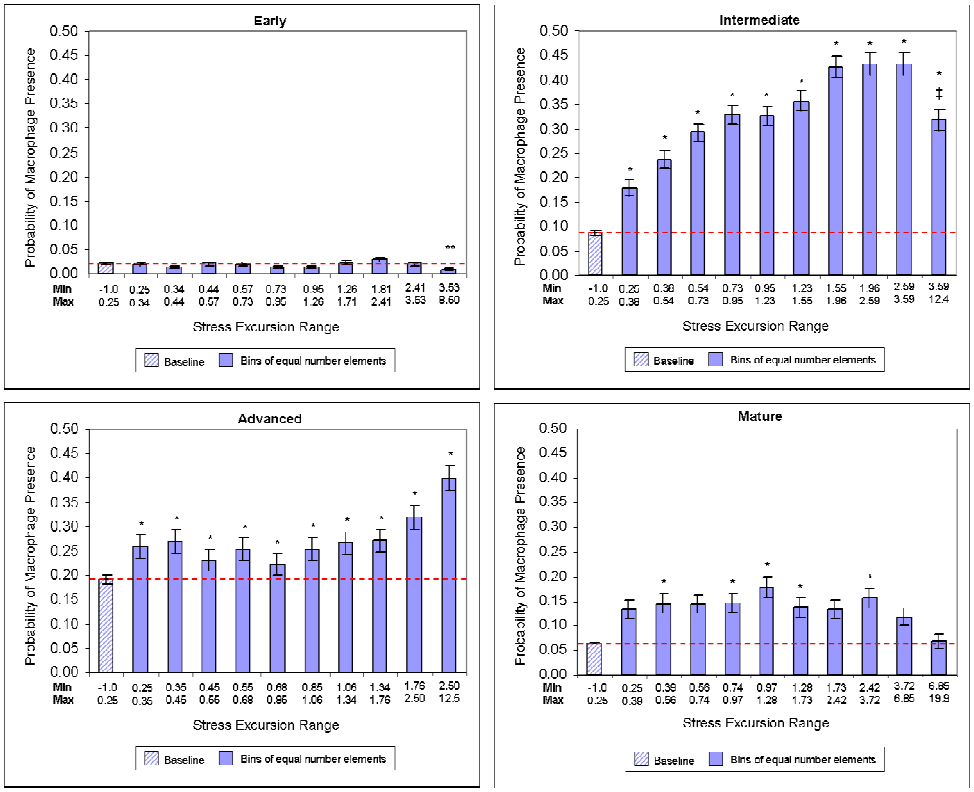

Figure 4.16 Probability of Macrophage presence as function of stress excursion for each disease category Early (Top Left), Intermediate (Top Right), Advanced (Bottom Left), and Mature (Bottom Right). * Significantly greater than baseline, † Significantly greater than preceding bin

significantly greater than the baseline ($p<0.0045$). In addition, the probability of macrophage presence followed the overall trend of for all cross-sections (Figure 4.15) – increasing monotonically, and then decreasing significantly for the highest stress bin. In contrast, expression in advanced plaque did not follow the overall trend seen in Figure 4.15. While all bins showed probabilities greater than the baseline, no real increasing or decreasing trend was seen for bins with mid-range stress excursions. Interestingly, though, the probability of macrophage presence was particularly increased at the highest levels of stress excursion. This disease category was the only category where high probability of presence was seen in the highest stress bin. In mature plaque, all bins except the highest stress bin showed expression greater than the baseline. There also seemed to be a trend of increasing expression, a peak, and then a decrease, as seen in the overall trend and in the intermediate category. For early plaque, no real relationship was seen between the probability of macrophage presence and stress.

The probability values seen in each of the graphs in Figure 4.16 reflect the overall macrophage concentrations for each disease category. As mentioned above, macrophage density in early plaques was very low. Densities in intermediate and advanced plaque was much higher. Overall densities in mature plaque was somewhat less than intermediate and advanced plaque.

Collocation of Macrophages and Von Mises Strain

The probability of macrophage presence decreased with increasing strain excursion, as shown in Figure 4.17 (ANOVA, $p<0.001$). While all bins showed probabilities greater than the baseline for stress excursion, in the case of strain excursion, all bins show expression probabilities less than the baseline. However, the difference

from baseline was only significant for the highest stress bin, where there was a significant drop in the probability of macrophage presence ($p<0.001$).

The relationship between macrophage presence and strain is dependent on the stage of plaque progression. Figure 4.18 shows the probability of macrophage presence as a function of strain excursion for each disease category (ANOVA, $p<0.001$ for all). As seen in the case of stress, no clear relationship was shown between macrophages and strain in early plaque, although the last two bins did have significantly lower expression probabilities than the baseline ($p<0.0045$). In intermediate and mature plaque, the probability of macrophage presence expression followed the overall trend of Figure 4.17 – decreasing with increasing strain, particularly in the highest strain bins. However, advanced plaque showed a slightly different trend. For all bins but the highest-strain

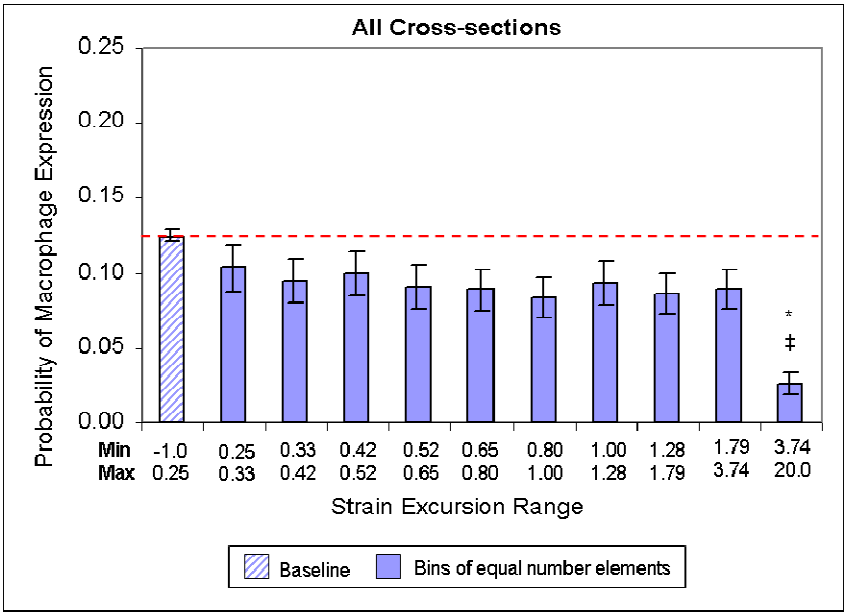

Figure 4.17 Probability of Macrophage presence as function of strain excursion over all cross-sections. * Significantly less than baseline, ‡ Significantly less than preceding bin

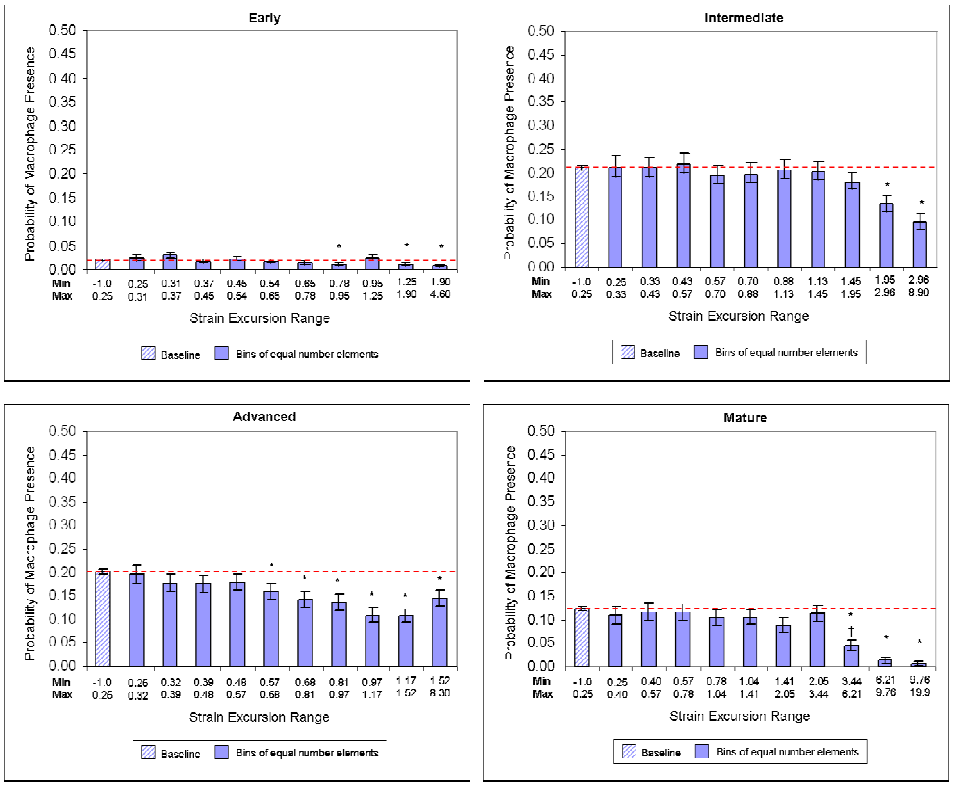

Figure 4.18 Probability of Macrophage presence as function of strain excursion by disease category. * Significantly less than baseline, ‡ Significantly less than preceding bin

bin, macrophages decreased with increasing strain. However, the probability of macrophage presence increased for the highest-strain bin, although the probability in this bin remained below the baseline.

MATRIX METALLOPROTEINASE 1 (MMP-1)

Overall Expression Levels of MMP-1

MMP-1 expression was less prevalent in mature plaque than in early, intermediate, and advanced plaque. Figure 4.19 shows the average percentage of area staining positive for MMP-1 for each disease category (ANOVA, $p<0.001$). MMP-1

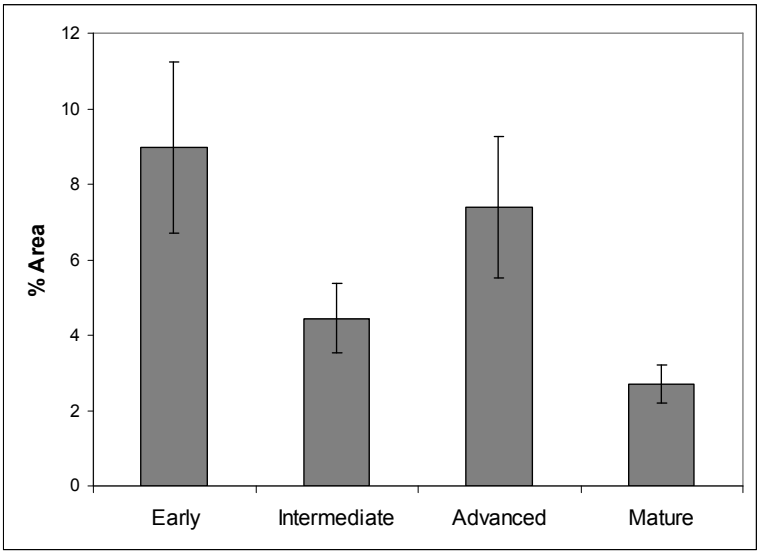

Figure 4.19 Overall % Area staining positive for MMP-1 by disease category

expression was greatest in early plaque, and least in mature plaques. The difference in expression between early, intermediate, and advanced plaque was not significant. Expression in mature plaque was significantly less than in early plaque ($p=0.006$), but was not significantly different from intermediate and advanced.

Collocation of MMP-1 expression and von Mises Stress

MMP-1 expression increased with increasing stress excursion. Figure 4.20 shows the probability of MMP-1 expression as a function of stress excursion (ANOVA, $p=0.001$). The trend was monotonic, and there was a significant jump in MMP-1 expression for elements in the highest stress bin ($p<0.001$). The probability of MMP-1 expression was greater than the baseline for all stress bins.

The relationship between MMP-1 expression and stress is quite dependent on the stage of plaque progression. Figure 4.21 shows the probability of MMP-1 expression as a

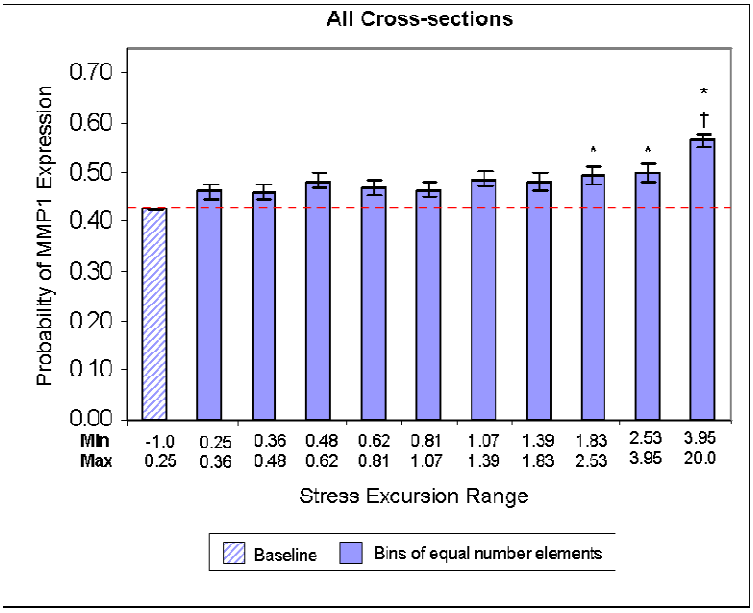

Figure 4.20 Probability of MMP-1 expression as a function of stress excursion over all cross-sections. * Significantly greater than baseline, † Significantly greater than preceding bin

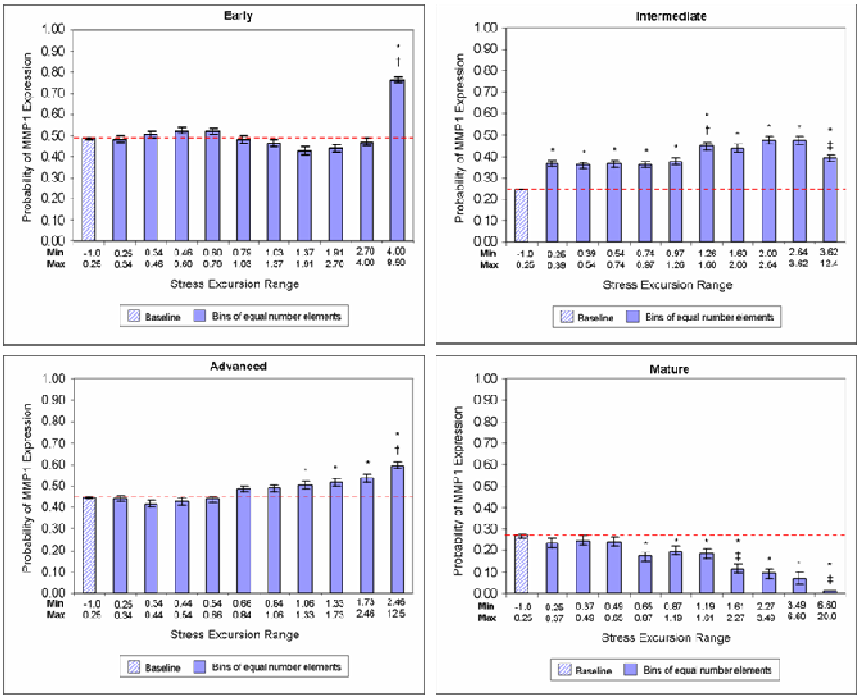

Figure 4.21 MMP-1 expression as a function of stress excursion for each disease category: Early (Top Left), Intermediate (Top Right), Advanced (Bottom Left), and Mature (Bottom Right). * Significantly greater than baseline, † Significantly greater than preceding bin

function of stress excursion for each disease category (ANOVA, $p<0.001$ for all). In early plaque, for moderate stress excursion values, no dependence on stress was seen. However, for the highest stress bin, there was a very large jump in MMP-1 expression. Interestingly, MMP-1 expression in intermediate and advanced plaque followed the same trend as macrophage expression in these groups (Figure 4.16). In intermediate plaque, expression in all bins was significantly greater than the baseline, but there was a significant drop in expression in the highest stress bin. In advanced plaque, MMP-1 expression increased monotonically with stress, and there was a significant jump in MMP-1 expression for elements in the highest stress bin. In contrast, MMP-1 expression in mature plaques decreased monotonically with increasing stress.

Collocation of MMP-1 expression and von Mises Strain

While MMP-1 expression showed a strong increasing trend with respect to stress, MMP-1 expression showed a weaker dependence on strain. Figure 4.22 shows the probability of MMP-1 expression as a function of strain excursion for all cross-sections (ANOVA, $p=0.047$). While the probability of MMP-1 expression was greater than the baseline for all bins, only the highest strain bin had a probability of expression that was significantly greater than the baseline.

The expression of MMP-1 as a function of strain was highly dependent on the state of disease. Figure 4.23 shows the probability of MMP-1 expression as a function of strain for each disease category (ANOVA, $p<0.001$ for all). In early plaque, MMP-1 expression increased monotonically with increased strain, with a particularly strong increase in the highest strain elements. In contrast, MMP-1 expression dramatically decreased with increasing strain in mature plaque. MMP-1 expression in intermediate and

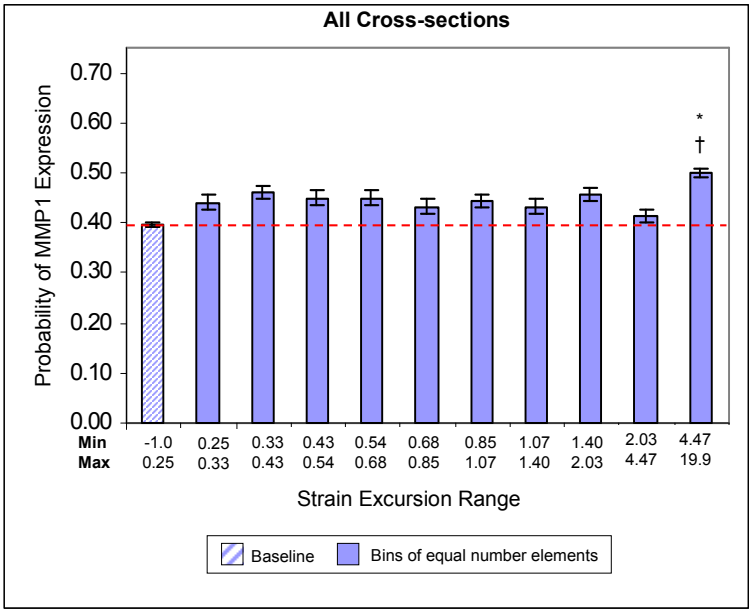

Figure 4.22 Probability of MMP-1 expression as a function of strain excursion over all cross-sections. * Significantly greater than baseline, † Significantly greater than preceding bin

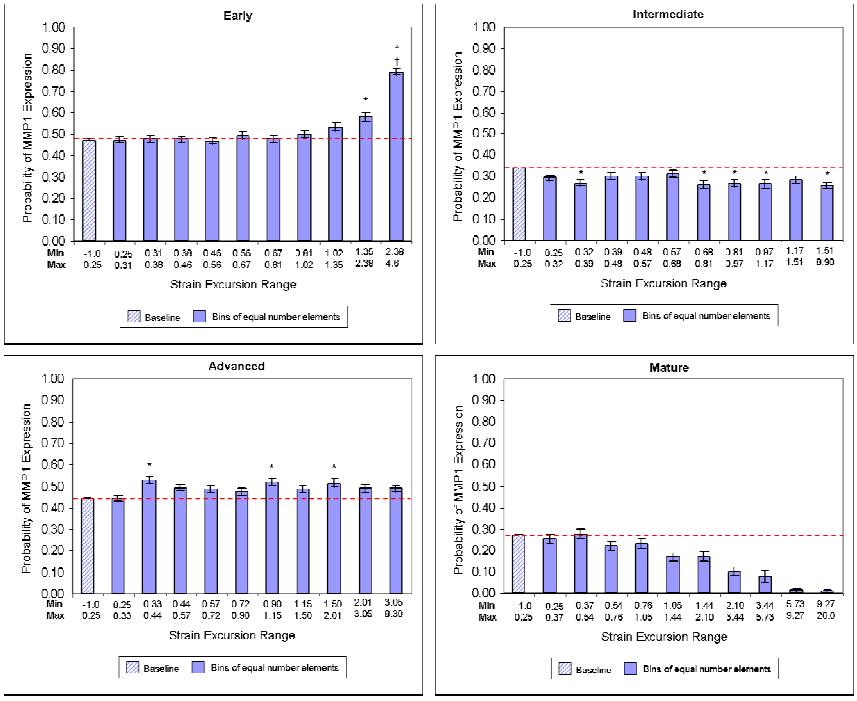

Figure 4.23 MMP-1 expression as a function of strain excursion for each disease category: Early (Top Left), Intermediate (Top Right), Advanced (Bottom Left), and Mature (Bottom Right). * Significantly greater than baseline, † Significantly greater than preceding bin

advanced plaque showed a very weak dependence on strain. In the intermediate group, all strain bins had expression probabilities less than the baseline, while in the advanced group, most strain bins had expression probabilities greater than the baseline.

NITROTYROSINE

Overall Expression Levels of Nitrotyrosine

Nitrotyrosine expression was similar among the disease categories, although it was slightly less for mature plaque. Figure 4.24 shows the average percentage of area staining positive for nitrotyrosine (a stable end-product of reactive oxygen species activity) for each disease category. Although expression was lower in mature plaque than in other categories, ANOVA showed no statistical difference in nitrotyrosine expression among disease categories ($p=0.4$).

Collocation of Nitrotyrosine Expression and von Mises Stress

When data from all cross-sections were considered together, nitrotyrosine expression showed no dependence on stress, as can be seen in Figure 4.25 (ANOVA, $p=0.26$) However, when the data was subdivided into disease categories, a weak dependence on stress was found, as shown in Figure 4.26 (ANOVA, $p<0.001$ for all). In early and intermediate plaque, nitrotyrosine seemed to decrease at high stresses, although no bins showed expression probabilities significantly lower than the baseline. In advanced and mature plaque, nitrotyrosine expression seemed to decrease for moderate values of stress, but then increase at very high stresses. In both groups, the probability of nitrotyrosine expression was significantly greater ($p<0.001$) than the baseline for the highest stress elements (stress excursion > ~2.4).

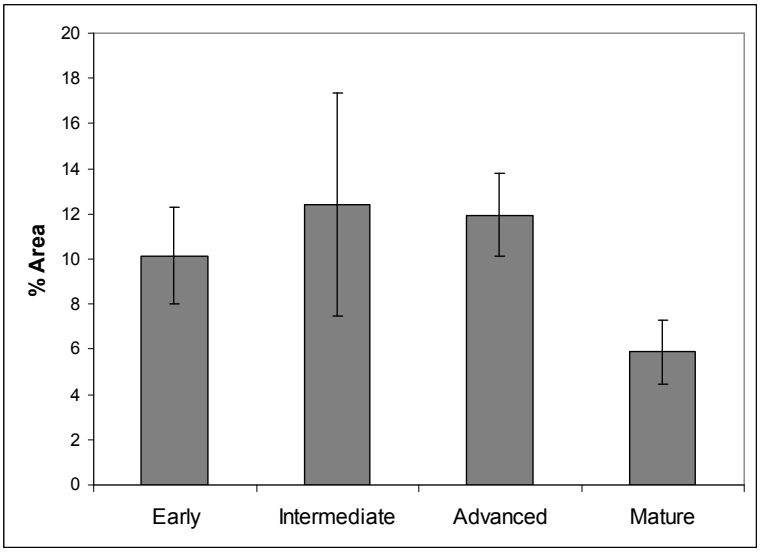

Figure 4.24 Overall % Area staining positive for Nitrotyrosine by disease category

Collocation of Nitrotyrosine Expression and von Mises Strain

Nitrotyrosine showed a stronger dependence on strain than stress. Figure 4.27 shows the probability of nitrotyrosine expression as a function of strain excursion for all cross-sections (ANOVA, $p<0.001$). For moderate values of strain excursion, nitrotyrosine showed no dependence on strain. However, there was as significant jump in nitrotyrosine expression for the highest two strain bins ($p<0.001$).

The expression of nitrotyrosine as a function of strain was dependent on the state of disease. Figure 4.28 shows the probability of nitrotyrosine expression as a function of strain for each disease category (ANOVA, intermediate: $p=0.003$; early, advanced and mature: $p<0.001$). Intermediate plaque showed no dependence of nitrotyrosine expression on strain. However, early and advanced plaque showed higher probability of nitrotyrosine expression in the highest strain bins. Mature plaque showed increasing nitrotyrosine expression with increasing strain, but then showed a significant drop in expression probability for the highest-strain bin.

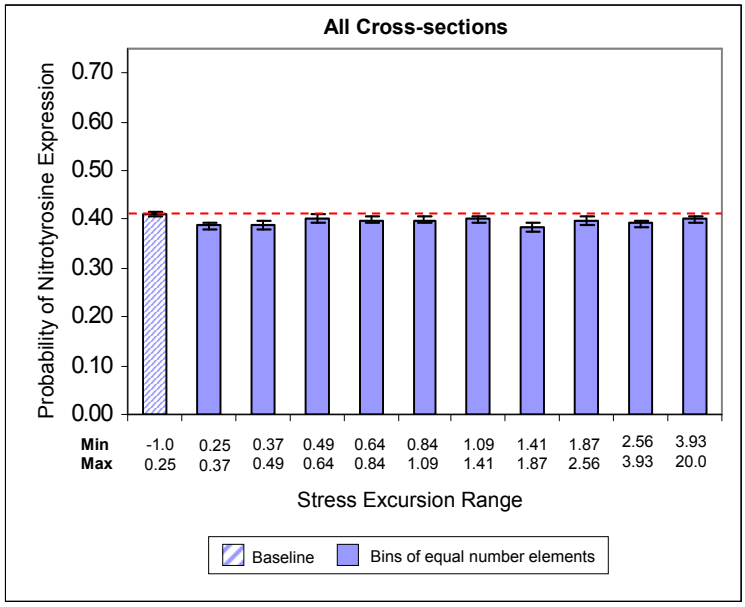

Figure 4.25 Probability of Nitrotyrosine expression as a function of stress excursion over all cross-sections. * Significantly greater than baseline, † Significantly greater than preceding bin

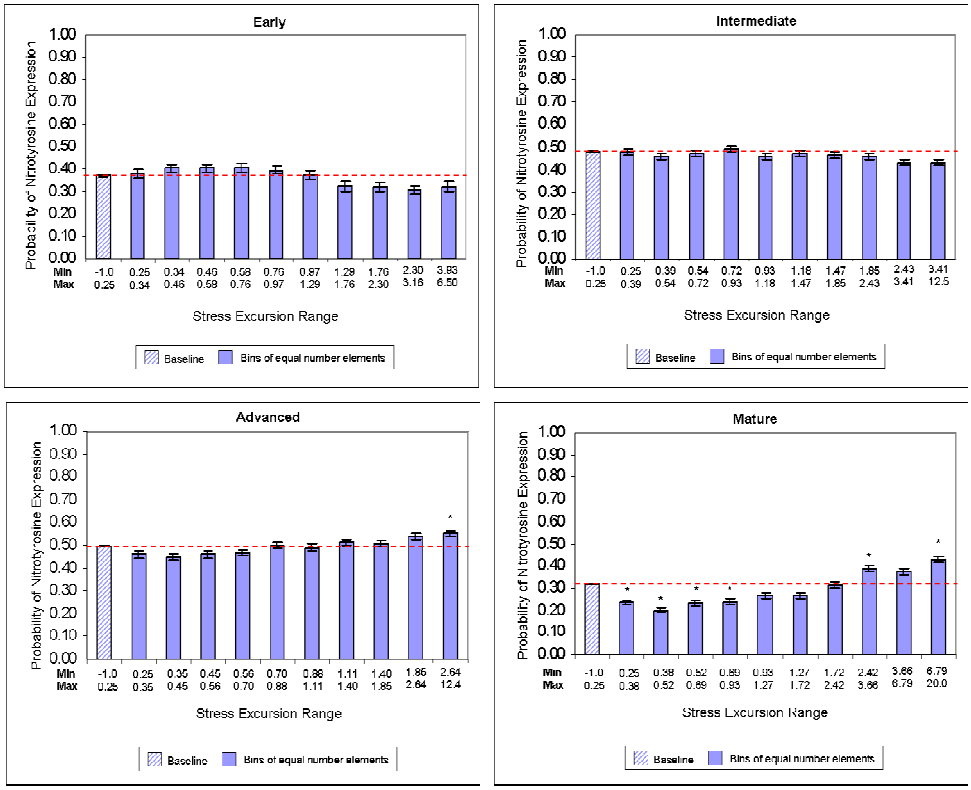

Figure 4.26 Probability of Nitrotyrosine expression as a function of stress excursion for each disease category. * Significantly greater than baseline, † Significantly greater than preceding bin

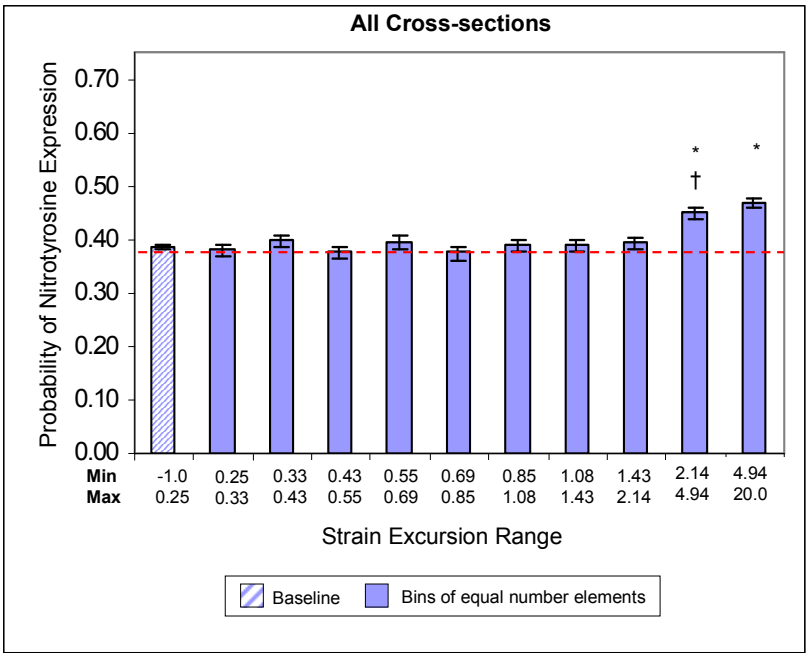

Figure 4.27 Probability of Nitrotyrosine expression as a function of strain excursion over all cross-sections. * Significantly greater than baseline, † Significantly greater than preceding bin

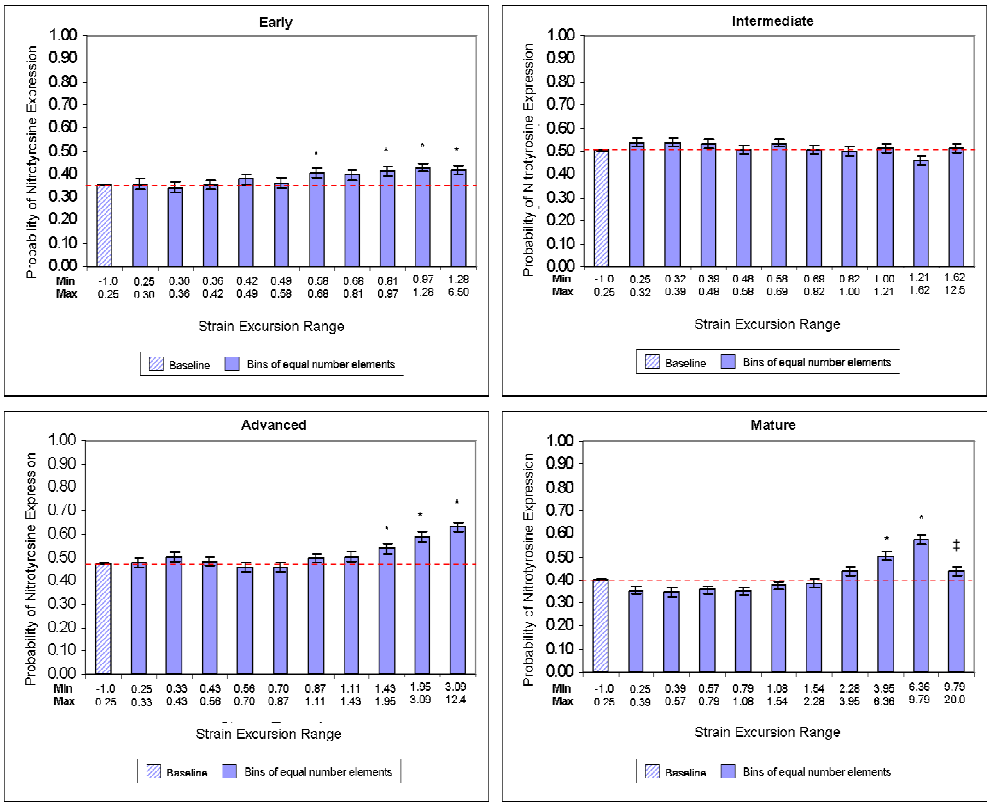

Figure 4.28 Probability of Nitrotyrosine expression as a function of strain excursion for each disease category * Significantly greater than baseline, ‡ Significantly less than preceding bin

MICROVESSELS

Overall Microvessel Density

Microvessel density appeared to increase slightly in the later stages of plaque progression. Figure 4.29 shows the average microvessel density for each disease category. Although microvessel density appears slightly higher in advanced and mature plaque, ANOVA showed that there was no statistical difference in the microvessel density between disease categories (p=0.56).

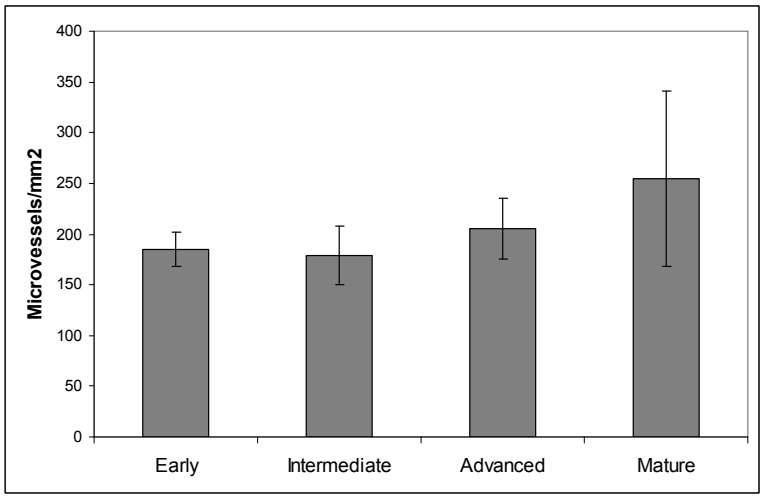

Figure 4.29 Overall Microvessel density by disease category

Collocation of Microvessels and von Mises Stress

Microvessels showed a weak, mixed dependence on stress. Figure 4.30 shows the probability of microvessel expression as a function of stress excursion (ANOVA, p=0.04). At moderate values of stress excursion, the probability of microvessel presence was lower than the baseline, and at high stress excursions, microvessel expression was

very near the baseline. However, no bins showed a probability of microvessel presence that was significantly different from the baseline.

When the data was subdivided into disease categories, a slightly stronger dependence on stress was found, as shown in Figure 4.31 (ANOVA, $p<0.001$ for all). The trends in these categories were mixed. In early, intermediate, and advanced plaque, microvessel expression followed the overall trend seen in Figure 4.30, although the trend was stronger in each category than in the overall data. For these categories, bins of moderate stress excursion had microvessel expression probabilities significantly lower than the baseline, while bins of high stress excursions had microvessel expression probabilities that were nearly equal to the baseline. In contrast, mature plaque showed a conflicting pattern of microvessel expression with respect to stress. At low-moderate stress, expression probability was above the baseline; at high-moderate stress, expression probability was near the baseline; and for the highest stress bin, there was a significant jump in microvessel expression probability.

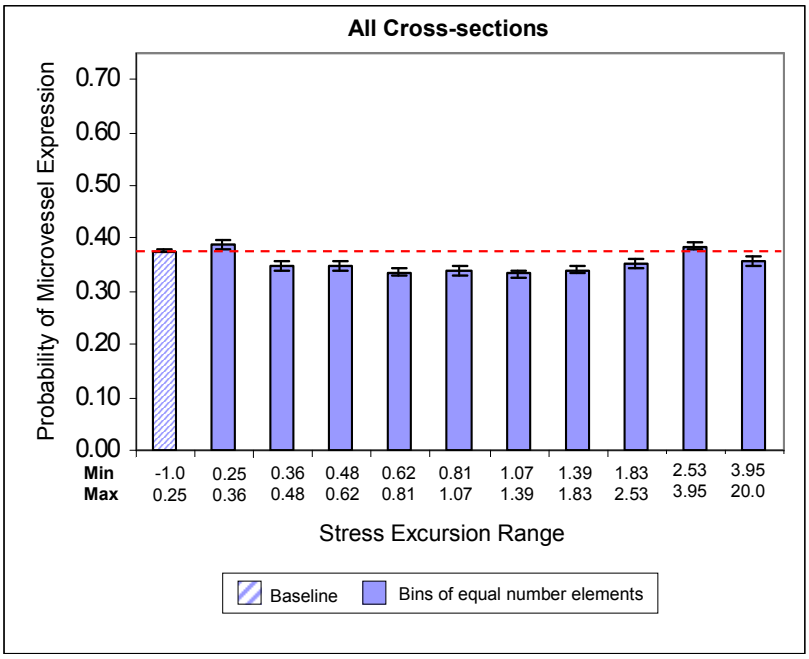

Figure 4.30 Probability of Microvessel expression as a function of stress excursion over all cross-sections. * Significantly greater than baseline, † Significantly greater than preceding bin

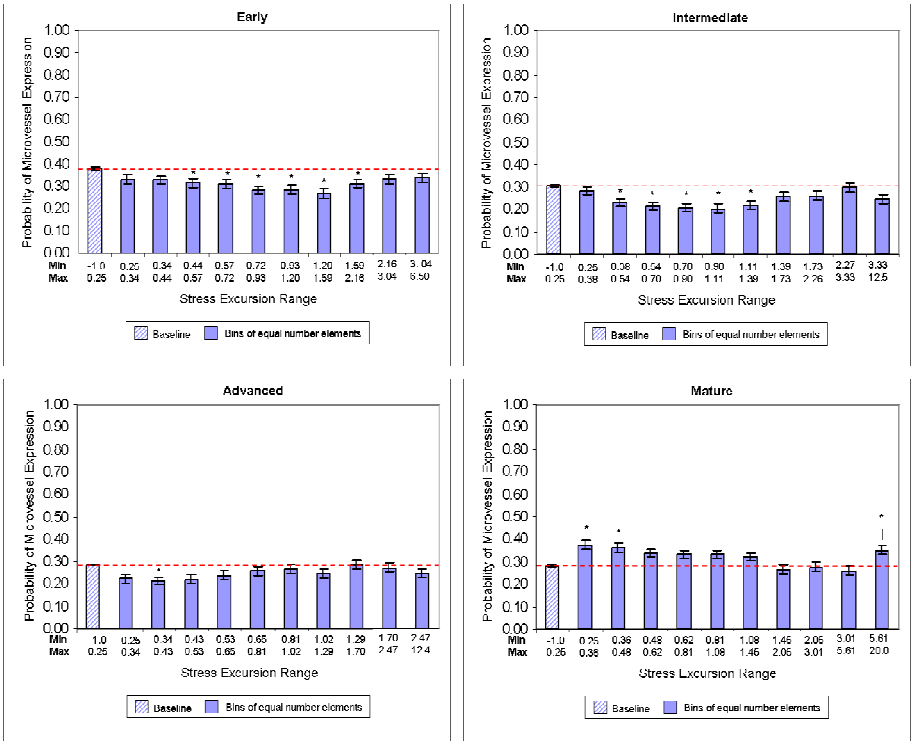

Figure 4.31 Probability of Microvessel expression as a function of stress excursion over all cross-sections. * Significantly greater than baseline, † Significantly greater than preceding bin

Collocation of Microvessels and von Mises Strain

Microvessels showed a weak, mixed dependence on strain. Figure 4.32 shows the probability of microvessel expression as a function of strain excursion (ANOVA, $p=0.02$). No bins showed expression probability significantly different from the baseline.

When the data was subdivided into disease categories, a stronger dependence on strain was found for some categories, as shown in Figure 4.33 (ANOVA, intermediate: $p=0.2$; early, advanced, and mature: $p<0.001$). In early plaque, microvessel expression decreased monotonically with increasing strain excursion. In intermediate plaque, no clear trend was seen. In advanced plaque, microvessel expression increased monotonically with increasing strain excursion, with particularly strong increases in the highest-strain bins. Expression in mature plaque followed a trend similar to the trend in advanced plaque, but there was also an increase in microvessel expression at low-moderate strain excursions.

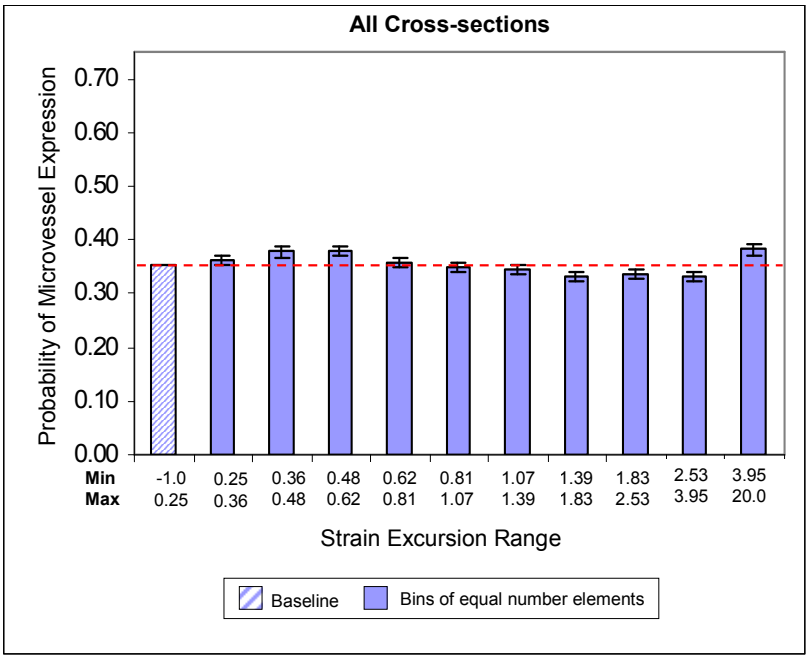

Figure 4.32 Probability of Microvessel expression as a function of strain excursion over all cross-sections. * Significantly greater than baseline, † Significantly greater than preceding bin

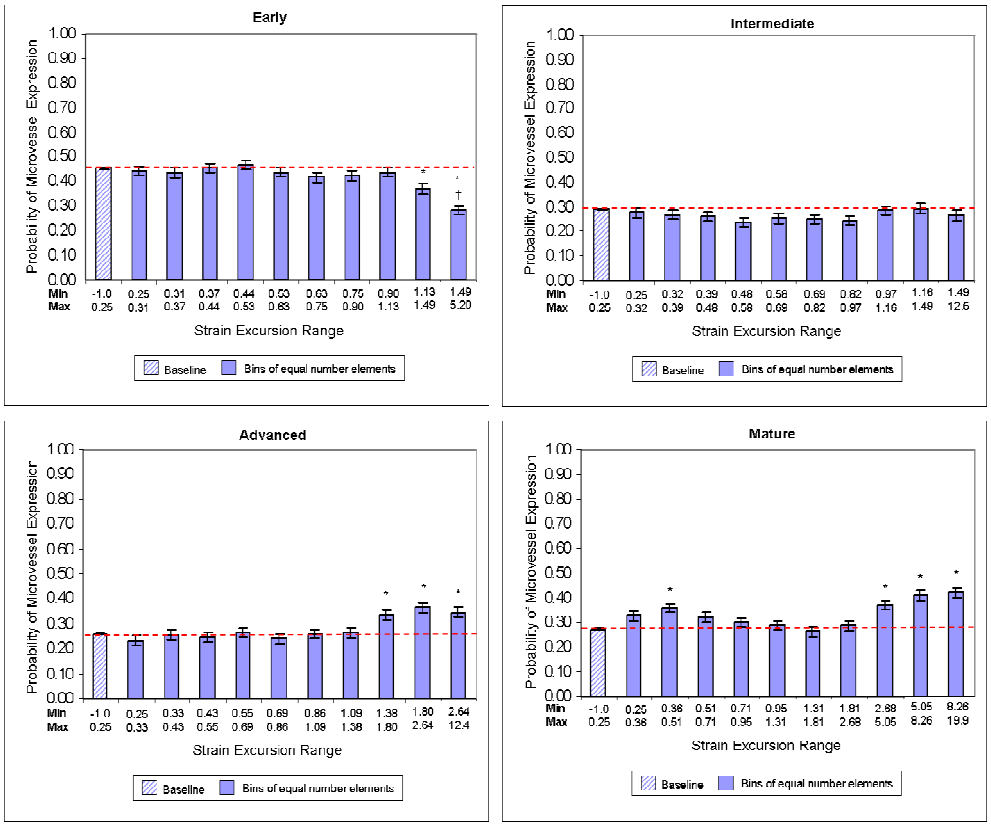

Figure 4.33 Probability of Microvessel expression as a function of strain excursion over all cross-sections. * Significantly greater than baseline, † Significantly greater than preceding bin

CO-EXPRESSION OF INFLAMMATORY MARKERS

To determine whether the inflammatory markers considered in this study were co-expressed, the spatial distribution of each of the five markers was compared with the spatial distribution of each of the other four markers. This comparison was performed for all cross-sections together and also for each disease category.

As discussed in Chapter 3, for each marker, elements were divided into two groups – either positive or negative – based on the presence of that marker. Then for each group, the proportion of elements positive for each of the remaining four markers was determined. These proportions can be found in Table A.2 – A.6 in the appendix. A two-proportion test was used to compare the proportions of the positive and negative groups. The results of this analysis are presented here.

Overall, activated NF-kB was found to be co-expressed with macrophages, MMP-1, and Nitrotyrosine, but was not co-expressed with microvessels. Table 4.2 shows the co-expression of NF-kB and each of these other four markers for all cross-sections, as well as for each disease category. For a given marker, a significant P-value means that elements expressing NF-kB were significantly more likely to express that marker than elements not expressing NF-kB. NF-kB showed significant co-expression with macrophages in intermediate and advanced plaque – the stages of plaque progression where large numbers of macrophages were present. In contrast, NF-kB was not co-expressed with macrophages in early and mature plaque – plaque where macrophages are much less prevalent. NF-kB showed significant co-expression with nitrotyrosine for all disease categories. NF-kB showed significant co-expression with MMP-1 in all stages of plaque progression except intermediate plaque. While NF-kB showed no significant co-

expression with microvessels overall, NF-kB did show co-expression with microvessels in the later stages of plaque progression.

Table 4.2 Co-expression of NF-kB and other inflammatory markers

Co-expression of **NF-κB** and other markers			
Marker	***Category***	***P-value***	***Significant?***
Macrophages	**All**	**p<0.001**	yes
	Early	p=0.98	no
	Intermediate	p<0.001	yes
	Advanced	p<0.001	yes
	Mature	p=0.53	no
MMP1	**All**	**p<0.001**	yes
	Early	p<0.001	yes
	Intermediate	p=0.52	no
	Advanced	p<0.001	yes
	Mature	p<0.001	yes
Nitrotyrosine	**All**	**p<0.001**	yes
	Early	p<0.001	yes
	Intermediate	p<0.001	yes
	Advanced	p<0.001	yes
	Mature	p<0.001	yes
Microvessels	**All**	**p=0.30**	no
	Early	p=0.08	no
	Intermediate	p=0.33	no
	Advanced	p<0.001	yes
	Mature	p<0.001	yes

As shown in Table 4.3, macrophages showed overall co-expression with NF-kB and Nitrotyrosine, but no co-expression with MMP-1 and microvessels. As expected based on the results for NF-kB in Table 4.2, macrophages and NF-kB were co-expressed in intermediate and advanced plaque, but were not significantly co-expressed in early and mature plaque. While macrophages did not show an overall collocation with MMP-1, analysis of each disease category showed that macrophages were co-expressed with MMP-1 in all stages of plaque progression except early plaque. Macrophages were co-

Table 4.3 Co-expression of Macrophage and other inflammatory markers

Co-expression of **Macrophage** and other markers			
Marker	***Category***	***Significant?***	***P-value***
NF-κB	**All**	yes	p<0.001
	Early	no	p=1
	Intermediate	yes	p<0.001
	Advanced	yes	p<0.001
	Mature	no	p=0.47
MMP1	**All**	no	p=0.26
	Early	no	p=0.70
	Intermediate	yes	p<0.001
	Advanced	yes	p<0.001
	Mature	no	p=0.003
Nitrotyrosine	**All**	no	p=0.008
	Early	no	p=0.14
	Intermediate	yes	p<0.001
	Advanced	no	p=0.811
	Mature	no	p=0.01
Microvessels	**All**	no	p=1
	Early	no	p=0.069
	Intermediate	no	p=0.98
	Advanced	no	p=0.90
	Mature	no	p=0.99

expressed with nitrotyrosine in intermediate and mature plaque, but not in early and advanced plaque. Surprisingly, macrophages showed no collocation with microvessels for any disease category.

Overall, MMP-1 showed strong co-expression with NF-kB, Nitrotyrosine, and microvessels, as shown in Table 4.4. While the overall co-expression of MMP-1 and macrophages was not significant, MMP-1 and macrophages were found to be co-expressed in all plaques except early plaque when disease categories were considered separately. Co-expression of MMP-1 with nitrotyrosine and microvessels was found in all disease categories, and co-expression of MMP-1 with NF-kB was found in all categories except intermediate.

Table 4.4 Co-expression of MMP-1 and other inflammatory markers

Co-expression of **MMP1** and other markers			
Marker	***Category***	***Significant?***	***P-value***
Macrophages	**All**	no	p=0.081
	Early	no	p=0.772
	Intermediate	yes	p<0.001
	Advanced	yes	p<0.001
	Mature	yes	p<0.001
NF-κB	**All**	yes	p<0.001
	Early	yes	p<0.001
	Intermediate	no	p=0.509
	Advanced	yes	p<0.001
	Mature	yes	p<0.001
Nitrotyrosine	**All**	yes	p<0.001
	Early	yes	p<0.001
	Intermediate	yes	p<0.001
	Advanced	yes	p<0.001
	Mature	yes	p<0.001
Microvessels	**All**	yes	p<0.001
	Early	no	p=0.039
	Intermediate	yes	p<0.001
	Advanced	yes	p<0.001
	Mature	no	p=0.031

Overall, nitrotyrosine was found to be co-expressed with all other markers, as shown in Table 4.5. When each disease category was considered separately, nitrotyrosine was found to be co-expressed with macrophages in intermediate and mature plaque, but not in advanced plaque. Nitrotyrosine was co-expressed with NF-kB in all but mature plaque, and was co-expressed with MMP-1 in all disease categories. Nitrotyrosine was co-expressed with microvessels only in early and advanced plaque.

Table 4.5 Co-expression of Nitrotyrosine and other inflammatory markers

Co-expression of **Nitrotyrosine** and other markers			
Marker	***Category***	***Significant?***	***P-value***
Macrophages	**All**	yes	p<0.001
	Early	no	p=0.10
	Intermediate	yes	p<0.001
	Advanced	no	p=0.16
	Mature	yes	p<0.001
NF-κB	**All**	yes	p<0.001
	Early	yes	p<0.001
	Intermediate	yes	p<0.001
	Advanced	yes	p<0.001
	Mature	no	p=0.053
MMP1	**All**	yes	p<0.001
	Early	yes	p<0.001
	Intermediate	yes	p<0.001
	Advanced	yes	p<0.001
	Mature	yes	p<0.001
Microvessels	**All**	no	p=0.037
	Early	yes	p=0.001
	Intermediate	no	p=1.0
	Advanced	yes	p<0.001
	Mature	no	p=0.828

Microvessels showed significant overall co-expression with both MMP-1 and nitrotyrosine, but surprisingly, did not show significant overall co-expression with macrophages or NF-kB. When each disease category was considered separately, microvessels were found to collocate with macrophages only in the earliest plaque. In contrast, macrophages collocated with NF-kB and with MMP-1 only in the later stages of plaque development. Results were mixed with respect to nitrotyrosine – microvessels and nitrotyrosine collocated in early and advanced plaque, but did not collocate in intermediate and mature plaque.

Table 4.6 Co-expression of Microvessels and other inflammatory markers

Co-expression of **Microvessels** and other markers			
Marker	***Category***	***Significant?***	***P-value***
Macrophages	**All**	no	p=1.0
	Early	no	p=0.026
	Intermediate	no	p=0.986
	Advanced	no	p=0.745
	Mature	no	p=1.0
NF-κB	**All**	no	p=0.10
	Early	no	p=0.074
	Intermediate	no	p=0.72
	Advanced	yes	p<0.001
	Mature	yes	p<0.001
MMP1	**All**	yes	p<0.001
	Early	no	p=0.056
	Intermediate	yes	p<0.001
	Advanced	yes	p<0.001
	Mature	no	p=0.047
Nitrotyrosine	**All**	no	p=0.004
	Early	yes	p=0.001
	Intermediate	no	p=1.0
	Advanced	yes	p<0.001
	Mature	no	p=0.805

Based on the co-expression results presented above, some pairs of markers showing significant co-expression were selected for further analysis of co-expression with respect to stress.

Co-expression of NF-kB and Macrophages. Figure 4.34 show the probability of the co-expression of NF-kB and macrophages as a function of stress excursion for intermediate and advanced plaque. Because NF-kB and macrophages were found to be co-expressed in intermediate and advanced plaque, but not in early and mature plaque (Table 4.2 and Table 4.3), analysis focused only on the intermediate and advanced categories. NF-kB and macrophages were more likely to be co-expressed at higher stresses in intermediate and advanced plaque, as shown in Figure

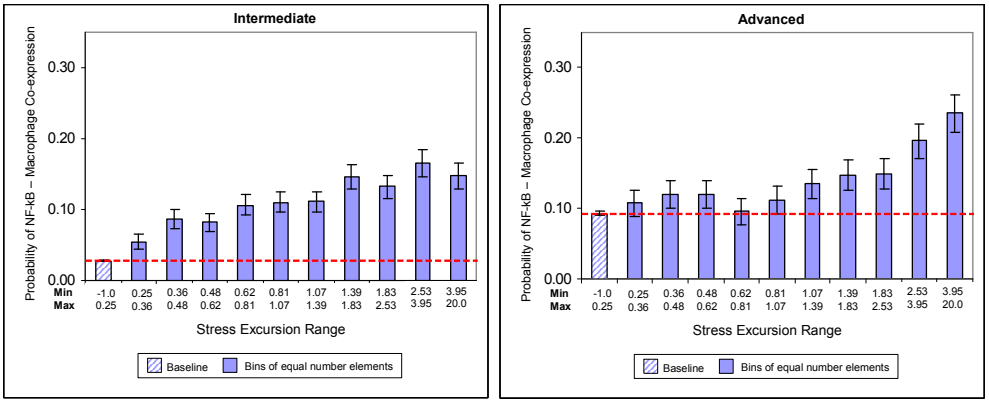

Figure 4.34 Probability of NF-kB and Macrophage Co-expression as a function of stress excursion for intermediate (left) and advanced (right) plaque.

4.34. For both categories, trend of monotonically increasing co-expression with increasing stress-excursion was found. Compare these trends with the trends of NF-kB alone with respect to stress (Figure 4.11) and macrophages alone with respect to stress (Figure 4.16). Because both NF-kB and macrophages alone monotonically increased with increasing stress for advanced plaque (Figure 4.11 and Figure 4.16), it is no surprise that their co-expression also increased with increasing stress. Note, however, that in Figure 4.16, for intermediate plaque, the probability of macrophage presence dropped significantly. However, while NF-kB and macrophage co-expression leveled off at highest stresses, there was not a significant drop in co-expression. This indicates that the trends in Figure 4.34 are not simply mirrors of the trend for macrophages alone.

Co-expression of NF-kB and MMP-1. As shown in Figure 4.35, the probability of NF-kB and MMP-1 co-expression increased with increasing stress for advanced plaque, but decreased with increasing stress for mature plaque. No real trend was seen in early plaque. The trend in intermediate plaque is also shown here for completeness: co-

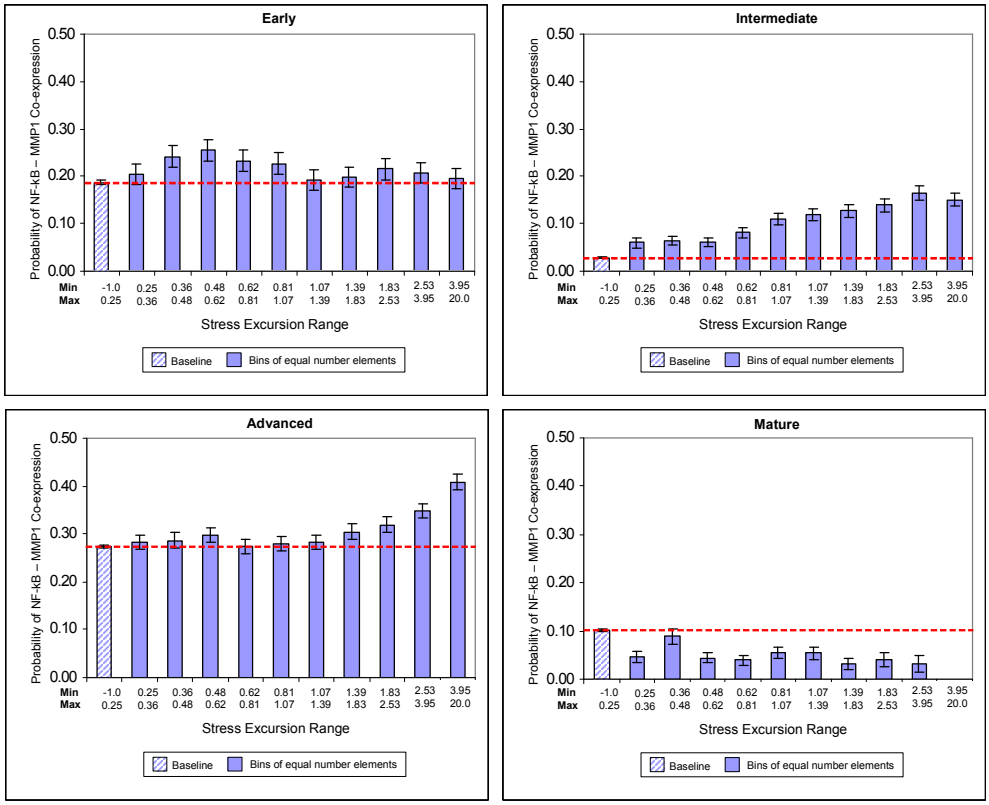

Figure 4.35 Probability of NF-kB and MMP-1 Co-expression as a function of stress excursion for each disease category.

expression increased with increasing stress; however, in general, NF-kB and MMP-1 were not significantly co-expressed in these plaques (Table 4.2, Table 4.4 above).

We can compare these trends with the trends of NF-kB only with respect to stress (Figure 4.11) and MMP-1 only with respect to stress (Figure 4.21). For advanced plaque, both markers alone monotonically increased with increasing stress for advanced plaque, so it is no surprise that their co-expression also increased with increasing stress. However, the trends in Figure 4.35 for early and mature plaque are quite different from the trends seen in Figures 4.11 and 4.21. When considered alone, MMP-1 expression greatly increased at highest stress excursions, but no such peak is seen here for co-expression of MMP-1 and NF-kB. For mature plaque, NF-kB expression greatly

increased for increasing stress, while MMP-1 expression greatly decreased with increasing stress. The co-expression trend follows the trend for MMP-1 alone, suggesting that when MMP-1 is expressed, NF-kB is also expressed but that the reverse is not true.

Macrophages and MMP-1 co-expression. As shown in Figure 4.36, macrophage and MMP-1 co-expression with respect to stress followed the same trends seen for macrophages alone for all disease categories (Figure 4.16). As expected, no trend was seen in early plaque since macrophages are present in these plaques only in very low levels.

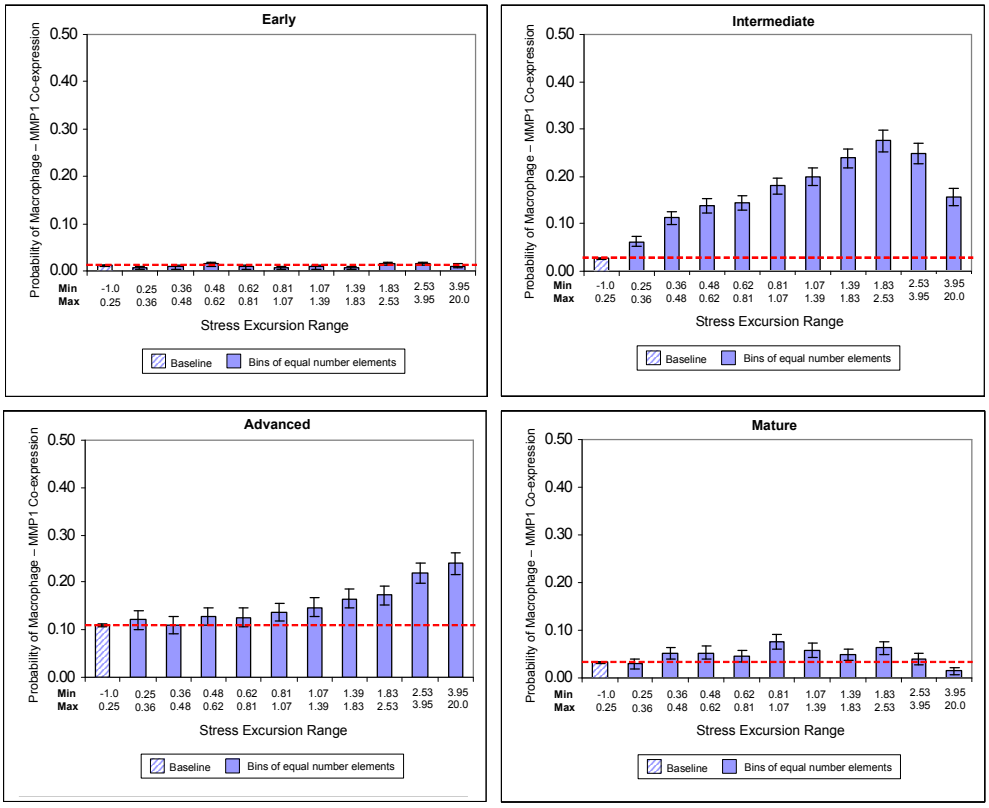

Figure 4.36 Probability of Macrophage and MMP-1 Co-expression as a function of stress excursion for each disease category.

NF-kB and Nitrotyrosine co-expression. NF-kB and nitrotyrosine co-expression increased with increasing stress for all disease categories except early plaque, as shown in Figure 4.37. This trend is of interest, since nitrotyrosine alone showed very little dependence on stress (Figure 4.24). The trends shown in Figure 4.37 for NF-kB and nitrotyrosine co-expression are very similar to the trends seen for NF-kB expression alone (Figure 4.11).

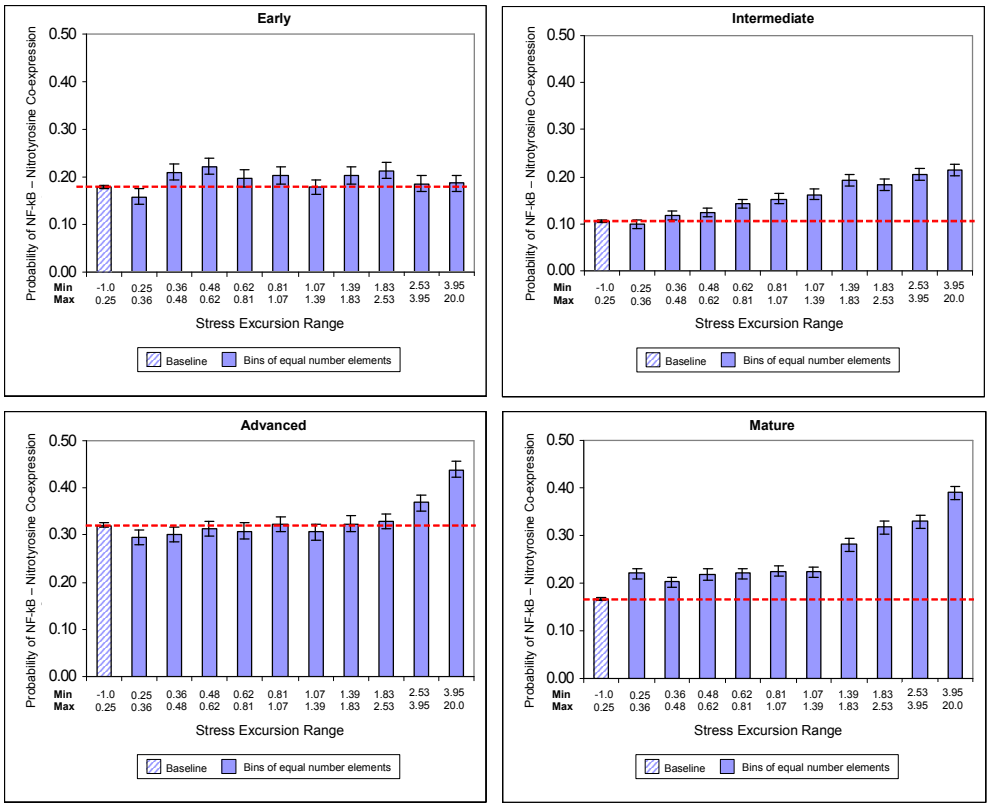

Figure 4.37 Probability of NF-kB and Nitrotyrosine Co-expression as a function of stress excursion for each disease category.

MMP-1 and Nitrotyrosine co-expression. MMP-1 and nitrotyrosine increased with increasing stress for intermediate and advanced plaque, but showed little relationship to stress for early and mature plaque(Figure 4.38). For intermediate and advanced plaque, the trends seen are very similar to the trends seen for MMP-1 alone (Figure 4.21). Interestingly, for advanced plaque, the probability of MMP-1 and nitrotyrosine expression did not decrease with increasing stress, even though the probability of MMP-1 expression alone significantly decreased for increasing stress.

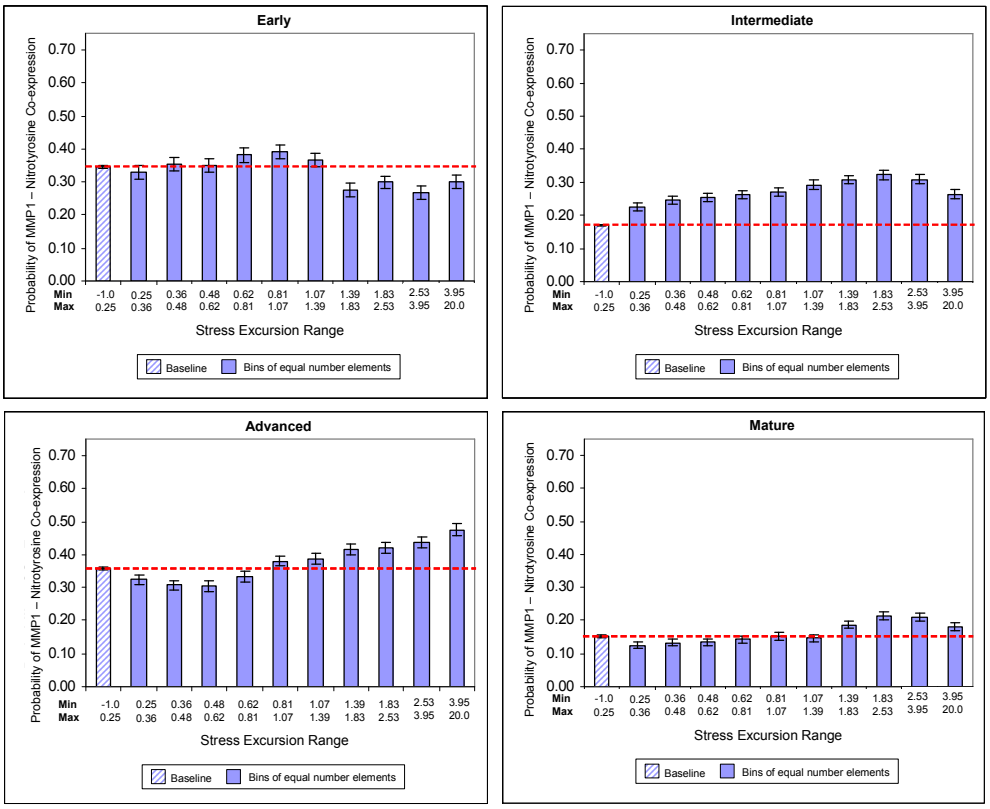

Figure 4.38 Probability of MMP-1 and Nitrotyrosine Co-expression as a function of stress excursion for each disease category.

CHAPTER 5

DISCUSSION

Cells within the vascular wall are subjected to mechanical loads due to contact with the surrounding extracellular matrix. These cells are capable of sensing mechanical stimuli and converting these stimuli to biochemical signals that lead to a variety of cellular responses, including induction or upregulation of inflammation. In addition, the inflammatory response is involved in vascular remodeling through the regulation of ECM turnover. Thus, the mechanical environment may stimulate inflammation, while the inflammatory response may also change the local mechanical environment within the vessel wall through remodeling.

In this study we hypothesized that there are spatial relationships between the local mechanical environment and expression of markers of inflammation. We further hypothesized that these relationships are plaque progression dependent. To test these hypotheses, we analyzed cross-sections at regular intervals along the length of human coronary atherosclerotic arteries. For each cross-section, a 2D heterogeneous finite element model was developed to determine the spatial distribution of stress in the cross-section. In addition, novel techniques for quantifying inflammatory markers at high spatial resolution were used to determine the distributions of a set of inflammatory markers. The distributions of stress and inflammation were then compared to determine whether a spatial relationship exists.

Because fresh human diseased tissue was used, the results of this study relate directly to human disease. This is a significant advantage over animal models and cell

culture studies, which have limited application to actual human pathology. In addition, because we were able to obtain fresh tissue within 2-4 hours of removal from heart transplant patients, we were able to control the tissue almost immediately from the time of removal from the body.

However, the use of tissue from human patients also means that we have no control over the tissue before it is harvested from the explanted heart. The artery provides a snap-shot of what is occurring at the time of removal. Therefore, it is not possible to control inputs to the artery and study the effects of these inputs over time. This makes it difficult to definitively determine causal effects. Thus, while we propose logical causal mechanisms in the following discussion, we recognize that collocation does not necessarily imply causation.

The results of this study are given in the previous chapter, and are discussed below. The discussion first focuses on mechanical modeling, followed by the quantification of the spatial distributions of inflammatory markers. The remainder of the chapter then focuses on the comparison of the spatial distributions of mechanical stress and inflammatory markers. Lastly, the significance of this work is discussed.

SPECIFIC AIM 1: MECHANICAL MODELLING

A histology-based two-dimensional heterogeneous finite element model was developed to determine the mechanical stress distributions in cross-sections of diseased arteries. The results of our model agree with the general trends found in previous finite element studies of diseased arteries (see Table 1.2 for a list of previous finite element studies).

As previously observed (Hayashi and Imai 1997), our models showed that stress in early and intermediate plaque is fairly uniformly distributed around the circumference of the lumen (Figure 4.2 A and B). This is expected, since the structures of these arteries are much more homogeneous and less eccentric relative to later stage plaques. Also as found in previous studies (Cheng et al 1993, Lee et al 1993, Keeny and Richardson 1987, Beattie et al 1998, Imoto et al 2005, Finet et al 2004, Li et al 2005, Huang et al 2001), stress in advanced plaque is concentrated in the fibrous cap and shoulder regions (Figure 4.2C), while in mature plaque stress is shifted to the relatively plaque-free portion of the vessel wall opposite the bulk of the plaque (Figure 4.2D). This difference in stress distribution between advanced and mature plaque is most likely due to the fact that advanced plaque are characterized by large lipid pools, while mature plaque are characterized by large calcium deposits (Figure 4.1 C and D). In advanced plaque, the soft lipid core is unable to bear mechanical loads, and thus the load is shifted to the fibrous cap and shoulder region. However, in mature plaque, the lipid core is replaced by rigid calcification, which helps reinforce the cap. In addition, because of the thick, rigid plaque bulk, stresses are shifted to the thinner elastic wall opposite the bulk of the plaque.

Our model provides increased confidence in the resulting spatial distributions of stress relative to previous models in the literature by more accurately representing the in vivo arterial geometry and plaque microstructure. Accurate spatial distributions are imperative when comparing the local mechanical environment with locally expressed biological markers.

For physiologically meaningful stress results, it is essential that finite element models are based on geometries that approximate the in vivo state as closely as possible,

and that the arterial microstructure is modeled as accurately as possible. As discussed in Chapter 1, histology is currently the gold standard for obtaining geometries of diseased arteries for finite element analysis. However, histologic processing introduces distortions in geometry. While previous histology-based models used paraffin embedded tissue and in most cases non-pressure fixed tissue, which is subject to large geometric distortions, this study limited histologic distortions by using pressure-fixed MMA-embedded tissue, so that the model geometries obtained from histologic cross-sections more closely represent the in vivo vessel geometry.

In addition, the models developed here include heterogeneity of the plaque microstructure that, to our knowledge, has been neglected in previous models. As discussed in Chapter 3, the heterogeneous microstructure is modeled by using a semi-automatic segmentation algorithm to segment images of the cross-sections into constituents pixel-by-pixel, and then using rule-of-mixtures to assign material properties to individual elements based on the constituent material properties and their area fractions within each element. In contrast, previous studies have manually divided the plaque into discrete constituent regions, and each region was meshed separately. Our method improves on these previous models in two ways. First, our method includes the effects of intermixing of constituents or small deposits of one constituent within another constituent. Because previous models meshed each constituent region separately, it was necessary to limit the number of separate constituent regions, making it impossible to include intermixing effects. Also, in these models it was not possible to include very small constituent regions, due to the difficulty of obtaining a good-quality mesh for such small areas. Secondly, our segmentation method is less subjective than previous methods.

As mentioned, while previous studies have manually segmented images, we used a semi-automatic segmentation approach. Because there are not always clearly distinguishable constituent regions within plaque, manual segmentation of plaque microstructure is quite subjective. However, in this study, subjectivity was limited by using a "trained" algorithm to segment the microstructure of each cross-section pixel-by-pixel based on image RGB values.

Limitations of Specific Aim 1. There are several limitations to the developed mechanical models. First of all, while the use of pressure-fixation is necessary in order to obtain physiologically accurate model geometries, use of this technique means that stresses cannot be determined based on the zero stress state. Justification for this approach is given in Chapter 3. However, this method is not suitable for applications where the absolute rather than the relative spatial distributions of stress are required.

In addition, while both pressure-fixation and MMA embedding are essential in limiting geometrical distortions, use of these tissue processing methods limit the histologic markers that can be considered. Some histologic techniques (i.e. in situ zymography) cannot be applied to fixed tissue, and we have also found that some antibodies are not as effective in acrylic tissue sections. Furthermore, even with pressure fixation and MMA embedding, differences may be present between the obtained geometry and the actual in vivo geometry. While the techniques used here are currently the best available, advances in medical imaging technology may eventually allow direct in vivo determination of vessel geometry and microstructure.

Although there is substantial anisotropy present in plaque, data on anisotropic material properties of plaque constituents is not currently available, and therefore,

isotropic material properties were used. In addition, the rule-of-mixtures for determining material properties is a simplification that ignores directional effects present within the plaque such as the orientation or disorganization of collagen fibers. This method also ignores structural interactions among constituents and variations in constituent biochemistry.

While significant residual stresses due to differences in strains among plaque constituents may be present within plaque, no technique is currently available to quantify these stresses in geometrically complex diseased arteries. In addition, the effects of axial stretch may be substantial, but because no information on axial stretch of these vessels was available to us, the effects of axial stretch were not included in our analysis. Because we are focused on the *relative* spatial distributions of stress, we expect that ignoring axial stretch does not affect the conclusions of this study.

Mechanical models in this study are two dimensional, and assume plane strain. However, plaque geometries may vary significantly in the axial direction. Comparison with results of three dimensional stress analyses are needed to determine in which cases the 2D plane strain assumption is reasonable and the calculated stress distributions are correct.

Lastly, the loading conditions used in the developed model are valid only for plaques of low to moderate stenosis. In the case of severe stenosis, loading conditions are more complex due to pressure drop across the stenosis and possible negative pressure downstream of the stenosis.

SPECIFIC AIM 2: QUANTIFICATION OF SPATIAL DISTRIBUTIONS OF INFLAMMATORY MARKERS

In this study, a novel method for determining high resolution spatial distributions of inflammatory markers in cross-sections of diseased human coronary arteries was developed. Briefly, as discussed in Chapter 3, inflammatory markers of interest were identified by immunohistochemistry, and cell-tagging or color image thresholding was used to identify locations of positive staining in the cross-section. Then, the same mesh used for finite element analysis of the cross-section in Aim 1 was overlaid on the immunostained image, and cell densities or area fractions were calculated for each element in the mesh.

The developed technique has several advantageous features. First, using the same finite element mesh used in determining spatial distributions of stress facilitates direct comparison of inflammatory marker distributions with mechanical stress. In addition, because the spatial resolution is coupled to the fineness of the finite element mesh, the resolution that can be obtained is limited only by alignment errors between cross-sections (As discussed in Chapter 3, the lower limit of element size is set so that elements are substantially larger than the cross-section alignment error).

Lastly, while this method was designed here to facilitate comparison of inflammatory markers with mechanical stress, its application is not limited to these variables. Instead, these techniques may be more broadly applied to spatial comparisons of any two variables, immunohistochemical, structural, or otherwise, that are distributed within the cross-section.

Limitations of Specific Aim 2. The method developed here for determining the spatial distribution of inflammatory markers is still semi-quantitative. There is some uncertainty in cell densities due to the difficulty of identifying individual cells when they are present in tight clusters. In addition, immunohistochemistry is not capable of determining exact concentrations of immunological expression. Still, this method gives a relative measure of the distribution of inflammatory markers, and does so at much higher resolution than previous studies.

The spatial distributions determined here do not take into account regional variation in cellularity within the cross-section. These differences in cell density may have an effect on the determined spatial distributions. Also, in determining the spatial distribution of non-cellular markers (NF-kB, MMP-1, Nitrotyrosine), we did not include information on the cell types in which these markers are expressed. This information could be valuable in determining how different cell types within plaque respond to stress, and should be considered in future studies.

SPECIFIC AIM 3: COMPARISON OF SPATIAL DISTRIBUTIONS OF INFLAMMATION AND MECHANICAL STRESS

The goal of this aim was to use the methods developed in Aim 1 and Aim 2 to address the overall hypotheses of this work: that spatial relationships exist between markers of inflammation and the mechanical environment in human atherosclerotic plaque, and that these relationships are plaque progression dependent. In this section, the comparison of the spatial distributions of inflammation and mechanical stress will be discussed in detail.

Each inflammatory marker will be discussed in turn – NF-κB, macrophages, MMP-1, nitrotyrosine, and microvessels. For each marker, first the overall expression of the marker will be considered. Then, the spatial relationship between the marker expression and mechanical stress and strain will be discussed. This will be followed by a discussion of the implications of any spatial relationships for plaque progression and plaque rupture.

After discussing each marker in turn, the co-expression of the markers will be considered. This discussion will be framed in terms of hypotheses for mechanisms relating markers to other markers and to stress, and the data will be used to either lend support to or detract from these hypotheses.

It has been shown that growth and remodeling in arteries correlate better with stress than strain (Taber and Humphrey 2001), and it is established practice in the field of vascular biomechanics to use stress rather than strain in the development of growth and remodeling laws (Humphrey 2002). Therefore, the discussion here will focus primarily on relationships between inflammatory markers and mechanical stress, although relationships with strain are included for completeness.

Nuclear Factor – kappa B

Overall Expression of NF-κB

Activated NF-κB, a transcription factor that initiates and maintains the inflammatory response through the regulation of a large number of genes (Kumar et al. 2004), was expressed in all stages of plaque progression (Figure 5.9), although its expression was highest in early and mature plaque. Because it has previously been

implicated in atherogenesis, it is not surprising that it was highly expressed in its activated form in the early stage of plaque development. Also, the fact that it was found in substantial levels in intermediate and advanced plaque indicates that it continues to play a role throughout plaque progression. However, it was quite surprising that activated NF-κB was found in relatively high levels in mature plaque, since these highly calcified plaques are typically thought to be senescent and biologically inactive. However, comparison of NF-κB expression with mechanical stress and strain distributions yielded possible explanations as to why NF-κB was so highly expressed in these mature plaques, as discussed below.

Comparison of Spatial Distributions of NF-κB and Mechanical Stress

This study found that the probability of NF-κB expression is greater in locations where stress is elevated, and that this probability increases monotonically with increasing stress (Figure 4.10). In addition, this trend is strengthened as plaques progress (Figure 4.11). To the best of our knowledge, this is the first study to spatially relate expression of activated NF-κB and mechanical stress in diseased human arteries.

These results strongly support the role of mechanics in instigating and maintaining the inflammatory process. As mentioned above, NF-κB is a transcription factor that, when activated, initiates and maintains the inflammatory response through the regulation of many genes, which can in turn lead to expression of other markers (Kumar et al. 2004). For instance, NF-κB expression may stimulate monocyte chemotactic protein-1 (MCP-1) expression, leading to macrophage recruitment. Thus, the fact that the probability of NF-κB expression is greater when stresses are higher directly links mechanical stress to the initiation and maintenance of inflammation in plaque.

NF-κB expression increases with increasing stress in all stages of plaque development, and this trend becomes stronger as plaques progress. While NF-κB expression has often been implicated in atherogenesis, these results show that the relationship between mechanics and NF-κB expression is involved in all stages of atherosclerotic plaque progression. In addition, while the probability of NF-κB expression increases with increasing stress in all categories, this trend is particularly strong in mature plaque. There was also a higher overall expression of NF-κB in mature plaque than in intermediate or advanced plaque. This was surprising, since mature plaques are typically considered to be stable and senescent, with less inflammation.

A closer look at the actual spatial distributions of NF-κB expression and stress yields insight into these results. While stresses in early and intermediate plaque are fairly evenly distributed around the circumference (Figure 4.2 A and B), stresses in advanced plaque (Figure 4.2C) are concentrated in the shoulder and fibrous cap regions, and NF-κB expression is also high in these regions. While stresses in advanced plaque were high in the shoulder and fibrous cap, high stresses in mature plaque were shifted to the relatively plaque-free portion of the vessel wall opposite the bulk of the plaque, as discussed above (Figure 4.2D), and NF-κB expression is also quite high in the opposite wall (Figure 4.4D). We conjecture that the shifting of stresses due to calcification leads also to a shifting and possibly new surge in NF-κB activation. This phenomenon helps explain the very strong trend seen in the data for the mature category, and highlights the spatial link between NF-κB expression and mechanical stress. We also speculate that this increase in NF-κB expression in the opposite wall may eventually lead to a new “wave” of

inflammation and remodeling in a plaque that appears to be stable and static. Further work is needed to determine whether this surge actually occurs.

Comparison of Spatial Distributions of NF-κB and Mechanical Strain

NF-κB expression, with the exception of mature plaque, showed a weaker dependence on strain than stress (Figure 4.12 and 4.13). This discrepancy is due to the fact that, as can be seen in Figures 4.2, stresses are higher in elements proximal to the lumen, while strains do not depend as strongly on proximity to the lumen. This trend occurs because the lumen is surrounded by fibrous plaque, while the media is more distant from the lumen. Elements consisting primarily of fibrous plaque tissue have a higher elastic modulus than elements consisting primarily of media, and since stress is the product of the elastic modulus and strain, for equal strain, stress is higher in fibrous plaque than in the media.

In light of this, there are several possible reasons why NF-κB correlates more strongly with stress than strain. First of all, cells expressing NF-κB may be inherently more likely to be found in fibrous tissue than in the media. However, because NF-κB can be expressed in both SMCs (found in large numbers in the media), and macrophages (found primarily in fibrous plaque), there is no reason to believe that this is the case.

Another possibility is that the cells found in the fibrous matrix are more sensitive to mechanical stretch than cells embedded in the media. Macrophages may more readily activate NF-kB in response to strain than SMCs. Also, it is known that smooth muscle cells are capable of exhibiting a spectrum of phenotypes – from contractile to synthetic to proliferative. In the intima most SMCs exhibit some degree of a synthetic or proliferative phenotype, while most medial smooth muscle cells exhibit a “contractile” phenotype

(Shenahan and Weissberg 1998). It may be these synthetic and proliferative cells in the plaque tissue are more sensitive to strain than the contractile cells in the media. Further research is needed to determine if this is the case.

Implications for plaque progression and plaque rupture

What does it mean that activated NF-κB expression increases with increasing stress? First of all, the fact that NF-kB expression increases with increasing stress in all four disease categories indicates that this is a general relationship that is important throughout the disease process; it is not specific to a certain disease state. Also, as mentioned above, these results suggest that mechanical stress, while not the only stimulus, is a stimulus for initiating and maintaining the inflammatory response.

This has implications for remodeling and plaque progression. It has long been known that arteries remodel in response to changes in stress within the wall. Because NF-κB controls a large number of genes, the connection found here between the mechanical environment and NF-κB expression helps explain how a mechanical input is able to direct the complex biological changes of remodeling. Activation of NF-κB by mechanical stress could provide the link between mechanotransduction leading to activation of NF-κB (Lehoux 2006) and the inflammatory signaling cascade beginning with NF-κB activation and leading to expression of MMPs, matrix synthesis, cell proliferation, or apoptosis

NF-κB is an important regulator of apoptosis, and thus the strong expression of NF-κB at high stresses provides a link between the mechanical environment and cell survival/cell death. As mentioned in Chapter 1, in most cases, NF-κB is thought to have a pro-survival, anti-apoptotic effect, but in some situations it has been shown to increase a

cell's sensitivity to apoptotic stimuli. Its effect is thought to depend on the environment and cell type in which it is expressed. Thus, expression of NF-κB at high stress may be an attempt by the cell to protect itself from apoptosis in this high stress environment. On the other hand, it may also be the cell's attempt to go through apoptosis in order to avoid necrosis that would lead to further inflammation.

The impact of NF-kB expression on cell survival may be different in different cells. This is supported by the fact that the probability of NF-κB expression is increased in the highest stress elements, even though the probability of macrophages being present is dramatically decreased in these elements. This trend will be discussed in detail later, but this result suggests that NF-κB is successful in protecting smooth muscle cells or other cell types (T-cells, mast cells, and dendritic cells are also present in plaque at very low concentrations) at very high stresses, while macrophages either die or do not migrate to regions of very high stress. Further research is needed to determine if this is indeed the case.

The relationship between NF-kB and stress also has implications for plaque rupture. In this study, we found that both mechanical stress and NF-kB were often concentrated in the shoulder and fibrous cap of advanced plaque (Figure 4.2C, Figure 4.4C). Also, as discussed later, NF-kB was co-expressed with MMP-1 (the primary enzyme that breaks down fibrillar collagen) in advanced plaque (Table 4.2), and this co-expression increased with increasing stress (Figure 4.35B).Although collocation of NF-kB and MMP-1 does not necessarily mean that NF-kB is causing MMP-1 expression, it is known that NF-kB *can* stimulate MMP-1 expression. Thus, it is possible that NF-kB

expression in the fibrous cap due to increased stresses leads to expression of MMP-1, degradation of the plaque cap, and subsequent plaque rupture.

Macrophages

Overall Expression of Macrophages

Macrophages, the primary cell type involved in inflammation, are found in high concentrations in intermediate and advanced plaque, but in lower concentrations in mature plaque, and in very low concentrations in early plaque (Figure 4.14). This result is interesting, although not surprising. Early plaque are relatively normal and healthy, and typically remodel slowly over the course of decades. On the other hand, intermediate and advanced plaques typically undergo substantial remodeling during a much shorter period of time. Mature plaques typically consist primarily of calcification and fibrous tissue with very low cellularity, and therefore are often considered senescent and biologically inert.

Comparison of Spatial Distributions of Macrophages and Mechanical Stress

Overall, the probability that macrophages are present increases with increasing stress for moderate stress ranges, but drops dramatically at very high stresses (Figure 4.15). This trend is very much dependent on the stage of plaque progression (Figure 4.16). In early plaque, no real relationship between macrophages and stress was seen, although there was a significant drop in macrophage expression at very high stresses. The trends of macrophage presence in both intermediate and mature plaque mimicked the overall trend of increasing with stress and then dramatically decreasing at very high stresses. On the other hand, in advanced plaque (plaques with the characteristic features

of instability), the probability of macrophage presence continued to increase even at highest stresses.

To our knowledge, only one previous study has investigated the collocation of macrophages and mechanical stress in diseased human arteries. In this study, Lee et al they found that macrophages were not increased in regions of high stress (Lee et al 1996). Our results do not agree with the results of this study. However, for reasons discussed in detail later, we believe that the limitations of the methods used in this previous study to compare spatial distributions of macrophages and stress may have precluded finding the same relationship between macrophages and stress found in our study. Also, while this previous study looked for general relationships between macrophages and stress, to our knowledge, our study is the first to consider the dependence of relationships between macrophage presence and mechanical stress on disease progression.

The relationship between the probability of macrophage presence and mechanical stress was highly progression dependent, and was seen most prominently in intermediate and advanced plaque. This is most likely due to the fact that overall macrophage density is high in intermediate and advanced plaque, while fewer macrophages are present in mature plaque, and even fewer in early plaque.

The increase in the probability of macrophage presence with increasing stress in advanced plaque was expected, since separate previous studies have reported that both macrophages (van der Wal 1994, Carr et al 1996, Pasterkamp et al 1999) and mechanical stress (Keeny and Richardson 1987, Cheng et al 1993) are concentrated in the fibrous cap and shoulder region, and our study found the same trend (Figure 4.2C, 4.5C). However, the dramatic drop in macrophage presence at highest stresses in all other disease

categories was quite unexpected. These results raise two questions: 1) Why is there such a dramatic drop in macrophages at very high stress? 2) Why is this dramatic drop at very high stress *not* seen in the more vulnerable advanced plaque?

To address the first question, there are several plausible reasons why macrophages were found to decrease at high stresses. The most obvious explanation is that very high stresses cause macrophage cell death – either by necrosis or apoptosis. In all three disease categories that showed a drop in macrophages at highest stress (early, intermediate, and advanced), this drop occurred for stresses greater than ~ 3.5 times the median. This suggests that there is a threshold stress level above which macrophages cannot survive.

Another possibility is that macrophages simply do not migrate to these very high stress regions. Macrophage infiltration of tissue is a three-step process. First, circulating monocytes (immature macrophages) in the blood stream respond to chemotactic signals by binding to adhesion molecules expressed on the endothelial surface. Next, these monocytes migrate into the vascular tissue by following additional chemotactic signals. Once they have reached their destination, they differentiate into true macrophages. It is possible that any of these three processes could be disrupted by high stress. First of all, pathologically high stresses could prevent other cells (SMCs and ECs) from producing chemotactic factors such as Monocyte Chemotactic Protein – 1 (MCP-1), so that macrophages are not attracted to regions of very high stress. Secondly, macrophages might be inherently prohibited from migrating into high stress regions (perhaps the cells sense that they would not be able to survive) even if chemotactic proteins are present. And lastly, pathologically high stresses may prevent monocytes from differentiating into monocytes in these locations.

While cell death or failure to migrate are plausible reasons for the drop in macrophage concentrations at very high stress, further research is needed to determine which of these mechanisms are playing a role, as well as other mechanisms that may contribute to the drop in macrophages at very high stress.

The second question raised by this study is: Why is this dramatic drop in macrophage presence at very high stress *not* seen in advanced plaque? This question is more difficult, and the results of this study are not sufficient to provide the answer. Plaques are structurally, biologically, and chemically complex, and mechanical stress is by no means the only factor involved in the behavior of cells within plaque. Is there some agent, biological, chemical, or otherwise, that allows macrophages to thrive at high stresses in advanced plaque, while in all other stages of plaque, they either die, migrate away from, or do not migrate to these high stress regions? Is there some other explanation for the different behavior of macrophages in advanced plaque than in other stages of plaque progression? Future studies are needed to elucidate the cause of this different behavior of macrophages at high stress in advanced plaque.

Comparison of Spatial Distributions of Macrophages and Mechanical Strain

Macrophage presence showed a different trend with increasing strain than with increasing stress. For all disease categories, the probability of macrophage presence tended to *decrease* with increasing strain (Figure 4.17). In addition, early, intermediate, and mature plaque showed a significant drop in macrophage presence at the highest strains. However, as with stresses, the trend was slightly different in advanced plaque (Figure 4.18). Although macrophages in advanced plaque decreased with increasing strain for moderate strains, there was no significant drop at highest strains. Instead, there

was a slight increase (still below baseline) at highest strain. Although further research is needed to determine why macrophage presence as related to strain is different in advanced plaque than in other stages of progression, the same conjectures discussed above with respect to stress are also valid with respect to strain.

There are several possible reasons that the trends may be different for strains than for stresses. As can be seen in Figure 4.2, and as was discussed above in the case of NF-κB, stresses tended to be higher in elements proximal to the lumen, while strains did not depend as strongly on proximity to the lumen. This occurs because the lumen is surrounded by stiff fibrous plaque, while the softer media is more distant from the lumen. Because of their different moduli, for equal strain, stresses are higher in fibrous plaque than in the media. For a migratory marker like macrophages, this trend is particularly important because, although some macrophages may enter the plaque through microvessels within the plaque or from the adventitia, most macrophages enter the plaque from the luminal bloodstream. Thus, macrophages are often found in higher concentrations near the lumen. This effect can be particularly noted in the intermediate and advanced plaque shown in Figure 5.7 and 5.8. Thus, macrophages may artificially be found to increase with increasing stress simply because stress is highest near the lumen, and macrophages are also found in higher concentrations near the lumen.

Even though proximity to the lumen may introduce bias into the stress data, it does not explain why there is such a dramatic drop in macrophage presence at high stresses/strains, or why this drop occurs in all stages of progression except advanced plaque – the plaque with characteristic features of vulnerability.

Implications for plaque progression and plaque rupture

As the primary inflammatory cell in plaque, macrophages release a large number of biological agents, including cytokines, chemokines, growth factors, tissue factor, reactive oxygen species, and MMPs. They also interact with and stimulate SMCs, endothelial cells, and other inflammatory cells like T lymphocytes and mast cells (Takahashi et al. 2002). Therefore, the fact that they are more likely to be present in advanced plaque in locations where stresses are high indicates that the inflammatory response is exacerbated in these locations of high stress. Because these locations coincide with locations where rupture most often occurs, this means that the inflammatory response is exacerbated at high stress in the most vulnerable regions of plaque.

This exacerbation of the inflammatory response has dire implications for plaque stability. Because macrophages release MMP-1 – which breaks down the primary structural component of the ECM – high concentrations of macrophages may cause mechanical weakening of the plaque cap. In fact, Lendon et al (1991) showed that fibrous caps are weakened when they are infiltrated with macrophages. In addition to weakening the cap, degradation of the fibrous cap means that loads previously born by the degraded portion of the cap are shifted to the remaining portion of the cap, thereby concentrating higher loads to thinner tissue. This trend will be considered in detail later when the discussion turns to MMP-1.

It should be noted here that the relationship between macrophage presence and stress discussed here describes only the *presence* of macrophages in different mechanical environments, and does not describe the *activity* of macrophages in these environments. Although with the exception of advanced plaque, macrophages were generally found to

decrease at very high stresses, this does not mean that macrophages are less active at these high stresses. Macrophages have been shown to be quite mechanically sensitive (Yang 2000), and it is likely that they behave differently in different mechanical environments within plaque. Because macrophages are found in high numbers, often outnumbering SMCs (van der Wal 1994) in plaque, the trends found for expression of NF-κB and MMP-1 with respect to stress and strain indicate that macrophage activity is changing in response to mechanical stress. This is discussed in detail later.

Comparison with previous studies. As mentioned above, to our knowledge, only one other study has considered the spatial relationship between macrophages and stress in diseased human arteries (Lee et al 1996). In the study by Lee et al, the cross-section was divided into 8 large sectors, and macrophage content in the highest-stress sectors was compared to macrophage content in the lowest stress sectors. While they found no relationship between macrophages and stress, we believe that the limitations of the methods used in this previous study to compare spatial distributions of macrophages and stress may have prevented them from finding the same relationship between macrophages and stress found in our study.

We believe there are several reasons why our study found a link between macrophages and mechanical stress, while this previous study did not. These reasons include the use of much higher spatial resolution, a broader approach for determining whether a relationship exists, and more accurate methods for quantifying macrophage distributions.

First of all, the spatial resolution of the study presented here was much higher. While we divided the cross-section into very small elements (1000 elements per cross-

section on average), Lee et al divided the cross-section into only 8 sectors. For each of these eight sectors, the macrophage content was determined over the whole sector area, while the stress level was determined from the peak stress value of the sector. Because the highest stresses typically occur at a very focal location, but macrophages were quantified over a very large area, the connection between macrophages and their local mechanical environment was lost.

Secondly, the methods used to determine whether a relationship exists between macrophages and stress were much broader in our study. Lee et al tested only to determine whether macrophage expression was higher at high stresses than at low stresses. However, our study simply looked for trends with respect to stress, and thus the analysis was not limited to monotonic trends only. Consider the trend shown in Figure 4.7 for macrophage expression as a function of stress. In our study, we found that macrophage concentrations increased with increasing stress for moderate stress values, but decreased dramatically at very high stresses; because of this, the macrophage content in the highest stress bin was not very different from the baseline. Because their analysis was limited to testing for positive collocation, a relationship between macrophages and stress may have been masked due to this trend of increasing and then decreasing expression with respect to stress. Therefore, the same trend found here may also have been present in their data; it was perhaps just not detected due to analytical and spatial resolution limitations.

A third major difference between our study and the previous study is the way in which macrophages were quantified. In our study, macrophages were quantified by tagging of individual cells, while in the study by Lee et al, macrophages were quantified

via image thresholding. In our experience, macrophages are typically found either sparsely distributed within the plaque, or in small clusters of cells in focal regions. Because of this, we have found that quantifying macrophages by image thresholding is difficult and unreliable. If the threshold is set too high, the result is very noisy, and non-cellular features are incorrectly labeled as macrophages. If the threshold is set too low, sparsely distributed macrophages are not detected. Therefore, for such sparsely distributed markers, cell tagging, as performed in this study, provides a more reliable method for quantifying spatial distributions than image thresholding.

Matrix Metalloproteinase - 1

Overall expression of MMP-1

MMP-1, the primary enzyme responsible for breaking down fibrillar collagen, was most strongly expressed in early and advanced plaque, while it was less strongly expressed in mature plaque (Figure 4.19). Strong expression in advanced plaque was expected, and agrees with previous studies that have shown that MMP-1 is strongly expressed in plaques showing characteristics of vulnerability (Nikkari et al. 1995, Galis et al. 1994, Guo et al. 2000). Also, weaker expression in mature plaque was expected, since these plaques are considered to be the "end-stage" of plaque remodeling and progression; lower MMP-1 expression is probably due to less overall remodeling and ECM turnover in these plaques (Guo et al. 2000)

The strong expression we found in this study in early plaque is in contrast to what has been found in previous studies, which have shown that MMP-1 is not highly

expressed in relatively non-diseased arteries (Nikkari et al 1995). However, the results of these studies were based on healthy arteries taken from patients who died of non-cardiovascular causes, while in this study the relatively non-diseased cross-sections still came from the arteries of cardiac transplant patients. Even though the cross-sections did not show the signs of advanced plaque, they are probably not in the same state of health as arteries from patients without cardiovascular disease.

Comparison of Spatial Distributions of MMP-1 and Mechanical Stress

Overall, the probability of expression of MMP-1 increases monotonically with increasing stress (Figure 4.20). This trend is highly dependent on the stage of plaque progression (Figure 4.21). In early plaque, MMP-1 expression does not change for moderate stresses, but there is a spike in MMP-1 expression at very high stress. In intermediate and advanced plaque, the probability of MMP-1 expression follows a pattern similar to that seen for macrophages: in intermediate plaque, expression increases monotonically for moderate stresses, but drops off to some extent at very high stresses, while in advanced plaque, the probability of MMP-1 expression continues to increase monotonically at very high stress. In mature plaque, the opposite trend is seen: the probability of MMP-1 expression decreases with increasing stress.

Our overall finding that MMP-1 expression increases with increasing stress agrees with the results found previously by Lee et al (1996). However, while they found that MMP-1 generally collocates with high stress, our study provides additional insight into the trends of this relationship with stress. Also, to our knowledge, this is the first study to investigate the dependence of the relationship between MMP-1 expression and stress on plaque progression.

The results of this study strongly support the role of mechanical stress in remodeling and ECM turnover in atherosclerosis. Because MMP-1 is responsible for breaking down the major structural component of the ECM, the fact that there is a relationship between mechanical stress and the probability of MMP-1 expression provides a link between mechanical stress and matrix degradation.

The nature of this relationship is dependent on the stage of plaque progression. In early, intermediate, and advanced plaque, MMP-1 expression generally increases with increasing stress, although the exact trends vary. In mature plaque, however, expression decreases with increasing stress. This difference between mid-stage plaques, which are developing and changing fairly rapidly, and mature plaque which are considered stable with little remodeling activity, suggests that the relationship between stress and MMP-1 expression is not a general relationship, but is plaque progression dependent.

A closer look at the spatial distributions of MMP-1 and mechanical stress in different stages of plaque progression yields insight into these results. In early plaque, there are very few macrophages present, and thus MMP-1 expression within the wall occurs primarily in smooth muscle cells within the media, as seen in Figure 4.6A. All of the cross-sections in this category came from patients who were on medication for high blood pressure at the time of transplantation. Therefore, while these cross-sections appear relatively undiseased, we speculate that MMP-1 expression in these plaques is facilitating positive remodeling due to increased stress caused by high blood pressure.

In intermediate plaque, most MMP-1 expression occurs in regions surrounding small lipid pools (Figures 4.1B and 4.6B). We know that as plaques progress, remodeling occurs in such a way that these small lipid deposits are consolidated into a larger lipid

pool. The fact that the probability of MMP-1 expression increases with increasing stress suggests that stress plays a role in this remodeling and consolidation of lipid pools.

In advanced plaque, MMP-1 expression is increased in the shoulder and fibrous cap regions, where stresses are also high. This has direct implications for plaque destabilization, since rupture most often occurs in these regions. This is discussed in more detail below.

In mature plaque, expression decreases with increasing stress. Looking at a representative cross-section (Figure 4.2D and 4.6D), mechanical stress is concentrated in the portion of the vessel wall opposite the bulk of the plaque, while MMP-1 is not expressed particularly strongly in this wall. Mature plaques consist primarily of calcification and fibrous tissue with very low cellularity, and therefore are considered senescent and relatively biologically inert. Thus, it would not have been surprising to find no increasing trend between MMP-1 and stress in these plaques, since very little remodeling is thought to be occurring, and MMP-1 is generally expressed in lower levels in mature plaque. However, it was surprising to find the *opposite* trend – that MMP-1 actually *decreases* with increasing stress in these plaques. Further research is needed to determine why MMP-1 shows the opposite trend with respect to stress in these "stable" plaques than in plaques currently undergoing remodeling.

As mentioned, the trends seen in intermediate and advanced plaque differ at very high stress. Because these trends follow the trends seen for macrophages, and macrophages are one of the two major cell types, along with SMCs, capable of expressing MMP-1 within the vessel wall, this difference can most likely be attributed to

a fewer number of macrophages at high stress in intermediate plaque than in advanced plaque .

Comparison of Spatial Distributions of MMP-1 and Mechanical Strain

MMP-1 expression shows a weaker dependence on strain than on stress (Figure 4.22 and 4.23). In intermediate and advanced plaque, MMP-1 expression showed no real dependence on strain at all. Because of the role of MMP-1 in ECM degradation and remodeling, stronger dependence of MMP-1 expression on stress than strains is corroborated by the fact that growth and remodeling in arteries has generally been found to correlate better with stress than strain (Taber and Humphrey 2001). As mentioned earlier, this is why stress rather than strain is used in the development of remodeling laws in the field of vascular mechanics.

Implications for plaque progression and plaque rupture

What do these results mean in terms of plaque progression and plaque rupture? It is well-known that arteries remodel in order to maintain baseline values of luminal shear stress and wall tension. Because MMP-1 is involved in matrix degradation, the finding that MMP-1 expression locally increases in regions with increased mechanical stress in plaques highlights the role that mechanical stress plays in the development and remodeling of plaque. In addition, the fact that MMP-1 expression is lower in more stable advanced plaque, and also that MMP-1 expression showed the opposite trend with respect to stress in these plaques indicates the relationship between mechanical stress and MMP-1 expression is not a general trend seen in all plaque, but is plaque progression dependent.

The relationship between mechanical stress and MMP-1 expression has serious implications for plaque stability. In advanced plaque, which exhibit the characteristic features of vulnerability to rupture, both MMP-1 and mechanical stress are collocated in the fibrous cap and shoulder, where rupture most often occurs. The current hypothesis is that plaque rupture occurs due to a combination of mechanical stress concentrations and disregulation of the ECM. The finding that MMP-1 is preferentially expressed in regions of high stress suggests that these two components of the plaque rupture hypothesis are not independent. There are two mechanisms by which stress concentrations and matrix disregulation may interact to contribute to plaque rupture. It is possible that cells in the fibrous cap sense increased stress and respond by upregulating MMP-1 expression (this process may be regulated by NF-kB, which, as we suggested earlier, may provide the link between the mechanotransduction signaling pathway and inflammatory signaling pathway). Increased MMP-1 expression results in degradation of the fibrous cap and increased risk of rupture. On the other hand, it is also possible that expression of MMP-1 leads to increased stresses in the fibrous cap and shoulder: breakdown of fibrillar collagen by MMP-1 may cause loads previously born by these collagen fibers to be shifted to the remaining fibrous cap. Because a thinner cap is now bearing more load, stresses are increased.

Because stress may induce MMP-1 expression, but MMP-1 expression may also lead to increased stress in the plaque cap, it is possible that, as the plaque progresses and small lipid pools are consolidated into a larger lipid pool with a true fibrous cap, the plaque enters a positive feedback cycle (see Figure 5.1, pg 171). In this cycle, increased stress in the fibrous cap and shoulder leads to increased MMP-1 expression, possibly

through NF-kB activation. This causes degradation of the extracellular matrix in these regions, leading to a further increase in stress, followed by an additional increase in MMP-1 expression. If nothing changes to cause an exit from this feedback cycle, it may eventually lead to plaque rupture. This positive feedback cycle, as well as possible means of exit from the feedback loop, is discussed in detail later.

While we considered *expression* of MMP-1 in this study, a limitation of this study is that we are not able to determine actual *activity* of MMP-1. As discussed in Chapter 1, MMP activity is highly regulated. Even after MMP-1 is synthesized, it requires activation, and even activated MMP-1 can be inhibited by Tissue Inhibitors of MMPs (TIMPs) which are also expressed in vascular tissue. Future studies into spatial relationships between MMPs and the mechanical environment should consider also the collocation of MMPs and TIMPs, as well as the activation state of MMPs.

Although MMP-1 activity can be detected within plaque through in situ zymography (Galis 1994), this method could not be applied in this study, since it requires the use of fresh frozen tissue. By choosing to use formalin-fixed, MMA imbedded tissue, our ability to detect some histologic end points such as MMP-1 enzymatic activity was limited. However, this tradeoff was necessary in order to develop mechanical models based on accurate vessel geometries.

Nitrotyrosine

Overall Expression of Nitrotyrosine

Nitrotyrosine expression, which is indicative of reactive oxygen species activity and oxidative stress, is found in relatively constant levels as plaques progress from early

to advanced, but is expressed less in mature plaque (Figure 4.24). The lower expression in mature plaque is most likely due to the fact that these plaques have lower cellularity and are generally less biologically active.

Comparison of Spatial Distributions of Nitrotyrosine and Mechanical Stress

When all stages of disease were considered together, nitrotyrosine expression showed no relationship to mechanical stress (Figure 4.25). A very weak dependency on stress was found when advanced and mature plaque were considered separately (Figure 4.26). Advanced plaque showed no dependence at moderate stresses, but showed a small increase in nitrotyrosine expression at very high stresses, while mature plaque showed a mixed trend. Expression decreased for moderate stresses, but expression increased at higher stresses. To our knowledge, this is the first study to investigate the spatial relationship between nitrotyrosine and stress.

Because no strong or consistent trend was found, we conclude that there is no general spatial relationship between nitrotyrosine expression and stress. While later stages of plaque do show a statistically significant dependence on stress, the trends seen are weak and incosistent. Also, examination of the spatial distributions of nitrotyrosine and stress provided no explanation or clear pattern of collocation. In advanced plaque (Figure 4.2C and 4.7C), nitrotyrosine shows a focal expression in the fibrous cap, where stresses are high, but is also highly expression in the outer layer of the vessel, where both stress and other inflammatory markers are low. In mature plaque (Figure 4.2C and 4.7C), nitrotyrosine expression was increased in the wall opposite the bulk of the plaque, where stresses were high, but was also increased in the fibrous cap, where stresses were low due to calcification reinforcement.

Comparison of Spatial Distributions of Nitrotyrosine and Mechanical Strain

While no spatial relationship was found between nitrotyrosine expression and mechanical stress, nitrotyrosine expression increased at high strains, particularly in advanced and mature plaque (Figure 4.27). This suggests that reactive oxygen species in atherosclerosis may be sensitive to mechanical strain rather than mechanical stress.

Implications

Because no spatial relationship was found between nitrotyrosine and mechanical stress alone, this suggests that interactions between mechanical stress and reactive oxygen species are not important in atherosclerosis development.

However, while we found no strong relationship between nitrotyrosine and stress, we did find data to suggest that reactive oxygen species *activity* depends on stress. ROS are capable of activating NF-kB, and we found that co-expression of nitrotyrosine with activated NF-kB is highly dependent on stress (Figure 4.37). This result is discussed in detail later, but briefly, this provides evidence to suggest that the ability of ROS to activate NF-kB is enhanced by increased stress.

It should be noted that while nitrotyrosine expression is used as a measure of reactive oxygen species activity, it has inherent limitations which may have affected the results of this study. First of all, because it is only one stable end-product of oxidative stress, it may not detect all ROS activity. In addition, as a stable end-product, it may accumulate over time, and thus the spatial distribution of nitrotyrosine may not directly represent the spatial distribution of current reactive oxygen species activity. Also, as mentioned in Chapter 3, the antibody for detecting nitrotyrosine has rather poor specificity, and this may have directly affected the determined spatial distributions.

Because nitrotyrosine detection is the only immunohistochemical method currently available for detecting reactive oxygen species, it was used here; however the limitations of nitrotyrosine as a marker for reactive oxygen species should be considered when interpreting the results of this study.

Microvessels

Overall Expression of Microvessels

Microvessels density was similar in all stages of plaque progression, although there was a slight, insignificant increase in density as plaques progressed (Figure 4.29). Microvessels are present in all vascular tissue, and are necessary to provide oxygen and nutrients to the vascular tissue. As plaques progress, the amount of tissue in the wall increases, and thus the amount of oxygen and nutrients needed increases. Because the density of microvessels is relatively even as this growth progresses, it may be that there is an optimum density of microvessels required to sustain vascular tissue.

Comparison of Spatial Distributions of Microvessels and Mechanical Stress

No general trends were found relating the presence of microvessels and mechanical stress (Figure 4.30). When we considered expression in the different stages of plaque progression, we found very weak dependence on stress (Figure 4.31). Also, the trends that were found were mixed, and no clear pattern emerged. Based on these results, we conclude that the presence of microvessels does not depend on the local mechanical stress. To our knowledge, this is the first study to consider the collocation of microvessels and mechanical stress in diseased human arteries.

Comparison of Spatial Distributions of Microvessels and Mechanical Strain

We found no general trends relating the presence of microvessels and mechanical strain (Figure 4.32). When we considered expression in the different stages of plaque progression, we found a stronger dependence on strain (Figure 4.33). However, these trends were mixed, and no clear pattern emerged.

Implications

While the density of macrophages remained even throughout plaque progression, this result is based on the average density over the entire cross-section. It is possible that as the plaque grows, new vessels may be stimulated to grown preferentially in certain locations within the plaque, even though the overall density remains the same. Because microvessels have been suggested as conduits for macrophages infiltration of the vasculature, the locations of microvessels could be an important factor in plaque progression and plaque rupture. However, this study found no evidence to suggest that there is a spatial relationship between mechanical stress and the presence of microvessels. In addition, microvessels surprisingly were not found to significantly collocate with macrophages (Table 4.6). To try to understand this result, we referred to the actual serial immunostained slides. After inspection, we saw that in some cases, macrophages were closely associated with microvessels, but there were also many populations of macrophages in regions void of microvessels, as well as many microvessels in regions void of macrophages. Thus, while microvessels may sometimes facilitate macrophage infiltration, this does not appear to be the only role of microvessels in plaque, and also does not appear to be the only means for macrophage infiltration into plaque.

One limitation of this study is that we were not able to differentiate between newly formed microvessels and microvessels that were present in the plaque all along. Thus, we were only able to spatially compare mechanical stress with the *presence* of microvessels, rather than the formation of *new* microvessels. Because all microvessels in the cross-section were included, the effect of the formation of new microvessels in high stress regions (if this occurs) could have been missed due to the much larger overall number of vessels. Therefore, while this study finds no spatial relationship between mechanical stress and microvessels, it does not exclude a relationship between stress and angiogenesis. Future studies should investigate markers of angiogenesis, rather than markers for microvessels themselves.

Hypotheses for Biological Mechanisms Relating Mechanical Stress and Inflammation

In the following section, we propose plausible hypotheses of mechanisms relating to the spatial associations of mechanical stress and inflammatory markers discussed above based on the findings of this study, as well as what is currently known about these specific markers and about the general biology of atherosclerotic plaque (these hypotheses were each mentioned briefly in the discussion above). We then use the findings discussed above, along with additional findings on the co-expression of pairs of markers and the dependence of this co-expression on stress, to evaluate these hypotheses. Because spatial collocation does not imply causation, our data does not permit us to draw definitive conclusions on the validity of these hypotheses. However, our results are used here to either lend support to or to refute the proposed hypotheses.

Plausible Hypothesis 1: Mechanical stress increases MMP-1 activity through NF-kB activation in diseased human arteries.

It has previously been shown that activated NF-kB can upregulate genes controlling MMP-1 expression (Vincenti and Brinckerhoff 2002). Therefore, as suggested earlier, NF-kB activation may be the link between mechanotransduction pathways and inflammatory signaling pathways leading to vascular remodeling (Lehoux et al 2006).

This hypothesis is supported by the following findings:

- NF-kB expression monotonically increases with increasing stress in all stages of plaque progression (Figure 4.15)
- MMP-1 expression generally increases with increasing stress, with the exception of mature plaque (Figure 4.20 and 4.21)
- MMP-1 and activated NF-kB are significantly co-expressed in all stages of plaque progression except intermediate plaque (Table 4.2 and 4.4)
- MMP-1 and activated NF-kB co-expression increases with increasing stress in all stages of plaque progression except mature plaque (Figure 4.36)
- Mechanical stress, activated NF-kB expression, and MMP-1 express are concentrated in the shoulder and fibrous cap of advanced plaque (Figure 4.2C, 4.4C, and 4.6C)

This hypothesis is *not* supported by the following finding:

- In mature plaque, NF-kB expression increases with stress, but MMP-1 *decreases* with mechanical stress (Figure 4.16D and 4.21D)

- In mature plaque, mechanical stress and NF-kB expression are very high in portion of the vessel wall opposite the bulk of the plaque, but MMP-1 expression is not high in this region. (Figure 4.2D, 4.4D, and 4.6D)

This hypothesis has implications for both plaque progression and plaque rupture. First of all, this hypothesis helps explain how a mechanical input is able to direct the complex biological changes of remodeling. As suggested earlier, activation of NF-κB by mechanical stress could provide the link between mechanotransduction leading to activation of NF-κB (Lehoux 2006) and the inflammatory signaling cascade beginning with NF-κB activation and leading to expression of MMP-1 and matrix degradation.

This has special importance for plaque rupture due to the fact that mechanical stress, NF-kB, and MMP-1 all collocate in the plaque shoulder and fibrous cap, where rupture most often occurs. As mentioned earlier, we propose a positive feedback cycle between stress, NF-kB activation, MMP-1 expression, and matrix degradation in the fibrous cap. This positive feedback mechanism is illustrated in Figure 5.1. In this positive feedback mechanism, as small isolated lipid pools are consolidated into a larger lipid pool (through the action of MMPs which degrade the matrix to allow the lipid to coalesce), stresses become increased in the fibrous cap and shoulder regions that separate the lipid from the lumen. This increase in mechanical stress activates NF-kB, which in turn increases expression of MMP-1 by macrophages and smooth muscle cells in the cap and shoulder. MMP-1 expression leads to degradation of fibrillar collagen and "thinning" of the fibrous cap. This thinning may be due to actual erosion of plaque cap tissue, but effective thinning may also occur without actual changes in plaque cap dimensions. Partial collagen degradation may locally weaken the matrix in the plaque cap, reducing

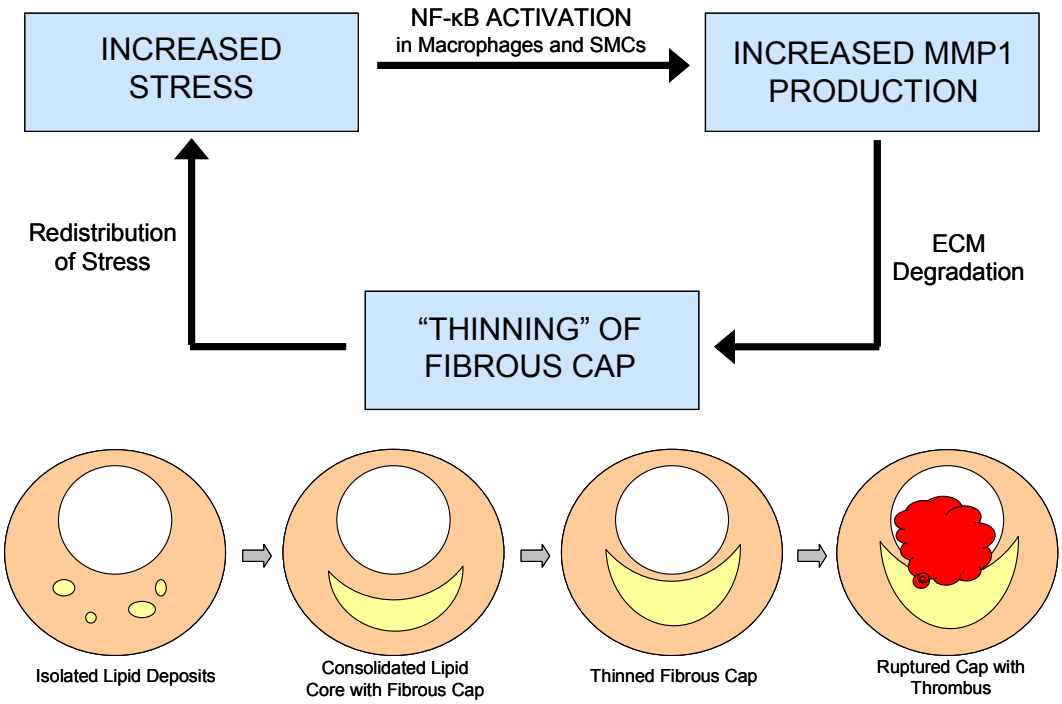

Figure 5.1 Hypothesized positive feedback mechanism between stress, NF-kB activation, MMP-1 expression, and ECM degradation of the fibrous cap.

the number of load bearing fiber. In either case, loads previously born by the degraded collagen fibers are shifted to the remaining intact collagen fibers. Because more loads are now concentrated in a "thinner" fibrous cap, stresses are increased. This increased stress in turn leads to further activation of NF-kB, further MMP-1 expression, and further degradation, until rupture occurs.

However, not all plaques with features of vulnerability (large lipid pool, thin fibrous cap) actually progress to rupture. One possible means of exit from this proposed positive feedback cycle leading to rupture could be provided by replacement of the lipid pool with calcification, as illustrated in Figure 5.2. It is thought that plaque progression to a mature state is brought about by the gradual filling of the lipid core with calcium or in some cases, fibrous matrix (Stary 1995). Thus, whether a plaque progresses to rupture or to

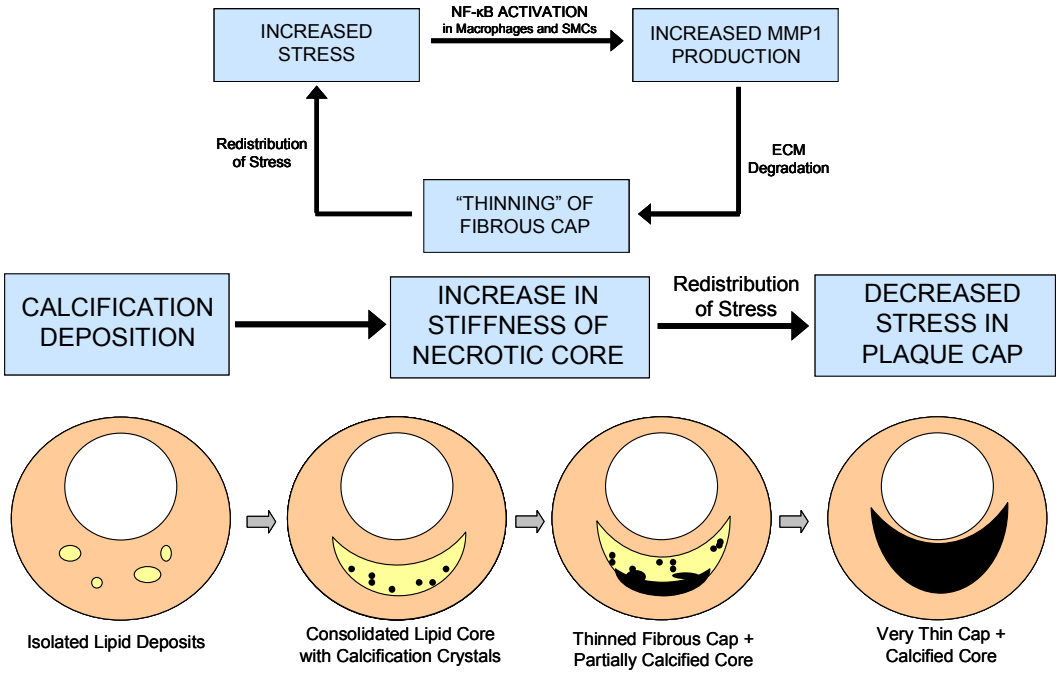

Figure 5.2 Calcification of lipid core may provide exit from positive feedback cycle by stiffening the necrotic core and decreasing the load born by the fibrous cap and shoulder.

stable maturity could be determined by the difference in the rate of plaque cap degradation and the rate of calcification or fibrosis of the lipid pool.

While there is data supporting the hypothesis that mechanical stress increases MMP-1 activity through NF-kB activation, some of the results found in this study do not support this hypothesis. If NF-kB activation by mechanical stress leads to MMP-1 expression, then why does MMP-1 expression decrease with stress in mature plaque, while NF-kB expression increases? One possible explanation is that the effect of NF-kB activation is different in different environments and cell types. Thus, NF-kB activation may have a different effect on MMP-1 expression at different stages of plaque progression. Further study is needed to determine the effects of NF-kB in different environments and cell types.

Plausible Hypothesis 2: High mechanical stress affects the activity of macrophage in atherosclerotic plaque.

In this study, we found that the probability of the *presence* of macrophages increases with moderate mechanical stress but drops significantly at very high stress. This result gives an indication of the relationship between mechanical stress and the combined proliferation, apoptosis, and migration of macrophages. However, this result does not indicate *all* activity of macrophages as a function of stress. We know that, at least in cell culture, macrophages respond to mechanical deformation in a variety of ways including changes in gene, protein, and receptor expression (Yang et al 2000, Ohki et al 2002). Therefore, it is likely that these activities also change in macrophages in environments of high mechanical stress.

To support this hypothesis, co-expression of macrophages and activated NF-kB, as well as co-expression of macrophages and MMP-1 increases with increasing stress (Figure 4.35 and 4.36). While macrophages alone show a significant drop in presence at very high stresses in intermediate plaque, the co-expression of macrophages and NF-kB does *not* drop significantly at very high stress. In addition, co-expression of macrophages and MMP-1 shows a slight drop at very high stress, but this drop is not nearly as significant as the drop seen for macrophages alone. Although not conclusive, these results suggest that NF-kB activation and MMP-1 expression are increased in macrophages at very high stress, indicating that changes in gene and protein expression occur in macrophages as stress increases.

One limitation that should be noted is that co-expression of macrophages and NF-kB or MMP-1 only indicates that both are present in the same element. In this study we do not differentiate between markers expressed by macrophages and markers expressed by other cell types when determining spatial distributions. Therefore, co-expression does not necessarily confirm that it is macrophages, as opposed to smooth muscle or other cell types, that are expressing NF-kB or MMP-1. In future studies, the gene and protein expression activity of macrophages may be evaluated more effectively by determination of co-expression on the cellular level when quantifying marker spatial distributions, rather than later at the element level.

Plausible Hypothesis 3: Mechanical stress enhances the activity of reactive oxygen species.

It is known that reactive oxygen species are capable of activating NF-kB and inducing MMP-1 expression (Bubici et al 2006, Rajagopolan 1996). In this study, we found that there is no spatial relationship between nitrotyrosine and mechanical stress. In addition, while NF-kB is present in its inactive form in all cells (thus, simple presence of NF-kB does not depend on stress), the *activated* form of NF-kB increases with increasing stress (Figure 4.10), and the *co-expression* of nitrotyrosine and NF-kB increases with increasing stress (Figure 4.37). The same trend is found in the case of MMP-1. While nitrotyrosine expression alone does not depend on stress, co-expression of MMP-1 and nitrotyrosine increases with increasing stress (Figure 4.38). Since ROS is an activator of NF-kB and is capable of inducing MMP expression, all of these results

taken together suggests, although they do not conclusively show, that the activity of ROS, at least on NF-kB and MMP-1, is enhanced in the presence of increased stress.

Limitations of Specific Aim 3

While specific limitations relating to each inflammatory marker are discussed above, some general limitations of this study are discussed here. First of all, while the use of tissue from human transplant patients provides results that relate directly to human pathology, there are also limitations associated with the use of human transplant tissue. Transplant patients are treated with a wide variety of medications (see Appendix A) and the effects of these drugs on the endpoints of this study are unknown. In addition, it is not possible to experimentally control inputs to the artery before analysis and to study the effects of these inputs over time; the artery provides a snap-shot of what is occurring at the time of removal from the patient. This makes it difficult to definitively determine causal effects. Thus, while we propose logical causal mechanisms to explain spatial relationships between stress and inflammatory markers, we recognize that collocation does not imply causation.

Also, the inflammatory markers studied here are not independent. For example, NF-kB activation may induce MMP-1 expression; MMP-1 and reactive oxygen species are commonly expressed in macrophages; macrophages may enter the tissue through microvessels. It is not practically possible to look at these markers in isolation in this study. Therefore, coupling effects may be present, so that the effects of relationships of one marker with respect to stress may have effects on the relationships found for other markers.

SIGNIFICANCE

Understanding the mechanisms that lead to atherosclerotic plaque rupture and subsequent myocardial infarction or stroke is critical to developing new, more effective treatment and prevention methods for a disease that is the leading cause of death in the United States. This study contributes to our understanding of the relationships between the mechanical and biological environment in atherosclerotic plaques as they progress, and provides insight into biological mechanisms by which mechanical stresses contribute to plaque progression and plaque rupture. Also, because these studies were conducted using diseased human arteries, these findings have direct implications for human disease pathology.

The research presented here provides *new* knowledge about the spatial relationships of mechanical stress and inflammation in atherosclerotic plaque. This study is the first to investigate relationships between mechanical stress and expression of NF-kB, nitrotyrosine, and microvessels in diseased human arteries. It is also the first study to find a significant spatial relationship between mechanical stress and macrophages. In addition, it corroborates previous results showing that MMP-1 collocates with stress, and provides more details about the patterns of this collocation. For all of these markers, this is the first time that the dependence of the relationship between mechanical stress and marker expression on plaque progression has been considered.

Because it was found that there is a spatial relationship between mechanical stress and activated NF-kB, macrophages, and MMP-1, this study motivates new research into the causal nature of these relationships on three fronts: First, investigations into mechanisms for controlling stresses within plaque could potentially be used to reduce or

manipulate the inflammatory response, with direct impact on plaque progression. Secondly, research into mechanisms to control the expression of these inflammatory markers could potentially be used to prevent progression of plaque to instability by preventing changes in the structure, composition, and material properties of plaque that lead to increased stresses. Third, research into mechanisms for disrupting the relationship between mechanical stress and inflammatory marker expression (for instance, by locally disrupting mechanotransduction signaling pathways) could change the course of plaque progression in a potentially beneficial way.

This research provides a scientific basis for potential clinical applications as well. As imaging technologies advance, higher resolution capabilities may provide a means for evaluating the mechanical environment of plaque clinically. Also, technologies are emerging that may allow detection of inflammation in vivo. Optical coherence tomography has shown potential for identifying macrophages in plaque in vivo (MacNeill et al. 2004, Tearney et al. 2003); use of activatable near-infrared fluorescence (NIRF) probes with fluorescence molecular tomography has been used to detect MMP activity in apoE deficient mice (Deguchi et al 2006); F-Fluoro-deoxyglucose positron emission tomography (F-FDG PET) has shown promise for indirectly detecting inflammation in plaque by detecting increased glucose metabolism at the cellular level (Arauz et al 2007); and focal loss of MR signal in ultra-small superparamagnetic particles of iron oxide (USPIO)-enhanced MRI has been shown to correlate with locations of macrophages (Tang et al 2006). Thus, the results of this study, coupled with in vivo imaging of plaque structural and biological features, may eventually aid in the clinical diagnosis of plaques at risk of rupture.

CHAPTER 6

CONCLUSIONS AND FUTURE RECOMMENDATIONS

Conclusions

The objectives of this study were to determine whether there is a spatial relationship between mechanical stress and markers of inflammation in human coronary atherosclerotic plaque, and whether this relationship depends on the state of plaque progression. To accomplish this, 2D heterogeneous mechanical models of cross-sections of atherosclerotic plaque were developed. These models provide improved confidence in the obtained spatial distributions of mechanical stress relative to previous models because they more accurately represent the microstructure and in vivo geometry of atherosclerotic arteries. In addition, improved methods for quantifying the spatial distribution of inflammation were developed. By using the same finite element mesh from the mechanical models to quantify the distribution of inflammatory markers, the methods developed here facilitate comparison of the distributions of inflammation and stress at high spatial resolution. In addition, these methods are not limited to comparisons between stress and inflammation, but can be applied to any variables that are spatially distributed in the cross-section.

In this study, we demonstrated that activated NF-kB is expressed in all stages of plaque progression, and that the probability of expression of activated NF-kB increases monotonically with increasing stress in all stages of progression. From this, we conclude

that the relationship between mechanical stress and NF-kB activation is a general relationship that is important throughout the disease process. Because activated NF-kB is involved in the regulation of a large number of genes involved in the inflammatory signaling cascade and in apoptosis, these findings support the role of the mechanical environment in instigating and maintaining inflammatory response, and also provide a link between mechanics and cell death.

We also demonstrated that the relationship between macrophages and stress is highly progression dependent, and is strongest in plaque where macrophages are present in high numbers – intermediate and advanced plaque. In early, intermediate, and mature plaque, macrophage presence increases with moderate stresses, but drops off sharply at high stresses. This decrease at high stress may be due to apoptosis, failure of monocytes to migrate to these high stress regions, or failure of monocytes to differentiate into full-fledged macrophages. In contrast, the presence of macrophages continues to increase at high stresses in advanced plaque, which have characteristic features of vulnerable plaque. Future studies are needed to elucidate the cause of this different behavior of macrophages at high stress in advanced compared to other stages of plaque progression. Because macrophages release a plethora of inflammatory markers, including matrix-degrading enzymes like MMP-1, this finding indicates that inflammation is exacerbated at locations of high stress. Since high stress locations coincide with locations where rupture most often occurs (the fibrous cap and shoulder) in advanced plaque, this trend has critical implications for plaque stability.

The relationship between MMP-1 expression and stress is highly dependent on the stage of disease progression. MMP-1 expression generally increases with stress in

developing plaque, while MMP-1 expression decreases with stress in mature stable plaques. Because MMP-1 is responsible for breaking down the major structural component of the ECM, this result highlights the role that mechanical stress plays in remodeling and ECM turnover. The relationship between mechanical stress and MMP-1 also has serious implications for plaque stability, particularly since both MMP-1 and mechanical stresses concentrate in the shoulder and fibrous cap region of advanced plaque. The current hypothesis of plaque rupture holds that rupture occurs due to a combination of stress concentrations and disregulation of the ECM. The finding that MMP-1 is preferentially expressed in regions of high stress suggests that these two components of the plaque rupture hypothesis are not independent.

There was no consistent trend relating nitrotyrosine expression and mechanical stress. This may be due to a true lack of relationship between stress and reactive oxygen species. However, it may also be due to limitations associated with the use nitrotyrosine as a marker of reactive oxygen species; nitrotyrosine is not the only end-product of oxidative stress, and the antibody used to detect nitrotyrosine has very poor specificity. However, while no relationship between *expression* of nitrotyrosine and stress was found, there is data to indicate that the *activity* of ROS may depend on stress. Reactive oxygen species are capable of activating NF-kB and of inducing MMP-1 expression. While nitrotyrosine expression alone does not depend on stress, the co-expression of nitrotyrosine and NF-kB and of nitrotyrosine and MMP-1 increases with increasing stress, suggesting that the activity of ROS on NF-kB activation and MMP-1 expression may be enhanced in regions of increased mechanical stress.

We found no spatial relationship between microvessels and mechanical stress. However, this study did not differentiate between newly formed microvessels and microvessels that were present in the plaque all along. Therefore, this finding does not exclude a relationship between *angiogenesis* and mechanical stress.

Although it is not possible to definitively determine causal relationships from this study, we use the results found here to suggest plausible hypotheses of mechanisms relating to the spatial associations of mechanical stress and inflammatory markers. We propose that mechanical stress increases MMP-1 activity through NF-kB activation in diseased human arteries. This hypothesis helps explain how a mechanical input is able to direct the complex biological changes involved in remodeling, and has special importance for plaque rupture, since mechanical stress, NF-kB, macrophages, and MMP-1 were all found to collocate in the plaque cap and shoulder regions. We also propose that a positive feedback cycle exists between mechanical stress, NF-kB activation, and MMP-1 expression. In this proposed theory, remodeling and coalescence of lipid into a lipid pool leads to increased stresses in the shoulder and fibrous cap. NF-kB is activated in cells in the fibrous cap and shoulder regions in response to this increased stress, leading to MMP-1 expression and degradation of collagen; this causes loads previously born by the degraded collagen fibers to be shifted to the remaining, thinner fibrous matrix, further increasing stress in the cap and shoulder and leading to additional NF-kB activation, MMP-1 expression, and matrix degradation, eventually ending in plaque rupture if nothing changes to cause an exit from this feedback cycle.

Future Recommendations

Refinement of methods

In the mechanical models developed in the current study, several assumptions were made due to lack of data on material properties, residual stresses, and axial stretch. In the future, new data may be provided in these areas, and this information should be incorporated into the models developed here. In addition, several assumptions were made in order to reduce the complexity of the model, and these assumptions may need to be modified for future applications.

The current mechanical models assume 2D plane strain, and this assumption is valid only when variations in the axial direction are small. Comparisons with 3D mechanical models are needed to determine when plane strain is valid, and when the calculated spatial distributions of stress are accurate. In cases where 2D plane strain is not valid, it may be beneficial to compare spatial distributions of inflammatory markers with distributions of stress determined from 3D models.

While the current models include the macroscopic heterogeneity of plaque, the microscopic heterogeneity due to variations in the component biochemistry and anisotropy due to orientation or disorganization of collagen fibers are not included. Also, local interactions among components are not considered. In future studies, modeling of heterogeneity on the microscopic level may give a better representation of the local mechanical environment. Understanding the mechanical conditions on the cellular level will likely be important in determining the exact mechanisms by which the cells interact with the mechanical environment.

In the current study, regional variation in cellularity over the cross-section was not included when quantifying the spatial distribution of inflammatory markers. In future studies, including effects of this variation may provide improved representation of the relative expression of inflammatory markers. In addition, the current methods do not include information about types of cells in which markers are expressed. This limits the ability of this study to definitively determine co-expression of markers, and particularly limits the ability to determine the activity of macrophages. In future studies, we recommend that an indication of type(s) of cell expressing the marker of interest be included when determining the marker concentration for each element (possibly by double-immunostaining). Among other things, this will allow relationships between mechanical stress and gene and protein expression of macrophages, as well as other cell types, to be more effectively evaluated.

Additional Endpoints

Based on the results of this study, we recommend that some additional endpoints for investigation with respect to mechanical stress. First of all, because NF-kB activity has been implicated in apoptosis, and because apoptosis is a possible cause of the drop in macrophage expression seen at high stress in some plaques, apoptosis is an interesting target for future comparison with mechanical stress.

Secondly, while this study looked at expression of MMP-1, MMPs are highly regulated, and thus expression does not necessarily indicate activity. Therefore, future studies should also investigate the expression of TIMPs (Tissue inhibitors of MMPs) with respect to stress. While methods to evaluate collagenolytic *activity* of MMP-1 are

currently limited to in situ zymography in frozen tissue, attempts should be made to evaluate this activity with respect to stress if additional methods become available.

In addition, while this study found no relationship between the presence of microvessels and mechanical stress, angiogenesis was not explicitly considered. Future studies should focus specifically on angiogenesis, rather than on overall microvessel presence. Also, while no strong relationship was found in this study between nitrotyrosine and mechanical stress, nitrotyrosine has several limitations as a marker for reactive oxygen species. Therefore, as improved antibodies or additional detection methods for ROS become available, further studies may show that a relationship does indeed exist.

And lastly, the list of inflammatory markers included in this study is by no means exhaustive. While we attempted to choose markers that cover a wide range of inflammatory processes, there are still many inflammatory markers present in plaque which may be sensitive to mechanical stress. Further studies into these markers may identify additional relationships between the mechanics and inflammation.

Future Research Directions

This study has laid the foundation for future studies focusing on the mechanisms and impacts of relationships between inflammation and the local mechanical environment. While plausible mechanisms underlying these relationships were proposed here, research is needed to validate these mechanisms, and to improve of understanding of the causal nature of these relationships.

Further investigation is needed to elucidate the role of NF-kB activation at high stress in atherosclerotic plaque. A significant trend of increasing NF-kB expression with increasing stress was found in all stages of plaque progression. However, the effects of NF-kB activation remains ambiguous, and the results of this study and previous studies suggest that NF-kB activation may have a different effect in different cell types and different environments. What genes are specifically affected by NF-kB activation at high stress? Does it protect against apoptosis at high stress, or does it have a pro-apoptotic effect? Does it have a different effect in macrophages than in smooth muscle cells exposed to high stress? Does it have a different effect in medial smooth muscle cells than in intimal smooth muscle cells?

In most stages of plaque progression, macrophages were found to increase with increasing stress, but then decrease significantly at very high stress. However, in advanced plaque macrophages continue to increase at high stress. Further studies are first needed to determine why the presence of macrophages drops at very high stress in most plaque. Is this due to apoptosis, failure to migrate, failure to differentiate, or some other mechanism? In addition, further study is needed to determine why a different relationship between macrophages and stress was found in advanced plaque. Because macrophages and high stress collocate at the site of rupture, this could be crucial to understanding the pathology of plaque rupture.

The results of this study raise many additional research questions which require further investigation. What are the specific biological mechanisms relating mechanical stress and inflammation? Because stresses are sensed on the cellular level, how do changes in the microstructure surrounding cells during remodeling affect the loads that

are transmitted to the cells? In what specific ways do interactions between mechanical stress and the inflammatory markers studied here affect the course of plaque progression? Using the findings of this study as a basis for investigation, it may even be possible to eventually develop a dynamic model of plaque progression that incorporates interactions between the local mechanical environment and NF-kB activation, macrophage recruitment, proliferation, apoptosis, and activity, and MMP-1 expression to direct changes in vessel morphology.

Long Term Clinical Applications

Because this research was conducted using diseased human tissue, the finding that there are spatial relationships between mechanical stress and markers of inflammation has direct implications for human pathology. These results provide a scientific basis for research into potential therapies that manipulating these relationships.

First, research into mechanisms for controlling stresses within plaque could potentially be used to reduce or manipulate the inflammatory response, with direct impact on plaque progression. Secondly, research into mechanisms to control the expression of these inflammatory markers could potentially be used to prevent progression of plaque to instability by preventing changes in the structure, composition, and material properties of plaque that lead to increased stresses. And third, research into mechanisms for disrupting the relationship between mechanical stress and inflammatory marker expression (for instance, by locally disrupting mechanotransduction signaling pathways) could change the course of plaque progression in a potentially beneficial way.

APPENDIX A: SUPPLEMENTAL DATA

Table A.1 Medical Data on Heart Transplant Patients

	Date of Transplant	Date of Birth	Age	Sex	Medications	Medical History
1	**3/13/2005**	12/20/1952	52	M	Amiodarone, Prevacid, Effexor, Prevacid, Lisinopril, Toresamide	MI in 2004, severe ischemic cardiomyopathy
2	**4/13/2005**	1/13/1962	43	M	Amiodarone, Elanapril, Coumadin, Imdur, Aldactone, Singulair, Advair, Flovent, Tessalon	hypertrophic cardiomyopathy, increased abdominal girth, weight gain, found to be in ARF
3	**8/19/2005**	11/10/1960	44	M	Coreg, K-Dur, Aldactone, Demadex, Coumadin, ASA, Protonix	CHF, A fib, hypercholesterolemia, dilated cardiomyopathy
4	**9/27/2005**	12/13/1942	62	M	Dobutamine, Cozaar, Amiodarone, Coumadin, Nitro, Digoxin, Demadex, Zoloft, Aldactone	iscemic cardiomyopathy, hiatal hernia, anemia, CABG, BiV pacer, cataract surgery, inguinal hernia repair
5	**10/20/2005**	5/30/1945	60	M	Amiodarone, Losartan, Aspirin, Coumadin, Spironolactone, Furosemide, Ambien, Milrinone, Citalopram	idiopathic dilated cardiomyopathy
6	**11/24/2005**	5/7/1961	44	M	Amiodarone, Coreg, Colace, Folic Acid, Hydralazine, Imdur, Demadex, Coumadin	non-ischemic dilated cardiomyopathy
7	**4/19/2006**	5/1/1961	44	M	Milrinone, Toprol, Coumadin, Demadex, Amiodarone, Lanoxin, Zocor	ischemic cardiomyopathy, MI, CABG
8	**4/27/2006**	7/13/1961	45	M		CHF, congenitally malformed trileaflet valve

CO-EXPRESSION OF INFLAMMATORY MARKERS

As discussed in Chapter 3, for each marker, elements were divided into two groups – either positive or negative – based on their content of that marker. Then for each group, the proportion of elements positive for each of the remaining four markers was then determined. These proportions are given below for all cross-sections (Table A.2), and for each disease category (Table A.3 – A.6).

Table A.2 Co-expression proportions for all cross-sections considered together

All Cross-sections										
Marker	nfkb neg	nfkb pos	macs neg	macs pos	mmp1 neg	mmp1 pos	nt neg	nt pos	mvs neg	mvs pos
NFKB	-	-	0.13	0.20	0.35	0.59	0.55	0.68	0.36	0.38
MACS	0.27	0.39	-	-	0.43	0.46	0.53	0.61	0.41	0.22
MMP1	0.20	0.40	0.14	0.17	-	-	0.49	0.70	0.28	0.48
NT	0.21	0.31	0.15	0.21	0.25	0.43	-	-	0.30	0.33
MVs	0.29	0.31	0.22	0.11	0.31	0.49	0.58	0.62	-	-

Table A.3 Early category co-expression proportions

Early										
Marker	nfkb neg	nfkb pos	macs neg	macs pos	mmp1 neg	mmp1 pos	nt neg	nt pos	mvs neg	mvs pos
NFKB	-	-	0.02	0.01	0.51	0.71	0.58	0.71	0.64	0.67
MACS	0.28	0.19	-	-	0.57	0.53	0.63	0.69	0.63	0.73
MMP1	0.19	0.37	0.02	0.02	-	-	0.51	0.66	0.61	0.64
NT	0.19	0.30	0.02	0.02	0.42	0.58	-	-	0.64	0.69
MVs	0.25	0.28	0.02	0.02	0.50	0.53	0.60	0.65	-	-

Table A.4 Intermediate category co-expression proportions

Intermediate										
Marker	nfkb neg	nfkb pos	macs neg	macs pos	mmp1 neg	mmp1 pos	nt neg	nt pos	mvs neg	mvs pos
NFKB	-	-	0.21	0.33	0.27	0.27	0.61	0.69	0.22	0.23
MACS	0.21	0.34	-	-	0.27	0.45	0.59	0.73	0.24	0.20
MMP1	0.21	0.21	0.20	0.30	-	-	0.60	0.72	0.19	0.29
NT	0.19	0.26	0.15	0.25	0.20	0.31	-	-	0.30	0.22
MVs	0.30	0.28	0.28	0.24	0.25	0.35	0.65	0.56	-	-

Table A.5 Advanced category co-expression proportions

Advanced										
Marker	nfkb neg	nfkb pos	macs neg	macs pos	mmp1 neg	mmp1 pos	nt neg	nt pos	mvs neg	mvs pos
NFKB	-	-	0.22	0.33	0.33	0.51	0.66	0.74	0.16	0.25
MACS	0.31	0.47	-	-	0.33	0.49	0.66	0.64	0.21	0.19
MMP1	0.32	0.52	0.21	0.34	-	-	0.63	0.79	0.12	0.33
NT	0.32	0.40	0.27	0.28	0.27	0.45	-	-	0.12	0.22
MVs	0.39	0.53	0.29	0.28	0.31	0.67	0.67	0.81	-	-

Table A.6 Mature category co-expression proportions

Mature										
Marker	nfkb neg	nfkb pos	macs neg	macs pos	mmp1 neg	mmp1 pos	nt neg	nt pos	mvs neg	mvs pos
NFKB	-	-	0.10	0.10	0.23	0.31	0.47	0.59	0.24	0.35
MACS	0.32	0.32	-	-	0.30	0.47	0.50	0.59	0.31	0.18
MMP1	0.32	0.41	0.05	0.09	-	-	0.44	0.55	0.32	0.36
NT	0.39	0.41	0.06	0.10	0.24	0.33	-	-	0.32	0.30
MVs	0.27	0.41	0.12	0.07	0.26	0.29	0.44	0.42	-	-

APPENDIX B: HISTOLOGY PROTOCOLS

B.1 Methyl Methacrylate Embedding of Soft Tissue

Purpose: Methyl methacrylate embedding of soft tissue for histology purposes.
Fixation: 10% buffered formalin
Hazards: Reagents used in this procedure are carcinogenic, neurotoxic, and explosive. User should wear gloves, goggles, and perform all work under a fume hood. Care must be taken to limit the addition of the catalyst and activator. Do not place solutions with catalyst and activator at temperatures greater than 37 C.

Method:

1. Pressure fix the sample in room temperature 10% neutral buffered formalin for 2 hours. (Fixative volume should be approximately twenty times that of tissue volume.) Fix for approximately 36 hours after pressure has been removed. (Fixation rate is approximately 1mm per 24 hours.)

2. Tissue is transferred to 70% alcohol post fixation and stored here until ready for processing.

3. Dehydrate tissue via the following schedule (can be done on processor):
   70% alcohol for 1 hr
   80% alcohol for 1 hr
   95% alcohol for 1 hr
   100% alcohol for 1 hr x 2
   Prepare infiltration solution 30 minutes prior to completion of dehydration.

4. Place samples in MMA infiltration solution:

Infiltration Solution	20 ML	15 mL	7.5 mL
MMA	15 mL	11.25 mL	5.625 mL
Dibutyl Pthalate (softener)	5 mL	3.75 mL	1.875 mL
Benzoyl Peroxide (catalyst)	1 g	0.75 g	0.375 g

5. Infiltrate in two changes of infiltration solution for 1 hour. Infiltrate in a further change overnight. The overnight infiltration step is performed on a rotator at room temperature.

6. Prepare the embedding solution:

Embedding Solution	15 mL	7.5 mL	9 mL
MMA	11.25 mL	5.625 mL	6.75 mL
Dibutyl Pthalate (softener)	3.75 mL	1.875 mL	2.25 mL
Benzoyl Peroxide (catalyst)	0.75 g	0.375 g	0.455 g
N,N-dimethyl-p-toluidine (activator)	94 µL	47 µL	56.4 µL

7. In a separate tube, combine the first 4 ingredients of the embedding solution. Vortex and place on shaker for 30 minutes. Vortex periodically.

8. Add activator and mix by hand for 1 minute.

9. Pour solution into imbedding tube(s), and place tissue in tube. Do not worry about exact position yet.

10. After polymerization has begun (~1 hour), use forceps to carefully position tissue as desired, while avoiding formation of air bubbles in solution.

11. Polymerization should occur in 4-6 hours.

12. After polymerization, use dremel to cut tube away from section.

13. Use jeweler saw or dremel to cut off excess MMA

14. Use rotating grinder to grind down and flatten the ends of the block

15. Superglue the block to a polycarbonate base for sectioning.

Reagents:
Methyl Methacrylate: Fisher #AC127140025
Dibutyl Pthalate: Aldrich #15,243-9
Benzoyl Peroxide: Sigma #17998-1
N,N-dimethyl-p-toluidine (aka N-N, dimethylaniline): Aldrich #D18900-6

B.2 von Kossa's Calcium and Masson's Trichrome Stains

This protocol is a modified version of an original obtained from Tracey Couse.

Purpose: Detection of calcium phosphate, Collagen, and Smooth Muscle
References: Mallory, Sheehan & Hrapchak
Carson, FL: Histotechnology: A Self-Instructional Text.
American Society of Clinical Pathologists, 1990.
Hazards: Silver nitrate is dangerous. Wear goggles and gloves. Dispose to chemical waste. Dried picric acid is explosive. Keep container tightly sealed. Wet lid before opening. Discard as chemical waste by calling OEHS.

Method:

1. Deplasticize in Xylene and acetone and rehydrate to distilled water:
   Xylene 2x20 min
   Acetone 1x3 min
   100% Alcohol 3x2min
   95% alcohol 2x2 min
   75% alcohol 1x2min
   Distilled water 2x2min

2. Place sections in silver nitrate solution and expose to bright sunlight or a UV light source for 10 to 20 minutes. Check slides periodically and stop reaction when the calcium salts are brown to black.

3. Rinse in distilled water

4. Place slides in 5% sodium thiosulfate for 2 minutes.

5. Wash well in distilled water

6. Proceed to Masson's Trichrome stain, or dehydrate through graded alcohol to xylene and coverslip.

7. Mordant sections in Bouin's for 1 hour at 56^{o}C.

8. Remove slides from oven and allow cooling at room temperature. Wash in running tap water until yellow is no longer visible.

9. Rinse in distilled water.

10. Stain sections in Biebrich's scarlet-acid fuchsin for 5 minutes. Solution can be used twice before discarding.

11. Rinse in distilled water.

12. Place sections in phosphomolybdic-phosphotungstic acid for 30-60 seconds. Discard after use. This step removes red from collagen.

13. Stain sections in aniline blue for 5-10 minutes. Solution may be used twice before discarding.

14. Rinse the slides in 1% acetic acid solution for 30 seconds – 2 minutes. Discard solution after use.

15. Dehydrate in 95% and 100% alcohol, twice each.

16. Clear with 2-3 changes of xylene and mount with synthetic resin.

Results:

Calcium salts	Black
Cytoplasm, muscle fibers, keratin	Red
Collagen and mucus	Blue

Notes:

The silver reacts with the anions, mainly carbonate and phosphate of the calcium salts. Bright light reduces the silver salts to metallic silver. Unreduced silver is removed via sodium thiosulfate. The use of unbuffered formalin may cause false positive results. Formic acid can lead to the generation of formalin pigment, which will reduce silver and result in a brown reaction product.

Reagents and Solutions:

5% silver nitrate

Silver nitrate	1g
Distilled water	20 mL

5% Sodium Thiosulfate

5% sodium thiosulfate	5g
Distilled water	100 mL

Bouin's Solution:

Picric acid, saturated aqueous solution	75ml
Formaldehyde, 37% to 40%	25ml

Glacial acetic acid 5ml

Biebrich Scarlet-Acid Fuchsin Solution:
Biebrich scarlet (C.I. 26905), 1% aqueous solution 360ml
Acid fuchsin (C.I. 42685), 1% aqueous solution 40ml
Glacial acetic acid 4ml

Phosphomolybdic-Phosphotungstic Acid Solution:
Phosphomolybdic acid 25g
Phosphotungstic acid 25g
Distilled water 1200ml

Aniline Blue Solution:
Aniline blue 25g
Glacial acetic acid 20ml
Distilled water 1000ml

1% Acetic Acid Solution:
Glacial acetic acid 1ml
Distilled water 99ml

B.3 Immunohistochemistry Using ABC-Alkaline Phosphatase

Please note: All antibodies and related reagents are temperature sensitive. Please keep at 4 C or on ice at all times. This will maintain the longevity of the reagents and limit antibody or reagent related problems with experiments.

1. Fix embedded tissue is deparrafinized/deplasticized and rehydrated in descending grades of alcohol.

   Parrafin:
   Autostainer program
   Plastic:
   2x20 min Xylene
   1x3 min Acetone
   100% Alcohol 3x2min
   95% alcohol 2x2 min
   75% alcohol 1x2min
   Distilled water 2x2min

   Frozen sections are thawed immediately before use at room temp 10-30 min before start of procedure. The frozen sections are fixed in acetone **5 min.** and airdried **5 min**.

2. Wash slides in 1XPBS **5 min**

3. Pretreatment:

   Pressure Cooker:
   See HEIR protocol

   Proteinase K:
   Tissue is treated with 1 μg/mL Proteinase K for **10 min** at room temperature
   Dilute 7.5 μl of 20 mg/mL stock Proteinase K in 150 mL of 1XPBS

4. Wash slides in 1XPBS twice for **5 min** each

5. Block tissue using 1% gelatin/PBS mixture for **20 min**

6. Prepare working dilution of primary antibody in 1% crystalline grade BSA in 1XPBS. Refer to previous work done with the antibody to determine working dilution, or refer to spec sheet of antibody for starting dilution.

7. Blot off geletin/PBS. DO NOT wash in PBS. Apply 150 μL of primary antibody (use less or more antibody depending on size of section). Incubate sections in a humid chamber for **1 hour** at room temperature, or overnight at 4 C.

8. Blot off excess antibody and wash slides in 1XPBS twice for **5 min** each.

9. Prepare working dilution of the biotinylated secondary antibody in 1% crystalline grade BSA in 1XPBS, and add 2% of normal serum from source animal of the secondary antibody. Prepare secondary antibody at 1/400 dilution. Apply 150 μL of antibody and incubate in a humid chamber **30 min.**

10. MEANWHILE, prepare the working dilution of ABC-Vector Red complex from the alkaline phosphatase standard kit (Vector #AK-5000) after application of secondary antibody. Allow to sit at ROOM TEMPERATURE **30 min.**
Solution:
    5 mL 1XPBS
    1 drop Reagent A
    1 drop Reagent B

11. Blot off excess antibody and wash slides in 1XPBS twice for **5 min** each.

12. Apply 150 μL of prepared ABC mixture to each slide. Incubate in a humid chamber at room temperature for **1 hour.**

13. Blot off excess antibody and wash slides in 1XPBS twice for **5 min** each, followed by one wash in 100mM tris pH 8.2 for **5 min**.

14. Make up alkaline phosphatase substrate solution (Vectore #SK-5100) immediately before use. Add to a foil-wrapped bottle:
    5mL of 100mM tris pH 8.2
    one drop levamisole (Vector #SP-5000)
    two drops each of reagent 1, 2, and 3
Apply 2-3 drops per section.
Incubate in the dark for up to 1 hour, checking color reaction periodically. Stop reaction by blotting off substrate and rinsing in tap water twice for **5 min** each

15. Lightly counterstain sections with Gill's hematoxylin (about 30 sec). Rinse slides well in water until water is clear. Dehydrate through graded alcohols, then xylene and coverslip for viewing.
Hematoxylin for 10 seconds
Rinse in tap water until clear
Dip once in 1% acid alcohol
Rinse in water
Scott's solution for 20 seconds
Rinse in water
Dehydrate through graded alcohols then xylene
Coverslip.

REAGENTS AND SOLUTIONS

Proteinase K
Dissolve proteinase K (Sigma #P-4914) in dH2O for a stock concentration of 20 mg/mL. Aliquot and store at -20 C.

10X PBS
Boehringer Mannheim #1666789

1% BSA/PBS
1g fraction V BSA (Sigma #A2153) in 100mL 1XPBS
Mix until fully dissolved. Aliquot into 5 mL volumes and store at -20 C

Secondary antibody and normal animal serum
Vector

Alkaline Phosphatase Standard ABC kit
Vector #AK-5000

Alkaline Phosphatase Substrate Kit I
Vector #SK-5100

Hematoxylin
Dilute Gill's Hematoxylin no. 2 (Polysciences #04570) one to one with dH2O before use

1% Acid Alcohol
2 mL HCl (Fisher #A144s) in 198 mL of 70% ethanol

Scott's Solution

NaHCO3	2g
MgSO4*7H2O	20g
dH2O	1000mL

Mix Until dissolved

B.4 HIER Using the Princess Electric Pressure Cooker and Citrate Buffer

1. Deparaffinize/deplasticize sections.
2. Rinse slides in PBS for 5 minutes.
3. Prepare the Princess pressure cooker. It is comprised of a base, a pot, a steel rack, and a lid. Plug the pressure cooker base into an outlet.
4. Remove the lid from the pressure cooker pot. Ensure the steel rack resting in the pot is prong side up.
5. Add about 2 staining dishes worth of water to the pot (about 400ml).
6. Fill the staining dish with 200ml of 10mM citrate buffer, pH6.0. Add slide rack containing slides and cover with staining dish lid.
7. Place slides and staining dish into pressure cooker pot. Lock pressure cooker lid in place atop pressure cooker. Be sure that the vent (rapid release) is in the closed position (up position).
8. Set pressure mode to high by pressing the "Pressure Mode" button twice.
9. Set the time for 15 minutes by using the "up" arrow. Press the start button.
10. The time will begin once the pot reaches the correct pressure and temperature.
11. When the timer reaches zero, push the "off" button.
12. After waiting 5 minutes, carefully push the "Rapid Release" tap to the down position. This releases the pressure within the pot, which will result in some spray of hot water. The red pin will descend once all the pressure has been release. The lid can now be removed.
13. Let slides cool to room temperature for 20minutes.
14. Transfer slide rack to ihc wash buffer and proceed with ihc protocol.

Solutions:

10mM Citrate Buffer, pH 6.0 (500ml)

Solution A	9 ml
Solution B	41 ml
dH_2O	450 ml

Adjust pH to 6.0. Bring up to 500 ml. Final concentrations are 1.96mM citric acid and 8.2mM sodium citrate.

Solution A, Citric Acid (109mM)

Citric acid	4.2 g
dH_2O	200 ml

Solution B, Sodium Citrate (100mM)

Sodium citrate	14.7 g
dH_2O	500 ml

APPENDIX C: MATLAB AND ANSYS CODE

C.1 Building and Meshing of Mechanical Model in ANSYS

When run in ANSYS 9.0, this code does the following for a sample cross-section:

- Reads in keypoints for the inner and outer boundary of the arterial cross-section
  - Rca##_s#r#_lumen_reduced.csv
  - Rca##_s#r#_exterior_reduced.csv
- Generates lines connecting keypoints
- Generates areas withing the lines
- Glues areas to generate a single cross-sectional area
- Coarsely meshes area and saves mesh as:
  - Rca##_s#r#_coarse_nodes.txt
  - Rca##_s#r#_coarse_elements.txt
- Refines coarse mesh and saves mesh as:
  - Rca##_s#r#_fine_nodes.txt
  - Rca##_s#r#_fine_elements.txt

```
FINISH
/CLEAR, NOSTART
/begin
!Assign name to parameters (limited to 8 characters)
m1 = 'rca15_'
m4 = 's1r7'
m2 = '_course'
M3 = '_fine'

!set starting directory^^^^^^^^^^^^^^^^^^^^
/CWD, 'G:\RCA15 - final\%m4%'

/PREP7

!Read in keypoints of inner and outer boundary
/INPUT, '%m4%_lumen_reduced','csv',,,0
/INPUT, '%m4%_exterior_reduced','csv',,,0



!Create lines for inner vessel wall
KPbegin=1
KPend=105    !number of keypoints on lumen surface !^^^^^^^^^^^^^^^
n=KPbegin
*Do,n,KPbegin,KPend-1
  L,n,n+1
*EndDo
```

```
L,KPend,KPbegin

!Create lines for outer vessel wall
KPbegin=KPend+1
KPend=KPend+128         !Add number of keypoints on !exterior surface^^^^^^^^^^^^^
n=KPbegin
*Do,n,KPbegin,KPend-1
  L,n,n+1
*EndDo
L,KPend,KPbegin

KPlines=KPend

!create lines dividing into four quadrants
L,63,159
L,36,195
L,14,220
L,83,136

!Create areas from lines
Lsel,s,,,236
Lsel,a,,,220,233
Lsel,a,,,106,135
Lsel,a,,,83,105
Lsel,a,,,1,13
Lsel,a,,,237
AL,all
Allsel,all

Lsel,s,,,236
Lsel,a,,,195,219
Lsel,a,,,235
Lsel,a,,,14,35
AL,all
Allsel,all


Lsel,s,,,235
Lsel,a,,,36,62
Lsel,a,,,234
Lsel,a,,,159,194
AL,all
Allsel,all

Lsel,s,,,237
Lsel,a,,,63,82
```

```
Lsel,a,,,234
Lsel,a,,,136,158
AL,all
allsel,all


!Glue areas to form a single area
Allsel,all
Aglue,all

!Pick Element Type
ET,1,PLANE42
KEYOPT,1,3,2          !set option for plane strain
KEYOPT,1,5,0
KEYOPT,1,6,0

!Set shape warnings for meshing
SHPP,WARN,ASPECT,4
SHPP,WARN,MAXANG,65

!coarsely mesh area
Asel,all
smrt,5
amesh,all

!Write course node and element data to text files and save model
nwrite,%m1%%m4%%m2%_nodes,txt,,0
ewrite,%m1%%m4%%m2%_elements,txt,,0

!refine mesh
*IF, m3, EQ, '_fine', THEN
  erefine,ALL, , ,1,0,clean
*ENDIF

!Write node and element data to text files and save model
nwrite,%m1%%m4%%m3%_nodes,txt,,0
ewrite,%m1%%m4%%m3%_elements,txt,,0
```

C.2 Determination of Segmentation Values for Each Constituent

This code uses manual segmentations of representative cross-sections to determine the average RGB values for each arterial constituent. Based on these values, the minimum distance segmentation algorithm in Appendix C.3 is used to segment the remaining cross-sections.

```
clear all
%set parameters for names of saved pre-segmented images
artery='rca33_';
nSeg=2;            %number of manually segmented images


nMat=4; %number of materials present in presegmented images

%Create matrix to contain sum of all values in each segmentation region
segCentroid=zeros(nMat,3);

%Create matrix to contain total number of pixels in each segmentation region
segPixCount(1:nMat)=0;

%for each pre-segmented image
for k=1:nSeg

   %set directory where manually segmented files are located
   cd 'F:\RCA33\manually segmented'
   if k==1
      section='s1r1';     %manually segmented section
   end
   if k==2
      section='s2r22';    %manually segmented section
   end


   %load manually segmented image
   Iseg=imread([artery,section,'_massons.png']);

   %change into directory where original image is located
   cd(['F:\RCA33\',section])
```

```
   %load original image
   I=imread([artery,section,'_massons.png']);

   I=double(I);
   Iseg=double(Iseg);
   Iseg=Iseg./255;


segIndex=zeros(nMat,3);
segIndex(1,:)=[0 1 0];  %RGB values for HEALTHY tissue in segmented image (gre(n)
segIndex(2,:)=[0 0 1];  %RGB values for FIBROUS (blue)
segIndex(3,:)=[1 1 1]; %RGB values for LIPID (white)
segIndex(4,:)=[1 0 0]; %RGB values for CALCIUM (red)

for i=1:nMat
   [a,b]=find(Iseg(:,:,1)==segIndex(i,1) & Iseg(:,:,2)==segIndex(i,2) &
Iseg(:,:,3)==segIndex(i,3));
   L=length(a);
   segPixCount(i)=segPixCount(i)+L;
   for j=1:L
      t(1:3)=I(a(j),b(j),:);
      segCentroid(i,:)=segCentroid(i,:)+t;
   end
end

end

for i=1:nMat
   segCentroid(i,:)=segCentroid(i,:)./segPixCount(i);
end

%change to directory where segmentation ranges should be saved ^^^^^^
cd 'F:\RCA33/Segmentation Range Files'
save 'rca33_rgb_segRanges' segCentroid
```

C.3 Auto-Segmentation of Cross-Sections Using Minimum-Distance Criteria

This code uses the average RGB values determined from manually segmented cross-sections (Appendix C.2) to assign each pixel of a Massons-stained image to a plaque constituent.

```
clear all

cd 'F:\RCA33'  %set starting directory
artery='rca33_';        %set artery number

for x=1:2
     y=1;
    while y<48

section=['s' num2str(x) 'r' num2str(y)]         %set section number

cd 'Segmentation Range Files'

%Load pre-determined segmentation values for each constituent
load([artery,'rgb_segRanges'])

cd ..
%segCentroid(3,:)=255; %add lipid/external segmentation if missing
segCentroid(4,:)=0; %add calcium segmentation if missing

 cd(section)
origImage='_massons';
extension='.png';

%Load image to be segmented
I=imread([artery,section,origImage,extension]);
I=double(I);

%set color index values for each constituent
codeRGB(1,:)=[0 1 0];  %healthy --> green
codeRGB(2,:)=[0 0 1];   %fibrous --> blue
codeRGB(3,:)=[1 1 1];   %lipid --> white
codeRGB(4,:)=[1 0 0];   %calcium --> red
```

```
%set grayscale index values for each constituent
codeGray(1)=175;
codeGray(2)=125;
codeGray(3)=225;
codeGray(4)=75;

nMat=size(segCentroid);
nMat=nMat(1);

%for each material
for i=1:nMat
        % calculate the distance between the RGB value of each pixel in the image of
        % interest and the segmentation value for the material under consideration
        Idist(:,:,i)=(I(:,:,1)-segCentroid(i,1)).^2+(I(:,:,2)-segCentroid(i,2)).^2+(I(:,:,3)-
        segCentroid(i,3)).^2;
end

L=size(I);
Iind=zeros(L);
Igray=zeros(L(1),L(2));

%Assign each pixel to the constituent for which its distance is smallest
for i=1:L(1)
   for j=1:L(2)
      a=min(Idist(i,j,:));
      ind=find(Idist(i,j,:)==a);
      Iind(i,j,:)=codeRGB(ind,:);
      Igray(i,j)=codeGray(ind);
   end
end

Iind=Iind.*255;
Iind=uint8(Iind);
Igray=uint8(Igray);

gray='_gray';
indexed='_indexed';

%Save indexed, segmented images
imwrite(Igray,strcat(artery,section,gray,origImage,'.png'))
imwrite(Iind,strcat(artery,section,indexed,origImage,'.png'))

cd ..
y=y+1;
end
end
```

C.4 Calculation of Element Material Properties

This code can be used in Matlab to calculate the material properties of each element of a mesh from the segmented image using rule-of-mixtures. The code does the following:

- Loads segmented image (see Appendix C.2 and C.3):
  - rca##_s#r#.png
- Loads corresponding fine mesh (see Appendix C.1):
  - Rca##_s#r#_fine_elements.txt
  - Rca##_s#r#_fine_nodex.txt
- For each element:
  - determines the number of pixels of each constituent
  - calculates the area fraction of each constituent
  - uses rule of mixtures to determine young's modulus
- Saves material property data in a format that can be read by ANSYS:
  - Rca##_s#r#_ElementMaterialProps.csv
- Saves pixel-count data in a matlab file:
  - Rca##_s#r#_pixelCounts.mat

```
%determine material properties for each element using rule of mixtures
%this program may take quite a while to run (~45 min per image)
close all
clear all

%list of cross-sections to be segmented
pindex=[ 19 ];

%for each cross-section
for kk=1:length(pindex)
k=pindex(kk);

% set directory where segmented images are located
cd 'C:\Documents and Settings\VitoLab\Desktop\Melissa\data\RCA15 - final'

%set cross-section name
artery='rca15_';
section=['s1r' num2str(k)];
cd(section)

%Load segmented image
I = imread([artery section '.png']);
I=double(I);

%Load corresponding fine mesh
```

```
X = load([artery section '_fine_nodes.txt']);
nodes = [X(:,2:3)];  % Strip off node # and add z
elements = load([artery section '_fine_elements.txt']);
elements = elements(:,1:4);

%plot elements on top of segmented image
imshow(uint8(I))
hold on
h=patch('Vertices', nodes, 'Faces', elements, 'FaceVertexCData', ones(size(nodes),1),
'FaceColor', 'none', 'EdgeColor', 'k')

%convert color segmented image to grayscale segmented image
exterior = 0
calcium = 50
fibrous = 100
healthy = 200
lipid   = 255

Inew=zeros(size(I));
Inew=Inew(:,:,1);
[a,b]=find(I(:,:,1)==255 & I(:,:,2)==0 & I(:,:,3)==0);
for i=1:length(a)
   Inew(a(i),b(i))=calcium;
end
[a,b]=find(I(:,:,1)==0 & I(:,:,2)==0 & I(:,:,3)==255);
for i=1:length(a)
   Inew(a(i),b(i))=fibrous;
end
[a,b]=find(I(:,:,1)==0 & I(:,:,2)==255 & I(:,:,3)==0);
for i=1:length(a)
   Inew(a(i),b(i))=healthy;
end
[a,b]=find(I(:,:,1)==255 & I(:,:,2)==255 & I(:,:,3)==255);
for i=1:length(a)
   Inew(a(i),b(i))=lipid;
end

element_Nodeset=[];
numElements=length(elements);

for i=1:numElements
   for j=1:4
      nodeNum=elements(i,j);
      element_Nodeset(i,j,:)=nodes(nodeNum,:);
   end
end
```

```
%element_Nodeset(i,j,k)
%i --> Element Number
%j --> node number 1-4 (4 nodes per element)
%k --> 1-> Node Number  2->Xloc 3->Yloc


elem_materials=zeros(length(elements),5);
%column 1 - total number of pixels in element
%column 2 - number of healthy pixels in element
%column 3 - number of fibrous pixels in element
%column 4 - number of lipid pixels in element
%column 5 - number of calcified pixels in element

I2=I;
I=Inew;
I=double(I);
clear Inew
N=length(elements)


%%%%%%%%%%determine material properties for each element%%%%%%%%%

%for each element N
for i=1:N
   i
   Elem=I.*double(roipoly(I,element_Nodeset(i,:,1),element_Nodeset(i,:,2)));
   t=Elem(find(Elem~=exterior));
   elem_materials(i,1)=length(t);
   %determine number of healthy pixels (green)
   elem_materials(i,2)=length(find(t==healthy));
   %determine number of fibrous pixels (blue)
   elem_materials(i,3)=length(find(t==fibrous));
   %determine number of lipid pixels (white)
   elem_materials(i,4)=length(find(t==lipid));
   %determine number of calcified pixels (red)
   elem_materials(i,5)=length(find(t==calcium));
end


%Elastic material properties from Debbie's Thesis in Pascals
nuxy = 0.49;
LT_E2=3.875e4;
HT_E2=2.449e5;
FT_E2=1.821e6;
CT_E2=1.066e7;
```

```
%use rule of mixtures to calculate Young's modulus for each element
E2 = (elem_materials(:,2)*HT_E2 + elem_materials(:,3)*FT_E2 +
elem_materials(:,4)*LT_E2 + elem_materials(:,5)*CT_E2)./elem_materials(:,1);


%Save element materiarl property data in a format that can be read in by ANSYS
nuxy = 0.45;
fid = fopen([section '_ElementMaterialProps.csv'],'w');
for i = 1:length(elements);
   %       no tissue   lipid           healthy          fibrous         calcified
   % map1 = [0 0 0;    1 1 1;           0 1 0;           0 0 1;           1 0 0];
   MPtext = ['MP, EX, ' num2str(i), ', ' num2str(E2(i))];
   fprintf(fid, '%s\n', MPtext);
   MPtext = ['MP, NUXY, ' num2str(i), ', ' num2str(nuxy)];
   fprintf(fid, '%s\n', MPtext);
end

for i = 1:length(elements);
   MPCHGtext = ['MPCHG, ' num2str(i) ', ' num2str(i)];
   fprintf(fid, '%s\n', MPCHGtext);
end
fclose(fid);

% Plot elements color coded with material property values.
%figure('Color', 'w')
%patch('Vertices', nodes, 'Faces', elements, 'FaceVertexCData', E2, 'FaceColor','flat')
%set(gca,'Box','on')
%axis equal tight ij
%colorbar

% Save data to .mat file for later retrieval
save([section '_pixel_counts.mat'],'nodes','elements','E2','elem_materials');
end
```

C.5 Solution of Finite Element Model in ANSYS

This code assumes that the model has already been built and meshed in ANSYS 9.0 (see code in Appendix C.1). This code does the following:

- Sets the load to be applied to 40 mmHg
- Reads in previously calculated material properties (see Appendix C.4)
- Applies displacement constraints to prevent rigid body motion
- Solves for stresses and strain
- Prints out solutions

```
!must build model in ANSYS before running this file

!set incremental pressure in mmHg
*SET,nloads , 1
*DIM,TIMEV,array,nloads
*SET,TIMEV(1) , 40

!!!!!! Input material properties
/INPUT,'%m4%_ElementMaterialProps','csv',,,0
!set starting directory^^^^^^^^^^^^^^^^^^^^
!/CWD, 'C:\Documents and Settings\Administrator\Desktop\melissa'

!Set shape warnings
SHPP,WARN,ASPECT,4
SHPP,WARN,MAXANG,65

!Specify solution for large strain
NLGEOM,on
NSUBST,5
KBC,0

! Apply displacement constraints
KSEL,S,,,KPend
NSLK,S
D,ALL,UX,0
D,ALL,UY,0
ALLSEL,all
KSEL,S,,,KPend-25
NSLK,S
D,all,UY,0
ALLSEL,all

!!!solve for finite element solution
```

```
FINISH
/SOL
/STATUS,SOLU
OUTPR,NSOL,ALL,
lsel,s,,,1,KPlines
!!!apply pressure to lumen surface
*do,istep,1,nloads,1
time,timev(istep)
sfl,all,pres,timev(istep)*133.3
!!!solve
solve
*enddo

lsel,all
FINISH
/POST1
SET,LAST
/VIEW,1,0,0,-1
/VUP,1,-Y
/GLINE,1,-1
!AVPRIN,0, ,


!!!!!!!!Print out results and save to files
PLESOL,S,EQV,0,1
PRNSOL,DOF
!copy and paste into file s#r#_nodal_disp_cart.txt
!print nodal strain in cartesian coordinates
PRNSOL,EPTO,COMP
!copy and paste into file s#r#_nodal_strains_cart.txt
!make table of element data of interest

!print list of data in cartesian coordinates
etable,,s,1    !first principal stress
etable,,s,2 ! second principal stress
etable,,s,3 !third principal stress
etable,,s,eqv   !von mises
etable,,epto,1  !first principal strain
etable,,epto,2  !second principal strain
etable,,epto,3  !third principal strain
etable,,epto,eqv  !von Mises strain
PRETAB,S1,S2,S3,SEQV, EPTO1,EPTO2,EPTO3,EPTOEQV
!copy and paste into file s#r#_element_princresults_cartesion.txt
```

C.6 Calculation of Coarse Mesh Data from Fine Mesh FE Results

This code calculates stress and strain values for each element of the coarse mesh based on average values of corresponding elements in the fine mesh

```
%find average stresses and strains for course mesh based on average stresses and strains
of corresponding elements in fine mesh
 close all
clear all
 %cross-section names
 pindex=[17]

%for each cross-section
for kk=1:length(pindex)

close all
k=pindex(kk);

cd('C:\Documents and Settings\VitoLab\Desktop\Melissa\data\rca24')  %^^^^^^^^^^
artery='rca24_';
 section=['s1r' num2str(k)];

data_type='_Von Mises Stress_Strain_';
cd(section)

%load list of corresponding elements
FtoCelems=load([section,'_correspondingElements.csv']);


%%%%%find coarse mesh stress values

%load stress-strain data for the fine mesh
data=load([section,data_type,'fine.csv']);  %load element stress data ^^^^^^^^
A=size(data);

%find average stress for each element in course mesh
N=length(FtoCelems);
dataCourse=zeros(N,A(2));
for i=1:N
   sum=zeros(1,A(2));
   for j=1:4
      sum=sum+data(FtoCelems(i,j),:);
   end
   dataCourse(i,:)=sum./4;
```

```
end


%load course mesh
X = load([artery section '_course_nodes.txt']);
nodes = [X(:,2:3)];  % Strip off node # and add z
elements = load([artery section '_course_elements.txt']);
elements = elements(:,1:4);

nodes=nodes.*4; %account for resizing

%load fine mesh
Xf = load([artery section '_fine_nodes.txt']);
nodesf = [Xf(:,2:3)];  % Strip off node # and add z
elementsf = load([artery section '_fine_elements.txt']);
elementsf = elementsf(:,1:4);

%plot course mesh and fine mesh stress and strain maps
nodesf=nodesf.*4; %account for resizing
h=patch('Vertices', nodesf, 'Faces', elementsf, 'FaceVertexCData', data(:,1), 'FaceColor',
'flat', 'EdgeColor', 'k')
figure
h=patch('Vertices', nodes, 'Faces', elements, 'FaceVertexCData', dataCourse(:,1),
'FaceColor', 'flat', 'EdgeColor', 'k')

%save coarse mesh data
dlmwrite([section data_type 'course.csv'],dataCourse)
cd 'C:\Documents and Settings\VitoLab\Desktop\Melissa\Stress - Macrophage Statistical
Analysis\data\rca34'
dlmwrite([section data_type 'course.csv'],dataCourse)
end
```

REFERENCES

1. American Heart Association. Heart Disease and Stroke Statistics. Dalas, Texas: American Heart Association 2006.

2. Aplin AE, Howe A, Alahari SK, Juliano RL. Signal Transduction and Signal Modulation by Cell Adhesion Receptors: The Role of Integrins, Cadherins, Immunoglobulin-Cell Adhesion Molecules, and Selectins. Pharmacological Reviews 1998; 50: 197-261.

3. Arauz A, Hoyos L, Zenteno M, Mendoza R, Alexanderson E. Carotid plaque inflammation detected by (18)F-fluorodeoxyglucose-positron emission tomography Pilot Study. Clin Neurol Neurosurg 2007; 109(5):409-12.

4. Arroyo LH, Lee RT. Mechanisms of plaque rupture: mechanical and biologic interactions. Cardiovasc Res 1999; 41: 369-75.

5. Baker CS, Hall RJ, Evans TJ, Pomerance A, Maclouf J, Creminon C, Yacoub MH, Polak JM. Cyclooxygenase-2 is widely expressed in atherosclerotic lesions affecting native and transplanted human coronary arteries and colocalizes with inducible nitric oxide synthase and nitrotyrosine particularly in macrophages. Arterioscler Thromb Vasc Biol 1999; 19: 646-55.

6. Baldewsing RA, de Korte CL, Schaar JA, Mastik F, van der Steen AF. A finite element model for performing intravascular ultrasound elastography of human atherosclerotic coronary arteries. Ultrasound Med Biol 2004; 30: 803-13.

7. Bank AJ, Versluis A, Dodge SM, Douglas WH. Atherosclerotic plaque rupture: a fatigue process? Med Hypotheses 2000; 55: 480-4.

8. Barger AC, Beeuwkes R, 3rd. Rupture of coronary vasa vasorum as a trigger of acute myocardial infarction. Am J Cardiol 1990; 66: 41G-43G.

9. Beattie D, Vito R. Determination of stresses and strains in heterogeneous, diseased human aorta. ASME Advances in Bioengineering 1996; 215-216.

10. Beattie D, Xu C, Vito R, Glagov S, Whang MC. Mechanical analysis of heterogeneous, atherosclerotic human aorta. J Biomech Eng 1998; 120: 602-7.

11. Beckman JA, Ganz J, Creager MA, Ganz P, Kinlay S. Relationship of clinical presentation and calcification of culprit coronary artery stenoses. Arterioscler Thromb Vasc Biol 2001; 21: 1618-22.

12. Berliner JA, Navab M, Fogelman AM, Frank JS, Demer LL, Edwards PA, Watson AD, Lusis AJ. Atherosclerosis: basic mechanisms. Oxidation, inflammation, and genetics. Circulation 1995; 91: 2488-96.

13. Bostrom K, Watson KE, Horn S, Wortham C, Herman IM, Demer LL. Bone morphogenetic protein expression in human atherosclerotic lesions. J Clin Invest 1993; 91: 1800-9.

14. Bostrom K, Watson KE, Stanford WP, Demer LL. Atherosclerotic calcification: relation to developmental osteogenesis. Am J Cardiol 1995; 75: 88B-91B.

15. Boyle JJ, Weissberg PL, Bennett MR. Tumor necrosis factor-alpha promotes macrophage-induced vascular smooth muscle cell apoptosis by direct and autocrine mechanisms. Arterioscler Thromb Vasc Biol 2003; 23: 1553-8.

16. Brand K, Page S, Rogler G, Bartsch A, Brandl R, Knuechel R, Page M, Kaltschmidt C, Baeuerle PA, Neumeier D. Activated transcription factor nuclear factor-kappa B is present in the atherosclerotic lesion. J Clin Invest 1996; 97: 1715-22.

17. Bubici C, Papa S, Dean K, Franzoso G. Mutual cross-talk between reactive oxygen species and nuclear factor-kappa B: molecular basis and biological significance. Oncogene 2006; 25(51):6731-48.

18. Burke AP, Weber DK, Kolodgie FD, Farb A, Taylor AJ, Virmani R. Pathophysiology of calcium deposition in coronary arteries. Herz 2001; 26: 239-44.

19. Burleigh MC, Briggs AD, Lendon CL, Davies MJ, Born GV, Richardson PD. Collagen types I and III, collagen content, GAGs and mechanical strength of human atherosclerotic plaque caps: span-wise variations. Atherosclerosis 1992; 96: 71-81.

20. Carnell, PC. Personal communication, Ma y 2006.

21. Carr S, Farb A, Pearce WH, Virmani R, Yao JS. Atherosclerotic plaque rupture in symptomatic carotid artery stenosis. J Vasc Surg 1996; 23: 755-65; discussion 765-6.

22. Casscells W, Hathorn B, David M, Krabach T, Vaughn WK, McAllister HA, Bearman G, Willerson JT. Thermal detection of cellular infiltrates in living atherosclerotic plaque: possible implications for plaque rupture and thrombosis. Lancet 1996; 347: 1447-51.

23. Chandran KB, Mun JH, Choi KK, Chen JS, Hamilton A, Nagaraj A, McPherson DD. A method for in-vivo analysis for regional arterial wall material property alterations with atherosclerosis: preliminary results. Med Eng Phys 2003; 25: 289-98.

24. Chau AH, Chan RC, Shishkov M, MacNeill B, Iftimia N, Tearney GJ, Kamm RD, Bouma BE, Kaazempur-Mofrad MR. Mechanical analysis of atherosclerotic plaque based on optical coherence tomography. Ann Biomed Eng 2004; 32: 1494-503.

25. Cheng GC, Loree HM, Kamm RD, Fishbein MC, Lee RT. Distribution of circumferential stress in ruptured and stable atherosclerotic lesions. A structural analysis with histopathological correlation. Circulation 1993; 87: 1179-87.

26. Davies MJ. Going from immutable to mutable atherosclerotic plaque. Am J Cardiol 2001; 88: 2F-9F.

27. Davies MJ. Reactive oxygen species, metalloproteinases, and plaque stability. Circulation 1998; 97: 2382-3.

28. Davies MJ, Thomas AC. Plaque fissuring--the cause of acute myocardial infarction, sudden ischaemic death, and crescendo angina. Br Heart J 1985; 53: 363-73.

29. Davies MJ, Thomas T. The pathological basis and microanatomy of occlusive thrombus formation in human coronary arteries. Philos Trans R Soc Lond B Biol Sci 1981; 294: 225-9.

30. Davies MJ, Woolf N, Rowles P, Richardson PD. Lipid and cellular constituents of unstable human aortic plaque. Basic Res Cardiol 1994; 89 Suppl 1: 33-9.

31. de Boer OJ, van der Wal AC, Teeling P, Becker AE. Leucocyte recruitment in rupture prone regions of lipid-rich plaque: a prominent role for neovascularization? Cardiovasc Res 1999; 41: 443-9.

32. De Korte CL, Pasterkamp G, Van der Steen AF, Woutman HA, Bom N. Characterization of plaque components with intravascular ultrasound elastography in human femoral and coronary arteries in vitro. Circulation 2000; 102: 617-623.

33. Deguchi JO, Aikawa M, Tung CH, Aikawa E, Kim DE, Ntziachristos V, Weissleder R, Libby P. Inflammation in atherosclerosis: visualizing matrix metalloproteinase action in macrophages in vivo. Circulation 2006; 114(1):55-62.

34. Deng Y, Manjunath BS, Shin H. Color image segmentation. Proc IEEE Computer Society Conference on Computer Vision and Pattern Recognition 1999. 2:446-51.

35. Depre C, Havaux X, Renkin J, Vanoverschelde JL, Wijns W. Expression of inducible nitric oxide synthase in human coronary atherosclerotic plaque. Cardiovasc Res 1999; 41: 465-72.

36. Dollery CM, Owen CA, Sukhova GK, Krettek A, Shapiro SD, Libby P. Neutrophil elastase in human atherosclerotic plaque: production by macrophages. Circulation 2003; 107: 2829-36.

37. Dutta J, Fan Y, Gupta N, Fan G, Gelinas C. Current insights into the regulation of programmed cell death by NF-kappaB. Oncogene 2006; 25(51):6800-16.

38. Eliceiri BP, Cheresh DA. The role of alphav integrins during angiogenesis: insights into potential mechanisms of action and clinical development. J Clin Invest 1999; 103: 1227-30.

39. Ennis BW, Matrisian LM. Matrix degrading metalloproteinases. J Neurooncol 1994; 18: 105-9.

40. Escarcega RO, Fuentes-Alexandro S, Garcia-Carrasco M, Gatica A, Zamora A. The transcription factor nuclear factor-kappa B and cancer. Clin Oncol 2007; 19(2):154-61.

41. Felton CV, Crook D, Davies MJ, Oliver MF. Relation of plaque lipid composition and morphology to the stability of human aortic plaque. Arterioscler Thromb Vasc Biol 1997; 17: 1337-45.

42. Ferrans VJ. New insights into the world of matrix metalloproteinases. Circulation 2002; 105: 405-7.

43. Finet G, Ohayon J, Rioufol G. Biomechanical interaction between cap thickness, lipid core composition and blood pressure in vulnerable coronary plaque: impact on stability or instability. Coron Artery Dis 2004; 15: 13-20.

44. Fleiner M, Kummer M, Mirlacher M, Sauter G, Cathomas G, Krapf R, Biedermann BC. Arterial neovascularization and inflammation in vulnerable patients: early and late signs of symptomatic atherosclerosis. Circulation 2004; 110: 2843-50.

45. Fung YC. Biomechanics: Mechanical Properties of Living Tissues. New York: Springer-Verlag New York, Inc., 1993.

46. Galis ZS, Sukhova GK, Kranzhofer R, Clark S, Libby P. Macrophage foam cells from experimental atheroma constitutively produce matrix-degrading proteinases. Proc Natl Acad Sci U S A 1995; 92: 402-6.

47. Galis ZS, Sukhova GK, Lark MW, Libby P. Increased expression of matrix metalloproteinases and matrix degrading activity in vulnerable regions of human atherosclerotic plaque. J Clin Invest 1994; 94: 2493-503.

48. Giddens DP, Zarins CK, Glagov S. The role of fluid mechanics in the localization and detection of atherosclerosis. J Biomech Eng 1993; 115: 588-94.

49. Glagov S, Bassiouny HS, Sakaguchi Y, Goudet CA, Vito RP. Mechanical determinants of plaque modeling, remodeling and disruption. Atherosclerosis 1997; 131 Suppl: S13-4.

50. Golledge J, Greenhalgh RM, Davies AH. The symptomatic carotid plaque. Stroke 2000; 31: 774-81.

51. Green AE and Zerna W. Theoretical Elasticity. Dover Publications, 2002.

52. Gronholdt ML, Dalager-Pedersen S, Falk E. Coronary atherosclerosis: determinants of plaque rupture. Eur Heart J 1998; 19 Suppl C: C24-9.

53. Grote K, Flach I, Luchtefeld M, Akin E, Holland SM, Drexler H, Schieffer B. Mechanical stretch enhances mRNA expression and proenzyme release of Matrix-Metalloproteinase-2 (MMP-2) via NAD(P)H Oxidase-derived Reactive Oxygen Species. Circ Res 2003; 92: 80-86.

54. Guo A, Wei L, Shi H, Li X, You L. [Matrix metalloproteinase-1 and coronary atheroslerotic plaque rupture]. Zhonghua Bing Li Xue Za Zhi 2000; 29: 263-6.

55. Halloran BG, Grange JJ, So BJ, Baxter BT. Macrophage products inhibit human aortic smooth muscle cell proliferation and alter 1 alpha (I) procollagen expression. Ann Vasc Surg 1997; 11: 80-4.

56. Hanley JA, Negassa A, Edwardes MD, and Forrester JE. Statistical analysis of correlated data using Generalized Estimating Equations: An orientation. Am J Epidemiol 2003; 157:364-375.

57. Harrison DG, Widder J, Grumbach I, Chen W, Weber M, Searles C. Endothelial mechanotransduction, nitric oxide adn vascular inflammation. J Internal Med 2006; 259: 351-363.

58. Hayashi K, Imai Y. Tensile property of atheromatous plaque and an analysis of stress in atherosclerotic wall. J Biomech 1997; 30: 573-9.

59. Herman MP, Sukhova GK, Libby P, Gerdes N, Tang N, Horton DB, Kilbride M, Breitbart RE, Chun M, Schonbeck U. Expression of neutrophil collagenase (matrix metalloproteinase-8) in human atheroma: a novel collagenolytic pathway suggested by transcriptional profiling. Circulation 2001; 104: 1899-904.

60. Hishikawa K, Oemar BS, Yang Z, Luscher TF. Pulsatile stretch stimulates superoxide production and activates nuclear factor-kappa B in human coronary smooth muscle. Circ Res 1997; 81: 797-803.

61. Holzapfel GA, Sommer G, Regitnig P. Anisotropic mechanical properties of tissue components in human atherosclerotic plaque. J Biomech Eng 2004; 126: 657-65.

62. Horton DB, Libby P, Schonbeck U. Ligation of CD40 onvascular smooth muscle cells mediates loss of interstitial collagen via matrix metalloproteinase activity. Ann N Y Acad Sci 2001; 947: 329-36.

63. Huang H, Virmani R, Younis H, Burke AP, Kamm RD, Lee RT. The impact of calcification on the biomechanical stability of atherosclerotic plaque. Circulation 2001; 103: 1051-6.

64. Humphrey JD. Cardiovascular solid mechanics: cells, tissues, and organs. New York: Springer-Verlag New York, Inc., 2002.

65. Humphrey J D and Rajagopal KR. A Constrained Mixture Model for Growth and Remodeling of Soft Tissues. Mathematical Models and Methods in Applied Science 2002; 12(3):407-430.

66. Imoto K, Hiro T, Fujii T, Murashige A, Fukumoto Y, Hashimoto G, Okamura T, Yamada J, Mori K, Matsuzaki M. Longitudinal structural determinants of atherosclerotic plaque vulnerability: a computational analysis of stress distribution using vessel models and three-dimensional intravascular ultrasound imaging. J Am Coll Cardiol 2005; 46: 1507-15.

67. Ingber DE. Mechanical signaling and the cellular response to extracellular matrix in angiogenesis and cardiovascular physiology. Circ Res 2002; 91: 877-87.

68. Ingber DE. Cellular mechanotransduction: putting all the pieces together again. FASEB J 2006. 20(7):811-27.

69. Iyemere VP, Proudfoot D, Weissberg PL, Shanahan CM. Vascular smooth muscle cell phenotypic plasticity and the regulation of vascular calcification.J Intern Med 2006; 260:192-210.

70. James TW, Wagner R, White LA, Zwolak RM, Brinckerhoff CE. Induction of collagenase and stromelysin gene expression by mechanical injury in a vascular smooth muscle-derived cell line. J Cell Physiol 1993; 157: 426-37.

71. Jeziorska M, Woolley DE. Local neovascularization and cellular composition within vulnerable regions of atherosclerotic plaque of human carotid arteries. J Pathol 1999; 188: 189-96.

72. Jiang MJ, Yu YJ, Chen YL, Lee YM, Hung LS. Cyclic strain stimulates monocyte chemotactic protein-1 mRNA expression in smooth muscle cells. J Cell Biochem 1999; 76: 303-10.

73. Joung IS, Iwamoto MN, Yan-Ting S, Quam CT. Cyclic strain modulates tubulogenesis of endothelial cells in 3D tissue culture model. Microvasc Res 2006; 71: 1-11.

74. Kaartinen M, Penttila A, Kovanen PT. Mast cells accompany microvessels in human coronary atheromas: implications for intimal neovascularization and hemorrhage. Atherosclerosis 1996; 123: 123-31.

75. Kaartinen M, van der Wal AC, van der Loos CM, Piek JJ, Koch KT, Becker AE, Kovanen PT. Mast cell infiltration in acute coronary syndromes: implications for plaque rupture. J Am Coll Cardiol 1998; 32: 606-12.

76. Katsuda S, Kaji T. Atherosclerosis and extracellular matrix. J Atheroscler Thromb 2003; 10: 267-74.

77. Keeny S, Richardson PD. Stress analysis of atherosclerotic arteries. IEEE Engineering Medicine Biology 1987; 9: 1484-1485.

78. Kher N, Marsh JD. Pathobiology of atherosclerosis - a brief review. Semin Thromb Hemost 2004; 30(6):665-72.

79. Kilpatrick D, Goudet C, Sakaguchi Y, Bassiouny HS, Glagov S, Vito R. Effect of plaque composition on fibrous cap stress in carotid endarterectomy specimens. J Biomech Eng 2001; 123: 635-8.

80. Kilpatrick D, Xu C, Vito R, Glagov S. Correlation of mechanical behavior and MMP-1 presence in human atherosclerotic plaque. J Mech Med Biol 2002; 2: 1-7.

81. Kooi ME, Cappendijk VC, Cleutjens KB, Kessels AG, Kitslaar PJ, Borgers M, Frederik PM, Daemen MJ, van Engelshoven JM. Accumulation of ultrasmall superparamagnetic particles of iron oxide in human atherosclerotic plaque can be detected by in vivo magnetic resonance imaging. Circulation 2003; 107: 2453-8.

82. Kumar A, Takada Y, Boriek AM, Aggarwal BB. Nuclear factor-kappaB: its role in health and disease. J Mol Med 2004; 82: 434-48.

83. Lee RT. Atherosclerotic lesion mechanics versus biology. Z Kardiol 2000; 89 Suppl 2: 80-4.

84. Lee RT, Grodzinsky AJ, Frank EH, Kamm RD, Schoen FJ. Structure-dependent dynamic mechanical behavior of fibrous caps from human atherosclerotic plaque. Circulation 1991; 83: 1764-70.

85. Lee RT, Libby P. The unstable atheroma. Arterioscler Thromb Vasc Biol 1997; 17: 1859-67.

86. Lee RT, Loree HM, Cheng GC, Lieberman EH, Jaramillo N, Schoen FJ. Computational structural analysis based on intravascular ultrasound imaging before in vitro angioplasty: prediction of plaque fracture locations. J Am Coll Cardiol 1993; 21: 777-82.

87. Lee RT, Richardson SG, Loree HM, Grodzinsky AJ, Gharib SA, Schoen FJ, Pandian N. Prediction of mechanical properties of human atherosclerotic tissue by high-frequency intravascular ultrasound imaging. An in vitro study. Arterioscler Thromb 1992; 12: 1-5.

88. Lee RT, Schoen FJ, Loree HM, Lark MW, Libby P. Circumferential stress and matrix metalloproteinase 1 in human coronary atherosclerosis. Implications for plaque rupture. Arterioscler Thromb Vasc Biol 1996; 16: 1070-3.

89. Lehoux S, Castier Y, Tedgui A. Molecular mechanisms of the vascular responses to haemodynamic forces. Journal of Internal Medicine 2006; 259: 381-392.

90. Lehoux S, Tedgui A. Signal Transduction of Mechanical Stress in the Vascular Wall. Hypertension 1998; 32:

91. Lemarie CA, Esposito B, Tedgui A, Lehoux S. Pressure-induced vascular activation of Nuclear Factor-kB: Role in cell survival. Circ Res 2003; 93: 207-212.

92. Lendon CL, Davies MJ, Born GV, Richardson PD. Atherosclerotic plaque caps are locally weakened when macrophages density is increased. Atherosclerosis 1991; 87: 87-90.

93. Lendon CL, Davies MJ, Richardson PD, Born GV. Testing of small connective tissue specimens for the determination of the mechanical behaviour of atherosclerotic plaque. J Biomed Eng 1993; 15: 27-33.

94. Leskinen MJ, Lindstedt KA, Wang Y, Kovanen PT. Mast cell chymase induces smooth muscle cell apoptosis by a mechanism involving fibronectin degradation and disruption of focal adhesions. Arterioscler Thromb Vasc Biol 2003; 23: 238-43.

95. Li ZY, Howarth S, Trivedi RA, JM UK-I, Graves MJ, Brown A, Wang L, Gillard JH. Stress analysis of carotid plaque rupture based on in vivo high resolution MRI. J Biomech 2005; In Press:

96. Libby P, Geng YJ, Aikawa M, Schoenbeck U, Mach F, Clinton SK, Sukhova GK, Lee RT. Macrophages and atherosclerotic plaque stability. Curr Opin Lipidol 1996; 7: 330-5.

97. Lindstedt KA, Kovanen PT. Mast cells in vulnerable coronary plaque: potential mechanisms linking mast cell activation to plaque erosion and rupture. Curr Opin Lipidol 2004; 15: 567-73.

98. Liu J, Sukhova GK, Yang JT, Sun J, Ma L, Ren A, Xu WH, Fu H, Dolganov GM, Hu C, Libby P, Shi GP. Cathepsin L expression and regulation in human abdominal aortic aneurysm, atherosclerosis, and vascular cells. Atherosclerosis 2006; 184: 302-11.

99. Loftus IM, Naylor AR, Bell PR, Thompson MM. Matrix metalloproteinases and atherosclerotic plaque instability. Br J Surg 2002; 89: 680-94.

100. Loree HM, Grodzinsky AJ, Park SY, Gibson LJ, Lee RT. Static circumferential tangential modulus of human atherosclerotic tissue. J Biomech 1994; 27: 195-204.

101. Loree HM, Kamm RD, Atkinson CM, Lee RT. Turbulent pressure fluctuations on surface of model vascular stenoses. Am J Physiol 1991; 261: H644-50.

102. Loree HM, Kamm RD, Stringfellow RG, Lee RT. Effects of fibrous cap thickness on peak circumferential stress in model atherosclerotic vessels. Circ Res 1992; 71: 850-8.

103. Loree HM, Tobias BJ, Gibson LJ, Kamm RD, Small DM, Lee RT. Mechanical properties of model atherosclerotic lesion lipid pools. Arterioscler Thromb 1994; 14: 230-4.

104. Lowder ML, Li S, Carnell PC, Vito R. Correction of distortion of histologic sections of arteries. J Biomech 2006; In Press:

105. MacNeill BD, Jang IK, Bouma BE, Iftimia N, Takano M, Yabushita H, Shishkov M, Kauffman CR, Houser SL, Aretz HT, DeJoseph D, Halpern EF, Tearney GJ. Focal and multi-focal plaque macrophage distributions in patients with acute and stable presentations of coronary artery disease. J Am Coll Cardiol 2004; 44: 972-9.

106. Madamanchi NR, Vendrov A, Runge MS. Oxidative Stress and Vascular Disease. Arterioscler Thromb 2004; 2005: 29-38.

107. Martin DK, Bootcov MR, Campbell TJ, French PW, Breit SN. Human macrophages contain a stretch-sensitive potassium channel that is activated by adherence and cytokines. J Membr Biol 1995; 147: 305-15.

108. Meuwissen M, van der Wal AC, Koch KT, Van der Loos CM, Chamuleau SAJ, Teeling P, de Winter RJ, Tijssen JGP, Becker AE, Piek JJ. Association between complex coronary artery stenosis and unstable angina and the extend of plaque inflammation. Am J Med 2003; 114: 521-527.

109. Molloy KJ, Thompson MM, Jones JL, Schwalbe EC, Bell PR, Naylor AR, Loftus IM. Unstable carotid plaque exhibit raised matrix metalloproteinase-8 activity. Circulation 2004; 110: 337-43.

110. Monaco C, Paleolog E. Nuclear Factor kB: a potential therapeutic target in atherosclerosis and thrombosis. Cardiovasc Res 2004; 61: 671-682.

111. Moreno PR, Bernardi VH, Lopez-Cuellar J, Murcia AM, Palacios IF, Gold HK, Mehran R, Sharma SK, Nemerson Y, Fuster V, Fallon JT. Macrophages, smooth muscle cells, and tissue factor in unstable angina. Implications for cell-mediated thrombogenicity in acute coronary syndromes. Circulation 1996; 94: 3090-7.

112. Moreno PR, Falk E, Palacios IF, Newell JB, Fuster V, Fallon JT. Macrophage infiltration in acute coronary syndroms: Implications for plaque rupture. Circulation 1994; 90: 775-778.

113. Moreno PR, Lodder RA, Purushothaman KR, Charash WE, O'Connor WN, Muller JE. Detection of lipid pool, thin fibrous cap, and inflammatory cells in human aortic atherosclerotic plaque by near-infrared spectroscopy. Circulation 2002; 105: 923-7.

114. Moreno PR, Purushothaman KR, Fuster V, Echeverri D, Truszczynska H, Sharma SK, Badimon JJ, O'Connor WN. Plaque neovascularization is increased in ruptured atherosclerotic lesions of human aorta: implications for plaque vulnerability. Circulation 2004; 110: 2032-8.

115. Moreno PR, Purushothaman KR, Fuster V, O'Connor WN. Intimomedial interface damage and adventitial inflammation is increased beneath disrupted atherosclerosis in the aorta: implications for plaque vulnerability. Circulation 2002; 105: 2504-11.

116. Moulton KS, Vakili K, Zurakowski D, Soliman M, Butterfield C, Sylvin E, Lo KM, Gillies S, Javaherian K, Folkman J. Inhibition of plaque neovascularization reduces macrophage accumulation and progression of advanced atherosclerosis. Proc Natl Acad Sci U S A 2003; 100: 4736-41.

117. Newby AC, Zaltsman AB. Fibrous cap formation or destruction--the critical importance of vascular smooth muscle cell proliferation, migration and matrix formation. Cardiovasc Res 1999; 41: 345-60.

118. Nicholson AC, Han J, Febbraio M, Silversterin RL, Hajjar DP. Role of CD36, the macrophage class B scavenger receptor, in atherosclerosis. Ann N Y Acad Sci 2001; 947: 224-8.

119. Nikkari ST, O'Brien KD, Ferguson M, Hatsukami T, Welgus HG, Alpers CE, Clowes AW. Interstitial collagenase (MMP-1) expression in human carotid atherosclerosis. Circulation 1995; 92: 1393-8.

120. O'Malley SM, Vavuranakis M, Naghavi M, Kakadiaris IA. Intravascular ultrasound-based imaging of vasa vasorum for the detection of vulnerable atherosclerotic plaque. Med Image Comput Comput Assist Interv Int Conf Med Image Comput Comput Assist Interv 2005; 8: 343-51.

121. Ohayon J, Teppaz P, Finet G, Rioufol G. In-vivo prediction of human coronary plaque rupture location using intravascular ultrasound and the finite element method. Coron Artery Dis 2001; 12: 655-63.

122. Ohki R, Yamamoto K, Mano H, Lee RT, Ikeda U, Shimada K. Identification of mechanically induced genes in human monocytic cells by DNA microarrays. J Hypertens 2002; 20: 685-91.

123. Onorato JM, Thorpe SR, Baynes JW. Immunohistochemical and ELISA assays for biomarkers of oxidative stress in aging and disease. Ann N Y Acad Sci 1998; 854: 277-90.

124. Pasterkamp G, Schoneveld AH, van der Wal AC, Hijnen DJ, van Wolveren WJ, Plomp S, Teepen HL, Borst C. Inflammation of the atherosclerotic cap and shoulder of the plaque is a common and locally observed feature in unruptured plaque of femoral and coronary arteries. Arterioscler Thromb Vasc Biol 1999; 19: 54-8.

125. Rachev A, Manoach E, Berry J, Moore J. Model of stress-induced geometrical remodeling of vessel segment adjacent to stents and artery/graft anastomosis. J Theor Biol 2000; 206(3):429-443.

126. Rajagopalan S, Meng XP, Ramasamy S, Harrison DG, Galis ZS. Reactive oxygen species produced by macrophage-derived foam cells regulate the activity of vascular matrix metalloproteinases in vitro. Implications for atherosclerotic plaque stability. J Clin Invest 1996; 98: 2572-9.

127. Reddy JN. An Introduction to the Finite Element Method, 2nd Ed. McGraw-Hill, INc., 1993.

128. Rekhter MD. Collagen synthesis in atherosclerosis: too much and not enough. Cardiovasc Res 1999; 41: 376-84.

129. Robbesyn F, Salvayre R, Negre-Salvayre A. Dual role of oxidized LDL on the NF-kappaB signaling pathway. Free Radic Res 2004; 38: 541-51.

130. Saijo Y, Ohashi T, Sasaki H, Sato M, Jorgensen CS, Nitta S. Application of scanning acoustic microscopy for assessing stress distribution in atherosclerotic plaque. Ann Biomed Eng 2001; 29: 1048-53.

131. Sakamoto H, Aikawa M, Hill CC, Weiss D, Taylor WR, Libby P, Lee RT. Biomechanical strain induces class a scavenger receptor expression in human monocyte/macrophages and THP-1 cells: a potential mechanism of increased atherosclerosis in hypertension. Circulation 2001; 104: 109-14.

132. Salunke NV, Topoleski LD. Biomechanics fo atherosclerotic plaque. Crit Rev Biomed Eng 1997; 25(3):243-85.

133. Schroeder AP, Falk E. Vulnerable and dangerous coronary plaque. Atherosclerosis 1995; 118 Suppl: S141-9.

134. Shaalan WE, Cheng H, Gewertz B, McKinsey JF, Schwartz LB, Katz D, Cao D, Desai T, Glagov S, Bassiouny HS. Degree of carotid plaque calcification in relation to symptomatic outcome and plaque inflammation. J Vasc Surg 2004; 40: 262-9.

135. Shah PK. Mechanisms of plaque vulnerability and rupture. J Am Coll Cardiol 2003; 41: 15S-22S.

136. Shah PK, Falk E, Badimon JJ, Fernandez-Ortiz A, Mailhac A, Villareal-Levy G, Fallon JT, Regnstrom J, Fuster V. Human monocyte-derived macrophages induce collagen breakdown in fibrous caps of atherosclerotic plaque. Potential role of matrix-degrading metalloproteinases and implications for plaque rupture. Circulation 1995; 92: 1565-9.

137. Shanahan CM, Weissberg PL. Smooth muscle cell heterogeneity - patterns of gene expression in vascular smooth muscle cells in vitro and in vivo. Arterioscler Thromb Vasc Biol 1998; 18:333-338.

138. Stary HC, Blankenhorn DH, Chandler AB, Glagov S, Insull W, Richardson M, Rosenfeld ME, Schaffer SA, Schwartz CJ, Wagner WD, et al. A definition of the intima of human arteries and of its atherosclerosis-prone regions. A report from the Committee on Vascular Lesions of the Council on Arteriosclerosis, American Heart Association. Circulation 1992; 85: 391-405.

139. Stary HC, Chandler AB, Glagov S, Guyton JR, Insull W, Rosenfeld ME, Schaffer SA, Schwartz CJ, Wagner WD, Wissler RW. A definition of initial, fatty streak, and intermediate lesions of atherosclerosis. . A report from the Committee on Vascular Lesions of the Council on Arteriosclerosis, American Heart Association. Circulation 1994; 89: 2462-78.

140. Stary HC, Chandler AB, Dinsmore RE, Fuster V, Glagov C, Insull W, Rosenfeld ME, Schwartz CJ, Wagner WD, Wissler RW. A definition of advanced types of atherosclerotic lesions and a histological classification of atherosclerosis. A report from the Committee on Vascular Lesions of the Council on Arteriosclerosis, American Heart Association. Circulation 1995; 92: 1355-74.

141. Stary HC. Natural history and histological classification of atherosclerotic lesions: an updata. Arteriscler Thromb Vasc Biol 2000; 20(5):1177-8.

142. Stefanadis C, Diamantopoulos L, Vlachopoulos C, Tsiamis E, Dernellis J, Toutouzas K, Stefanadi E, Toutouzas P. Thermal heterogeneity within human atherosclerotic coronary arteries detected in vivo: A new method of detection by application of a special thermography catheter. Circulation 1999; 99: 1965-71.

143. Sukhova GK, Schonbeck U, Rabkin E, Schoen FJ, Poole AR, Billinghurst RC, Libby P. Evidence for increased collagenolysis by interstitial collagenases-1 and -3 in vulnerable human atheromatous plaque. Circulation 1999; 99: 2503-9.

144. Sukhova GK, Shi GP, Simon DI, Chapman HA, Libby P. Expression of the elastolytic cathepsins S and K in human atheroma and regulation of their production in smooth muscle cells. J Clin Invest 1998; 102: 576-83.

145. Takahashi K, Takeya M, Sakashita N. Multifunctional roles of macrophages in the development and progression of atherosclerosis in humans and experimental animals. Med Electron Microsc 2002; 35: 179-203.

146. Tang D, Yang C, Kobayashi S, Ku DN. Effect of a lipid pool on stress/strain distributions in stenotic arteries: 3-D fluid-structure interactions (FSI) models. J Biomech Eng 2004; 126: 363-70.

147. Tang TY, Howarth SP, Miller SR, Trivedi R, Graves MJ, King-Im JU, Li ZY, Brown AP, Kirkpatrick PJ, Guant ME, Gillard JH. Assessment of inflammatory burden contralateral to the symptomatic carotid stenosis using high-resolution ultrasmall, superparamagnetic iron oxide-enhanced MRI. Stroke 2006. 37(9):2266-70.

148. Tearney GJ, Yabushita H, Houser SL, Aretz HT, Jang IK, Schlendorf KH, Kauffman CR, Shishkov M, Halpern EF, Bouma BE. Quantification of macrophage content in atherosclerotic plaque by optical coherence tomography. Circulation 2003; 107: 113-9.

149. Topoleski LD, Salunke NV. Mechanical behavior of calcified plaque: a summary of compression and stress-relaxation experiments. Z Kardiol 2000; 89 Suppl 2: 85-91.

150. Topoleski LD, Salunke NV, Humphrey JD, Mergner WJ. Composition- and history-dependent radial compressive behavior of human atherosclerotic plaque. J Biomed Mater Res 1997; 35: 117-27.

151. van der Wal AC, Becker AE. Atherosclerotic plaque rupture--pathologic basis of plaque stability and instability. Cardiovasc Res 1999; 41: 334-44.

152. van der Wal AC, Becker AE, van der Loos CM, Das PK. Site of intimal rupture or erosion of thrombosed coronary atherosclerotic plaque is characterized by an inflammatory process irrespective of the dominant plaque morphology. Circulation 1994; 89: 36-44.

153. van der Wal AC, Becker AE, van der Loos CM, Tigges AJ, Das PK. Fibrous and lipid-rich atherosclerotic plaque are part of interchangeable morphologies related to inflammation: a concept. Coron Artery Dis 1994; 5: 463-9.

154. Vengrenyuk Y, Carlier S, Xanthos S, Cardoso L, Ganatos P, Virmani R, Elinav S, Gilchrist L, Weinbaum S. A hypothesis for vulnerable plaque rupture due to stress-induced debonding around cellular microcalcifications in thin fibrous caps. Proc Natl Acad Sci USA 2006; 103(40): 14678-83.

155. Versluis A, Bank AJ, Douglas WH. Fatigue and plaque rupture in myocardial infarction. J Biomech 2006; 39: 339-47.

156. Vincenti MP, Brinckerhoff CE. Transcriptional regulation of collagenase (MMP-1, MMP-13) genes in arthritis: integration of complex signaling pathways for the recruitment of gene-specific transcription factors. Arthritis Res 2002; 4(3):157-64.

157. Vito R, Whang MC, Giddens DP, Zarins CK, Glagov S. Stress analysis of the diseased arterial cross-section. ASME Advances in Bioengineering 1990; 273-276.

158. Vito RP, Dixon SA. Blood vessel constitutive models-1995-2002. Annu Rev Biomed Eng 2003; 5: 413-39.

159. Vonesh MJ, Cho CH, Pinto JV, Jr., Kane BJ, Lee DS, Roth SI, Chandran KB, McPherson DD. Regional vascular mechanical properties by 3-D intravascular ultrasound with finite-element analysis. Am J Physiol 1997; 272: H425-37.

160. Watson KE. Pathophysiology of coronary calcification. J Cardiovasc Risk 2000; 7: 93-7.

161. Yamamoto K, Ikeda U, Shimada K. Role of mechanical stress in monocytes/macrophages: implications for atherosclerosis. Curr Vasc Pharmacol 2003; 1: 315-9.

162. Yang JH, Sakamoto H, Xu EC, Lee RT. Biomechanical regulation of human monocyte/macrophage molecular function. Am J Pathol 2000; 156: 1797-804.